General Disclaimer

One or more of the Following Statements may affect this Document

- This document has been reproduced from the best copy furnished by the organizational source. It is being released in the interest of making available as much information as possible.

- This document may contain data, which exceeds the sheet parameters. It was furnished in this condition by the organizational source and is the best copy available.

- This document may contain tone-on-tone or color graphs, charts and/or pictures, which have been reproduced in black and white.

- This document is paginated as submitted by the original source.

- Portions of this document are not fully legible due to the historical nature of some of the material. However, it is the best reproduction available from the original submission.

Produced by the NASA Center for Aerospace Information (CASI)

NASA CR-156817

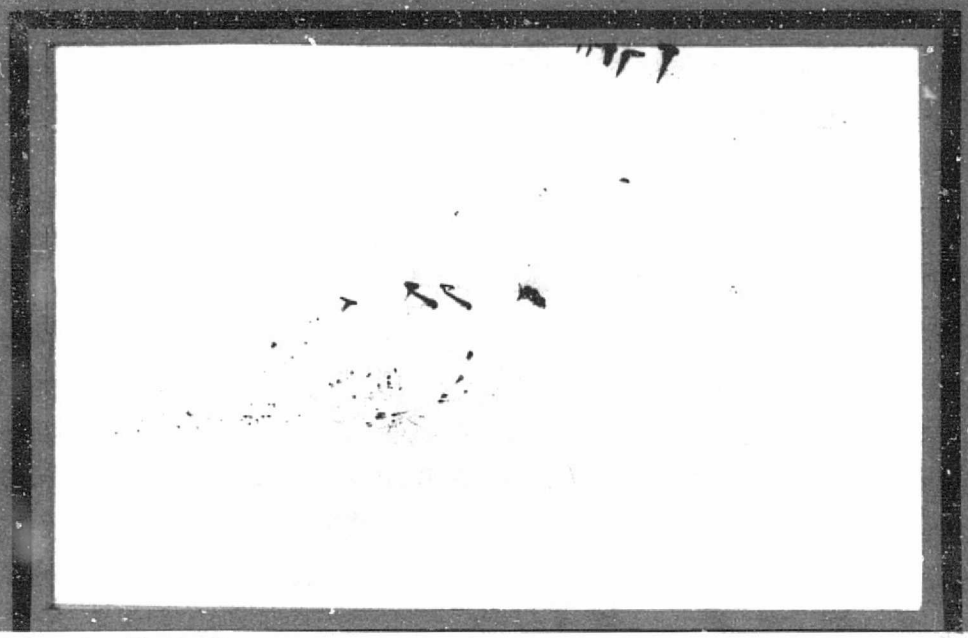

(NASA-CR-156817) MILLIMETER WAVE PROPAGATION MODELING OF INHOMOGENEOUS RAIN MEDIA FOR SATELLITE COMMUNICATIONS SYSTEMS (Virginia Polytechnic Inst. and State Univ.) 204 p HC A10/MF A01 CSCL 20N G3/32

N78-32315

Unclas 33197

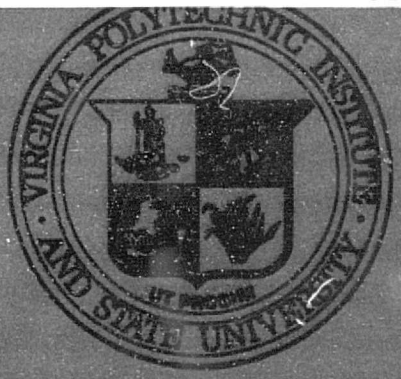

Virginia Polytechnic Institute
and State University
Electrical Engineering
BLACKSBURG, VIRGINIA 24061

Interim Report 1978-1

on

A DEPOLARIZATION AND ATTENUATION EXPERIMENT USING THE CTS AND COMSTAR SATELLITES

Millimeter Wave Propagation Modeling Of Inhomogeneous Rain Media For Satellite Communications Systems

Text by

R. R. Persinger and W. L. Stutzman

Electrical Engineering Department
Virginia Polytechnic Institute and State University
Blacksburg, Virginia 24061

Prepared for

NASA Goddard Space Flight Center
Greenbelt, Maryland 20771

This work was supported by NASA and DCA
under Contract NAS5-22577
and by the
U. S. Army Research Office
under Grant DAAG29-77-G-0083.

June, 1978

PRECEDING PAGE BLANK NOT FILMED

TABLE OF CONTENTS

LIST OF FIGURES

LIST OF TABLES

CHAPTER I

INTRODUCTION

The ever-increasing demand for additional communications capacity has led system design engineers to increase operating frequencies higher into the millimeter wave frequency band. Also, to effectively double communications capacity for a given satellite communications system, frequency reuse systems employing orthogonal polarizations have been suggested [1]. However, for operating frequencies above 10 GHz rain attenuation and depolarization become more severe because of the increased signal scattering and absorption by raindrops. Before future communications systems can be designed for maximum reliability and economy, a clearer understanding of these weather induced phenomena is necessary. Presently an experimental data base is being collected to describe the effects of rain on terrestrial and satellite communications links. Measured signal attenuation, orthogonal channel isolation, and phase shift data are being correlated with weather data to aid the design engineer in the prediction of rain effects on millimeter wave propagation. Since this collection of data is relatively expensive, especially for satellite communications links, theoretical models have been developed to predict weather effects on communications link performance. This report investigates the ability of a theoretical model to account for the *inhomogeneous rain conditions* present on a satellite communications link and thus accurately predict the effects of weather on system performance.

Theoretical modeling of the scattering properties of an ensemble

of particles was considered by Gustav Mie as early as 1908 [2]. The present development of theoretical modeling as related to a rain-filled space and the restrictions associated with the ensemble of raindrops will be discussed in Chapter II. In Chapter III a new deterministic theoretical model is presented with an associated rain propagation prediction program that can model an inhomogeneous rain and accurately predict the effects of precipitation on a satellite communications link for a variety of frequencies, elevation angles and locations. Finally in Chapter IV, the most recent multiple frequency data from various depolarization experiments are presented as verification of the new model.

The new model presented in Chapter III, although more general than previous models, is theoretically equivalent to each of the classical models presented in Chapter II under the assumptions of the respective model. By taking a slightly different approach in the theoretical derivation of the new model, the scattering properties of an arbitrary inhomogeneous ensemble of raindrops and ice crystals can be determined and the validity of other theoretical models can be verified. Unique aspects of the new model are: 1) attenuation and depolarization are computed directly in terms of the scattered fields from an ensemble of particles containing an arbitrary mixture of particle type (rain or ice), particle shape, particle size, particle density and particle orientation, 2) an inhomogeneous mixture of particles and the presence of a melting layer along the propagation path is accounted for directly in determining the scattering fields exiting the rain medium, 3) a

frequency independent synthetic storm algorithm models the nonuniform rain rates present on a satellite communications link, 4) antenna-wave interaction is considered, and 5) signal attenuation, channel isolation and phase as a function of ground rain rate can be determined for a variety of site locations from a knowledge of the operation frequency, system antenna polarization parameters, and the system elevation angle.

CHAPTER II

REVIEW OF CURRENT THEORETICAL PROPAGATION MODELS

Although Gustav Mie in 1908 [2] was responsible for the preliminary foundation for theoretical work relating to the attenuation and depolarization of electromagnetic waves propagating through rain, it was not until 1960 that Oguchi [3] first considered the depolarization of an incident field by an oblate spheroidal raindrop. Oguchi obtained the first-order change in the scattered field from a single oblate raindrop by expanding the scattered field directly in a series of spherical vector wave functions involving powers of the raindrop eccentricity. The single oblate raindrop scattering coefficients provided the foundation for all theoretical rain depolarization models that followed. The scattering coefficients of Oguchi were later verified using different theoretical methods by Morrison and Cross of Bell Labs in 1974 [4] and Uzunoglu, Evans, and Holt of the University of Essex, England in 1977 [5].

Using the theory of van de Hulst [6], Oguchi extended the single drop solution to an ensemble of identical, equioriented oblate spheroidal raindrops. By decomposing the incident field along the orthogonal axes defined by the principal planes of the canted oblate raindrop, Oguchi determined an effective complex refractive index of the rain medium. The application of the work of Oguchi to the problem of depolarization as related to a communications system was first made by Thomas of Bell Labs in 1971 [7]. He showed that a difference in attenuation for waves polarized along the major and minor axes of an

oblate raindrop would lead to depolarization of any wave not polarized parallel to one of the principal axes. However, Thomas neglected the effects of differential phase on the depolarization of an electric field. The assumptions of the theoretical model of Thomas are given below:

1) Uniform rainfall over the entire path,
2) Laws and Parsons [8] raindrop-size distribution,
3) Single scattering (which is to say that each raindrop is illuminated by an incident plane wave and wave interaction between drops is negligible),
4) 100% oblate spheroidal equioriented raindrops at an effective canting angle θ.

The theoretical models of Watson (1973) [9] and Chu (1974) [10] also employ the assumptions of Thomas; however, these models consider the effects of differential attenuation and differential phase. The work of Watson and Chu, referred to as the classical propagation constant formulation, predicted rather well the rain effects experienced on a terrestrial communications link with nearly uniform rain conditions.

Wiley [11] in 1973 checked the validity of the classical propagation constant model. He derived the same results by directly summing the scattered fields located within the first Fresnel zone from an arbitrary equioriented ensemble of raindrops. (A drop size distribution was not included.) Wiley also illustrated that theoretical models could represent an ensemble of raindrops that contained up to 60%

spherical raindrops and accurately predict measured depolarization data. This difference in opinion of the percent of oblate raindrops is complicated by the positions of meteorologists Jones [12] and Pruppacher and Pitter [13]. Using experimental vertical wind tunnel conditions and formulations relating surface tension to particle shape, Pruppacher and Pitter hypothesize that, except for only the largest drops, raindrops are oblate spheroidal particles. Based on real rain measurements, Jones indicates that a real rain is composed of spherical, oblate spheroidal, prolate spheroidal and irregular shaped raindrops for all size classes greater than 0.9 mm spherical radius. Depending on the assumption of the percent of oblate raindrops present in an ensemble of raindrops, channel isolation can vary by a significant amount for a given value of attenuation as indicated in Fig. 2-1. (This figure was obtained from the results of Chapter III.) Since the work of Jones indicates the presence of shapes other than oblate and the effect of different raindrop shapes has a significant impact on the prediction of channel isolation, a theoretical propagation model should include a particle shape distribution.

Although still assuming 100% oblate spheroidal raindrops, Uzunoglu, Evans, and Holt [5] and Nowland, Olsen, and Shkarofsky [14] in 1977 indicated that a distribution of canting angles should be included in a theoretical model. Since the classical propagation constant formulation is restricted to equioriented raindrops, a stochastic averaging process was implemented. By weighting the elements of the scattering matrix as seen in Eq. (2-1) with a Gaussian probability distribution

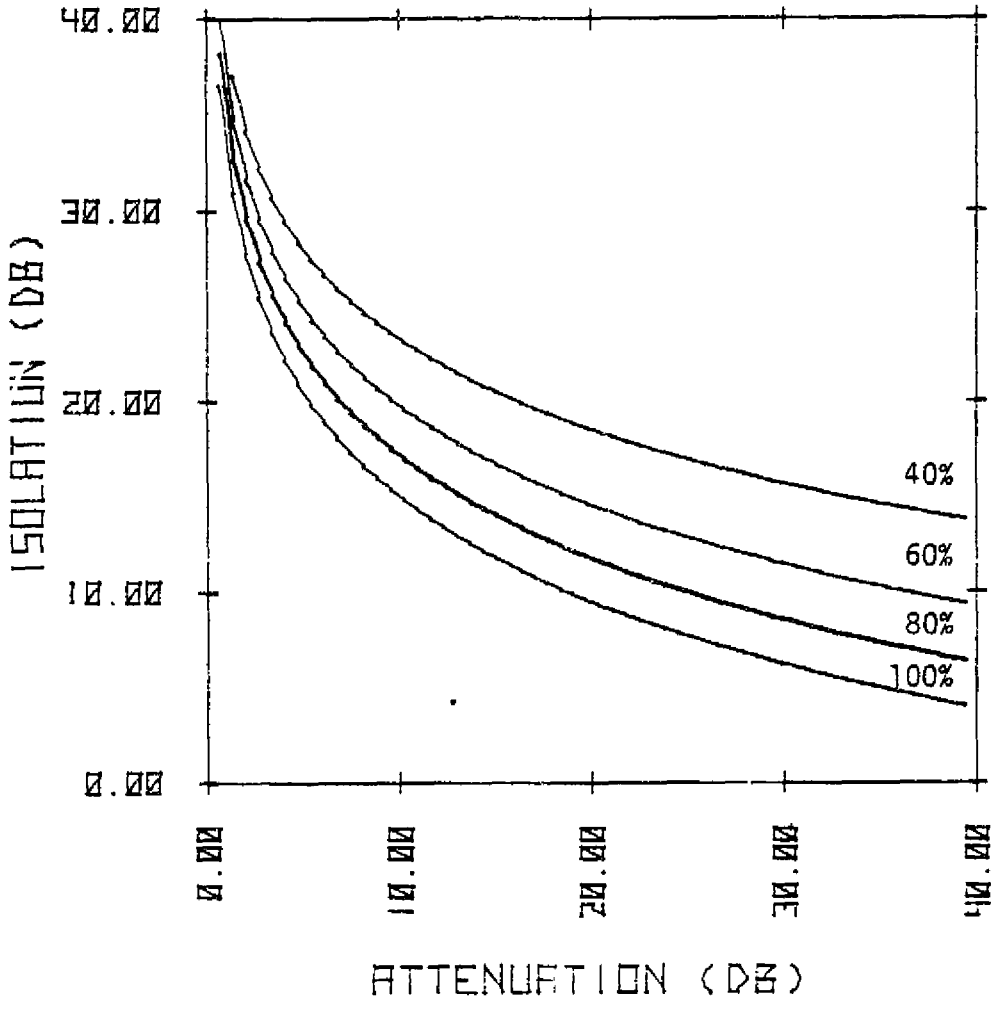

Figure 2-1. Isolation versus attenuation for different percentages of oblate raindrops. (f = 11 GHz, no canting angle distribution, circular polarization, L = 10 km).

function, a canting angle distribution can be modeled:

$$\begin{bmatrix} \dot{E}_x \\ \dot{E}_y \end{bmatrix} = \begin{bmatrix} \sum_i w\, D_{11}(\theta_i) & \sum_i w\, D_{12}(\theta_i) \\ \sum_i w\, D_{21}(\theta_i) & \sum_i w\, D_{22}(\theta_i) \end{bmatrix} \begin{bmatrix} \dot{E}_x^i \\ \dot{E}_y^i \end{bmatrix}$$

where

$$\begin{aligned} D_{11} &= d_h \cos^2\theta + d_v \sin^2\theta \\ D_{22} &= d_h \sin^2\theta + d_v \cos^2\theta \\ D_{12} &= D_{21} = (d_v - d_h)\cos\theta \sin\theta \end{aligned} \tag{2-1}$$

and the symbols w, $d_{v,h}$, θ, $f_{v,h}$, N, and L are defined as

w = normalized Gaussian weighting function

$d_{v,h} = e^{-j\lambda L \sum N(\bar{a})\, f_{v,h}(\bar{a})}$

θ = drop canting angle

$f_{v,h}$ = principal plane single drop scattering coefficients

$N(\bar{a})$ = number of raindrops per unit volume in the $\bar{a}$ to $\bar{a} + d\bar{a}$ equivolumetric drop radius interval.

L = rain extent length .

Because a stochastic averaging process was used, the above formulation ignores multiple scattering between arbitrarily oriented raindrops. However, the assumption was made that multiple scattering is negligible. This assumption can be verified by the more general model presented in the following chapter because it accounts for the arbitrarily oriented particles directly.

For satellite communications links the assumption of uniform rainfall over the entire rain extent is not adequate in describing the effects of precipitation on system performance. As peak rain rate increases, rain cells of higher rain rates decrease in size. Based on experimental attenuation measurements, researchers [15], [16], [17] have implemented an effective path length (L_e) that models the nonuniform rain rates present on a satellite communications link. However, it will be shown in Sec. 3.6 that this method is frequency dependent and overly restrictive. Therefore, a frequency independent synthetic storm algorithm will be presented.

The formulations of Uzunoglu, Evans and Holt [5] and Nowland, Olsen, and Shkarofsky [14] represent the current status in theoretical propagation models. However, these formulations do not consider the effects of an ensemble of arbitrary particles and an inhomogeneous rain medium. The theoretical model presented in the following chapter accounts for the scattering properties of an arbitrary inhomogeneous ensemble of particles without a significant increase in model complexity.

CHAPTER III

DEVELOPMENT OF THE THEORETICAL MODEL

A theoretical rain propagation model should represent accurately the physical nature of a rain medium and allow a wide range of rain parameters; thus, the effect of precipitation on communications system performance can be determined accurately. Parameters such as canting angle, particle size, particle shape and particle type should be described with deterministic distributions based on existing physical knowledge of their behavior. The model also should be flexible so that these parameters can be adjusted to best describe the true physical nature of the rain medium. In this chapter a model is presented that provides this generalized format and henceforth will be referred to as the *scattering model*.

3.1 Electromagnetic Scattering by an Oblate Spheroidal Particle

To develop a solid foundation for the derivation of the *scattering model*, the scattering properties of a single oblate raindrop will be considered first. The oblate raindrop is of extreme importance in any model that predicts the attenuation, depolarization, and phase shift of an electric field. The oblate particle through its differential attenuation and differential phase properties provides the key mechanism in the depolarization process. Oguchi and Hosoya [18], Morrison and Cross [4], and Uzunoglu, Evans, and Holt [5] have published single drop scattering coefficients as a function of drop size for the principal planes of the oblate drop. The drop size is represented by an

equivolumetric drop radius, and as the radius increases the drop becomes more oblate. The available scattering coefficients agree rather well and provide the basis for any theoretical model.

An oblate spheroidal raindrop canted at an angle θ with respect to an arbitrary x-y coordinate system is illustrated in Fig. 3.1-1. If the x-y coordinate system is aligned with true horizontal and vertical, θ is the drop canting angle. Following the notation of Oguchi, the h-v axis in Fig. 3.1-1 represents the orientation of the oblate raindrop where the h and v axis are aligned with the drop major and minor axes, respectively. Another important parameter needed in the calculation of the single drop scattering coefficients is the elevation angle. The elevation angle β is the angle between a plane parallel to the local horizontal and the direction of propagation represented by the vector $\vec{K}_i$. For a terrestrial communications link, this angle would be zero. A satellite link would have an elevation angle ranging from 0 to 90 degrees. Knowing the equivolumetric drop radius as defined by Uzunoglu, Evans and Holt and given in Fig. 3.1-1, the elevation angle, and the frequency of propagation, the vertical and horizontal scattering coefficients f_v and f_h can be determined.

Any incident field can always be decomposed into orthogonal linear components along the principal axes of the oblate spheroidal raindrop. Thus, single drop scattering coefficients are given only for the principal axes of the drop. Single drop scattering coefficients are defined in several ways in the literature; the definition of Oguchi will be used as follows:

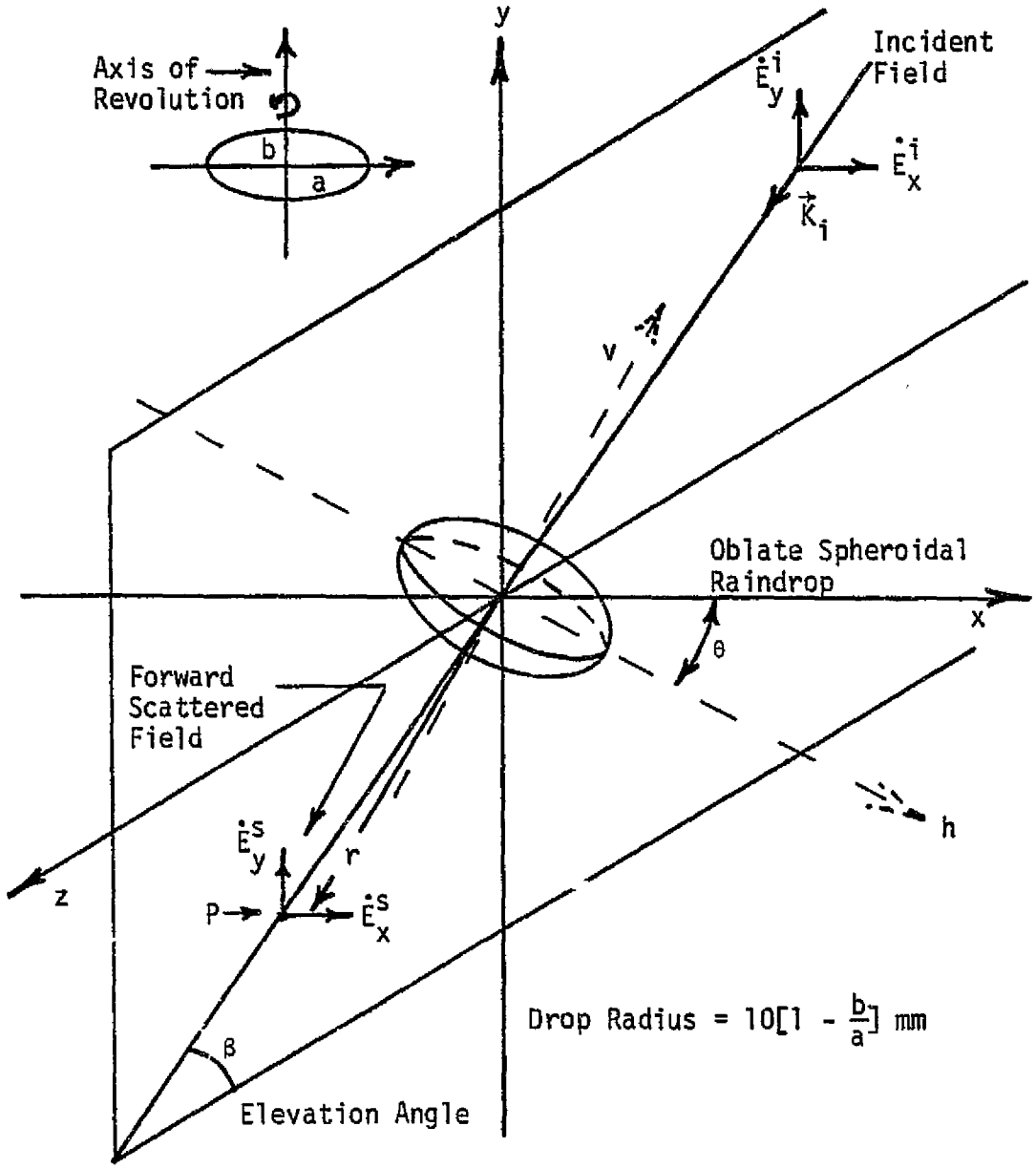

Figure 3.1-1. Arbitrary oblate spheroidal raindrop canted in an arbitrary x-y coordinate system.

f_v: ratio of the forward scattered electric field component along the drop minor axis to the incident electric field component along the drop minor axis

f_h: ratio of the forward scattered electric field component along the drop major axis to the incident electric field component along the drop major axis .

The incident electric field component along the drop major axis (h) experiences more attenuation and phase shift than the component along the minor axis (v). This effect causes the depolarization of incident fields that are not linearly polarized along one of the principal axes.

The hv decomposition is overly restrictive. Wiley [11] has shown that a generalized scattering coefficient can be defined as a function of θ and the single drop scattering coefficients. The generalized scattering coefficients allow the incident field to have any arbitrary angle with respect to the drop. These coefficients are easily derived (see Appendix 6.1.1) and are given below in terms of the arbitrary x-y coordinate system:

$$\begin{aligned} f_{xx} &= f_v \sin^2\theta + f_h \cos^2\theta \\ f_{xy} &= (f_v - f_h) \sin\theta \cos\theta \\ f_{yx} &= f_{xy} \\ f_{yy} &= f_v \cos^2\theta + f_h \sin^2\theta \quad . \end{aligned} \tag{3.1-1}$$

The symbol f_{pq} will be used to represent the general scattering coefficient.

Now the forward scattering effects of an oblate spheroidal raindrop can be examined. The incident field on the drop can be written in the general form

$$\vec{E}^i = \dot{E}_x \hat{x} + \dot{E}_y \hat{y} \tag{3.1-2}$$

for all polarization states where $\dot{E}_x$ and $\dot{E}_y$ are phasor quantities. The forward scattered electric field at point P in Fig. 3.1-1 is expressed by the relation

$$\vec{E}^s(P) = \{\dot{E}^s_{xx}(P) + \dot{E}^s_{yx}(P)\}\hat{x} + \{\dot{E}^s_{xy}(P) + \dot{E}^s_{yy}(P)\}\hat{y} \tag{3.1-3}$$

where

$$\dot{E}^s_{pq}(P) = \dot{E}^i_p(P)\, f_{pq}\, \frac{e^{-jk_o r}}{r} \tag{3.1-4}$$

= the scattered electric field component with polarization q as a result of an incident field with polarization p, evaluated at point P

and,

f_{pq} = the ratio of the forward scattered electric field with polarization q to the incident electric field with polarization p evaluated for a particular drop orientation, drop size, and frequency.

The $\frac{e^{-jk_o r}}{r}$ factor of Eq. (3.1-4) describes the spherical wave behavior

of the scattered field between the drop and point P. Although the oblate drop does have back and side scattering properties, these are of no consequence in the prediction of rain effects on a point to point millimeter wave communications link. However, back-scattering coefficients are available in the literature [18] and can be used in place of the forward scattering coefficients in Eqs. (3.1-1) and (3.1-4) to obtain the back-scattered electric field.

The forward scattering effects of an oblate raindrop can be described by Eq. (3.1-3) in terms of the drop orientation, drop size, and frequency. The generalized scattering coefficients of Wiley [11] also can be extended to *any* particle having two axes of symmetry. With this fact, the scattering effects of a slab of arbitrary particles can be investigated.

3.2 Electromagnetic Scattering by a Single Homogeneous Slab of Arbitrary Particles

To predict accurately the effects of precipitation on a given communications link, the propagation path may be subdivided into small intervals of thickness $\Delta\ell$ which are commonly called rain slabs. To describe the scattering properties of a slab, and hence the scattering properties of the entire propagation path, a physical understanding of the rain parameters is necessary. Jones [12] has indicated that rain consists of particles with a variety of shapes. An average rain consists of spherical, oblate spheroidal, prolate spheroidal, and irregular shaped raindrops. Furthermore, it is not uncommon to find

that a heavy concentration of ice crystals at higher altitudes affects the performance of a satellite link. The particle shape, particle orientation, and particle density influence electromagnetic waves propagating through a rain medium. All particle shapes except for spherical contribute to the depolarization of the incident field. For this reason the electromagnetic scattering from a single homogeneous slab of *arbitrary* particles is extremely important to the evaluation of rain effects on millimeter wave propagation.

In 1957 van de Hulst [6] addressed the problem of light scattering by a slab of particles. Although the scattering here is at high radio frequencies, van de Hulst's optical work will serve as a foundation for the development of the scattering model. Consider a homogeneous slab of particles $\Delta\ell$ meters thick and infinite in extent in the transverse plane as shown in Fig. 3.2-1. Since single drop scattering coefficients are not readily available for irregular and prolate spheroidal raindrops, the assumption will be made that all scattering effects of the slab are produced by spherical raindrops, oblate spheroidal raindrops, and ice crystals. However, if coefficients do become available for the irregular and prolate spheroidal raindrops, their inclusion in the theoretical development of the model would further refine the physical representation of the rain medium. With the exception of the work of Wiley [11], most researchers have assumed 100% oblate raindrops which is not physically accurate. Also, any model with the 100% oblate assumption inherently predicts more depolarization for a given rain rate and attenuation because non-depolarizing spherical scatterers are

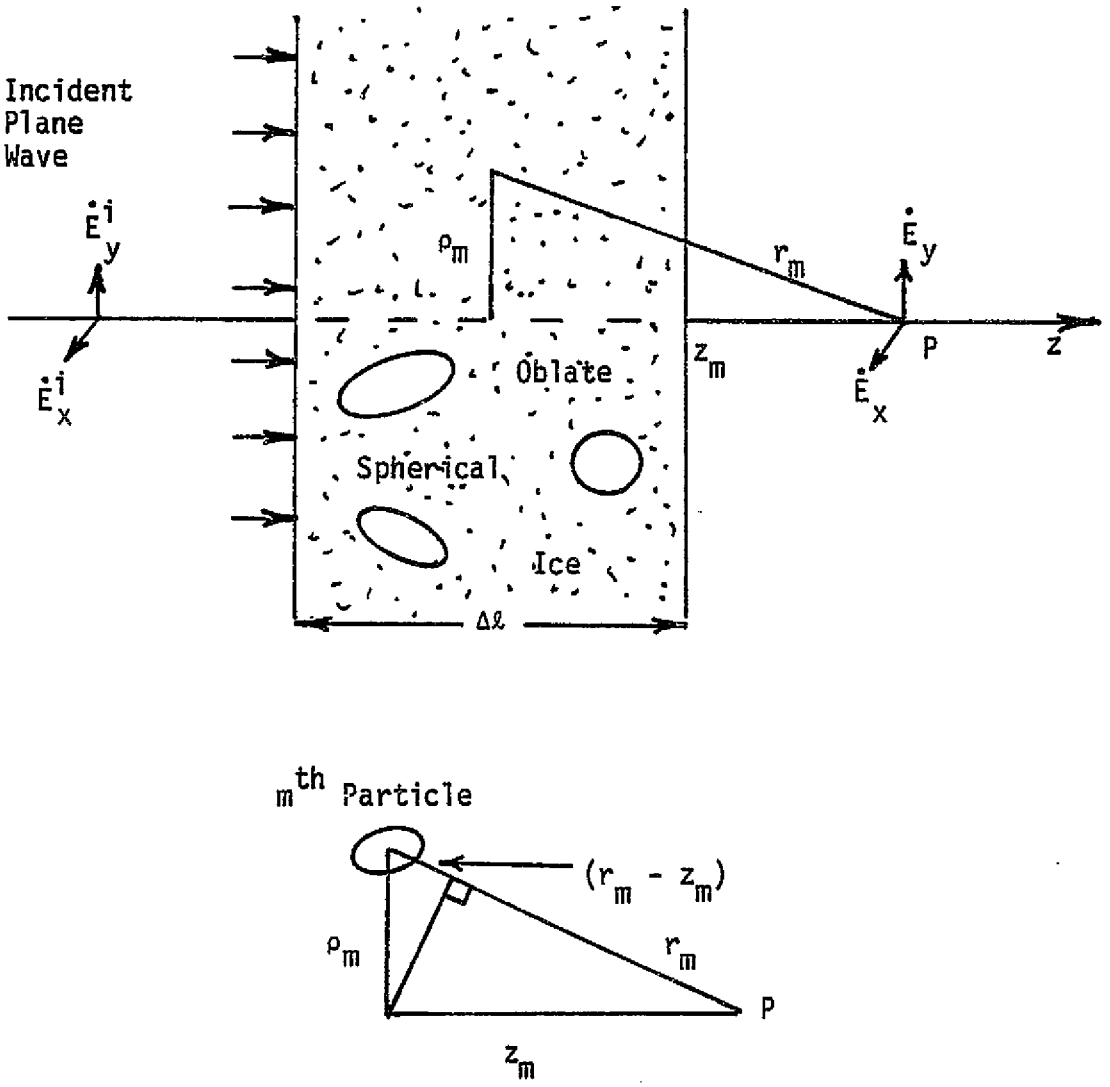

Figure 3.2-1. Homogeneous rain slab of arbitrary particles.

omitted.

The incident field on the slab of particles is assumed to be a uniform plane wave propagating in a direction perpendicular to the slab. Also, the magnitude of the incident field is the same for all particles within the slab. The incident field, regardless of polarization, can be represented by its x and y components as in the previous section. The rain slab is assumed to be large-scale homogeneous with a mixture of particles having varying shapes, sizes, and orientations within the volume of the slab. The distribution functions describing these parameters will be discussed in greater detail in Sec. 3.6. The purpose of this section is to determine the total electric field exiting the propagation medium.

The total electric field at point P is the sum of the incident field and the forward scattered field both evaluated at point P.

$$\vec{E}^{T}(P) = \vec{E}^{i}(P) + \vec{E}^{s}(P) \quad . \tag{3.2-1}$$

The total forward scattered field at point P is the sum of the scattered fields from all the particles within the slab. The total scattered electric field with polarization q resulting from an incident field with polarization p evaluated at point P is expressed by

$$\dot{E}^{s}_{pq}(P) = \dot{E}^{i}_{p}(P) \sum_{\substack{m \\ \text{All Particles}}} f_{pq_m}(\bar{a}, \bar{\theta}) \frac{e^{-jk_o(r_m - z_m)}}{r_m} \quad . \tag{3.2-2}$$

The factor $f_{pq_m}(\bar{a}, \bar{\theta})$ is the generalized complex forward scattering

coefficient for the m^{th} particle as found in Eq. (3.1-1) and represents the change in amplitude, phase, and polarization that the incident field experiences as a result of the m^{th} particle. Note that the scattering coefficient is a function of particle size ($\bar{a}$) and particle orientation ($\bar{\theta}$) and must remain within the summation. The factor $e^{-jk_o(r_m - z_m)}/r_m$ represents the spherical nature of the scattered waves and the effect of the location of the m^{th} particle on the phase of the scattered field at point P.

With a few assumptions Eq. (3.2-2) can be simplified. Consider the geometry for the location of the m^{th} particle as shown in Fig. 3.2-1. The relative phase difference corresponding to the path difference $(r_m - z_m)$ is all that need be considered in determining the phase of the scattered waves arriving at point P. If the assumption is made that $z_m >> \rho_m$, then $r_m \approx z_m$ and:

$$r_m^2 = \rho_m^2 + z_m^2$$

$$\rho_m^2 = r_m^2 - z_m^2 = (r_m - z_m)(r_m + z_m)$$

$$(r_m - z_m) = \rho_m^2/(r_m + z_m) \approx \rho_m^2/2\, z_m \quad (z_m >> \rho_m) \quad . \qquad (3.2\text{-}3)$$

The assumption $z_m >> \rho_m$ is reasonable because the scattered fields at point P are influenced coherently only by the particles located within the first few Fresnel zones. For a satellite link, the radius of the first Fresnel zone corresponding to a rain extent less than 15 km is less than 20 meters. Using Eq. (3.2-3) in Eq. (3.2-2) yields

$$\dot{E}^{s}_{pq}(P) = \dot{E}^{i}_{p}(P) \sum_{\text{All Particles}} f_{pq_m}(\bar{a}, \bar{\theta}) \frac{e^{-jk_o \rho_m^2/2 z_m}}{z_m} \quad . \tag{3.2-4}$$

Although the evaluation of the sum in Eq. (3.2-4) is a relatively simple procedure, several new symbols are needed to abbreviate the somewhat long and cumbersome summations. These symbols will be defined as they are needed.

Let N_p represent the total number of particles within the slab, and let Pe_S, Pe_O, and Pe_I represent the effective fraction of particles that are spherical raindrops, oblate raindrops, and ice crystals, respectively. Since there are three distinct particle shapes, Eq. (3.2-4) can be rewritten as

$$\dot{E}^{s}_{pq}(P) = \dot{E}^{i}_{p}(P) \sum_{m=1}^{Pe_S N_p} f^{SPH}_{pq_m}(\bar{a}) g_m + \dot{E}^{i}_{p}(P) \sum_{m=1}^{Pe_O N_p} f^{OBL}_{pq_m}(\bar{a}, \bar{\theta}) g_m$$
$$\text{Spherical Drops} \qquad \text{Oblate Drops}$$
$$+ \dot{E}^{i}_{p}(P) \sum_{m=1}^{Pe_I N_p} f^{ICE}_{pq_m}(\bar{a}, \bar{\theta}) g_m \tag{3.2-5}$$
$$\text{Ice Crystals}$$

where

$$g_m = \frac{e^{-jk_o \rho_m^2/2 z_m}}{z_m} \quad .$$

The superscripts SPH, OBL, and ICE denote the scattering coefficient for the respective particle type.

Within each class of particle shapes there exists a distribution

of particle size and for the oblate raindrop and ice crystal classes there is also a distribution of particle orientation. Let N_i^{SPH}, $N_{i,k}^{OBL}$, and $N_{i,k}^{ICE}$ represent the number of spherical, oblate, and ice particles within a rain slab that are in the i^{th} size class and k^{th} orientation class, respectively. The scattered field can now be expressed as a series of summations:

$$
\begin{aligned}
\dot{E}_{pq}^{s}(P) = \dot{E}_{p}^{i}(P) \left\{ \sum_{m=1}^{N_1^{SPH}} f_{pq}^{SPH}(\bar{a}_1)\, g_m + \cdots + \sum_{m=1}^{N_m^{SPH}} f_{pq}^{SPH}(\bar{a}_m)\, g_m \right\} \\
+ \dot{E}_{p}^{i}(P) \left\{ \sum_{m=1}^{N_{1,1}^{OBL}} f_{pq}^{OBL}(\bar{a}_1, \bar{\theta}_1)\, g_m + \cdots + \sum_{m=1}^{N_{n,1}^{OBL}} f_{pq}^{OBL}(\bar{a}_n, \bar{\theta}_1)\, g_m \right. \\
\left. + \cdots + \sum_{m=1}^{N_{1,m}^{OBL}} f_{pq}^{OBL}(\bar{a}_1, \bar{\theta}_m)\, g_m + \cdots + \sum_{m=1}^{N_{n,m}^{OBL}} f_{pq}^{OBL}(\bar{a}_n, \bar{\theta}_m)\, g_m \right\} \\
+ \dot{E}_{p}^{i}(P) \left\{ \sum_{m=1}^{N_{1,1}^{ICE}} f_{pq}^{ICE}(\bar{a}_1, \bar{\theta}_1)\, g_m + \cdots + \sum_{m=1}^{N_{n,1}^{ICE}} f_{pq}^{ICE}(\bar{a}_n, \bar{\theta}_1)\, g_m \right. \\
\left. + \cdots + \sum_{m=1}^{N_{1,m}^{ICE}} f_{pq}^{ICE}(\bar{a}_1, \bar{\theta}_m)\, g_m + \cdots + \sum_{m=1}^{N_{n,m}^{ICE}} f_{pq}^{ICE}(\bar{a}_n, \bar{\theta}_m)\, g_m \right\} .
\end{aligned}
\tag{3.2-6}
$$

Note that the summation over the spherical drops is independent of canting angle. Although Eq. (3.2-6) is somewhat cumbersome, it illustrates the physical significance of the particular class of particles involved in the summation process. The assumption has been made that the canting angle of a given particle is independent of the equivolumetric particle radius. Brussaard [19] has shown that this is not strictly true. As the radius and the terminal velocity of the falling particle increases, wind gradients have more effect on the orientation of the particle. However, the assumption of independence is reasonably accurate and it also leads to a relatively simple model.

Since the scattering coefficients in Eq. (3.2-6) are constant within their respective summations, they can be taken out of the summation signs leaving the summation $\sum_{m}^{N_{i,k}} g_m$ in every term. This summation is easily evaluated (see Appendix 6.1.2) and the result is a constant given below:

$$\sum_{m=1}^{N_{i,k}} g_m = -j\lambda\Delta\ell \; n_{i,k} \quad . \tag{3.2-7}$$

The symbol $n_{i,k}$ is the number of particles per unit volume in the i^{th} size class and the k^{th} orientation class. Equation (3.2-6) now becomes:

$$\dot{E}_p^s(P) = -j\lambda\Delta\ell \; \dot{E}_p^i(P) \left\{ n_1^{SPH} f_{pq}^{SPH}(\bar{a}_1) + \cdots + n_n^{SPH} f_{pq}(\bar{a}_n) \right\}$$

$$+ \left\{ n_{1,1}^{OBL} f_{pq}^{OBL}(\bar{a}_1, \bar{\theta}_1) + \cdots \right.$$
$$\left. + \quad \vdots \quad \cdots \quad n_{n,m}^{OBL} f_{pq}^{OBL}(\bar{a}_n, \bar{\theta}_m) \right\}$$

$$+ \left\{ n_{1,1}^{ICE} f_{pq}^{ICE}(\bar{a}_1, \bar{\theta}_1) + \cdots \right.$$
$$\left. + \quad \vdots \quad \cdots \quad n_{n,m}^{ICE} f_{pq}^{ICE}(\bar{a}_n, \bar{\theta}_m) \right\} \quad . \quad (3.2\text{-}8)$$

Recognizing that the individual bracketed terms are double sums over the discretized particle size and particle orientation distributions, Eq. (3.2-8) can be further simplified. Let $N_V(\bar{a}_i, \bar{\theta}_k)$ be the total number of particles per unit volume with particle size $\bar{a}_i$ and particle orientation $\bar{\theta}_k$. Then Eq. (3.2-8) can be rewritten as follows:

$$\dot{E}_{pq}^{s}(P) = -j\lambda\Delta\ell \; \dot{E}_{p}^{i}(P) \sum_{i=1}^{M_i} \sum_{k=1}^{M_k} N_V(\bar{a}_i, \bar{\theta}_k) F_{pq}(\bar{a}_i, \bar{\theta}_k) \qquad (3.2\text{-}9)$$

where,

$$F_{pq}(\bar{a}_i, \bar{\theta}_k) = \{Pe_S \; f_{pq}^{SPH}(\bar{a}_i) + Pe_O \; f_{pq}^{OBL}(\bar{a}_i, \bar{\theta}_k) + Pe_I \; f_{pq}^{ICE}(\bar{a}_i, \bar{\theta}_k)\}$$

(3.2-10)

and, the symbols M_i and M_k represent the number of discrete intervals in the respective distribution functions.

Although the scattered field expression has been simplified to a great extent, it is convenient to define an effective scattering coef-

ficient for the entire slab, S_{pq}, such that

$$\dot{E}^{s}_{pq}(P) = S_{pq}\,\dot{E}^{i}_{p}(P) \quad . \tag{3.2-11}$$

From Eq. (3.2-9), the effective scattering coefficient S_{pq} is expressed by the relation

$$S_{pq} = -j\lambda\Delta\ell \sum_{i=1}^{M_i}\sum_{k=1}^{M_k} N_V(\bar{a}_i, \bar{\theta}_k)F_{pq}(\bar{a}_i, \bar{\theta}_k) \tag{3.2-12}$$

= the ratio of the forward scattered electric field with polarization q to the incident electric field with polarization p representing the scattering properties of a thin rain slab with arbitrary particle shapes, sizes, and orientations.

Using Eq. (3.1-1) in Eq. (3.2-12), the effective scattering coefficients relative to the arbitrary x-y axes can be formulated as

$$\begin{aligned}
S_{xx} &= -j\lambda\Delta\ell \sum_{i=1}^{M_i}\sum_{k=1}^{M_k} N_V(\bar{a}_i, \bar{\theta}_k)\{Pe_S\, f^{SPH} + \sin^2\bar{\theta}_k(Pe_0\, f_v^{OBL} + Pe_I\, f_v^{ICE}) \\
&\qquad + \cos^2\bar{\theta}_k(Pe_0\, f_h^{OBL} + Pe_I\, f_h^{ICE})\} \\
S_{xy} &= S_{yx} = -j\lambda\Delta\ell \sum_{i=1}^{M_i}\sum_{k=1}^{M_k} N_V(\bar{a}_i, \bar{\theta}_k)\{Pe_0(f_v - f_h)^{OBL} \\
&\qquad + Pe_I(f_v - f_h)^{ICE}\}\sin\bar{\theta}_k\cos\bar{\theta}_k \\
S_{yy} &= -j\lambda\Delta\ell \sum_{i=1}^{M_i}\sum_{k=1}^{M_k} N_V(\bar{a}_i, \bar{\theta}_k)\{Pe_S\, f^{SPH} + \cos^2\bar{\theta}_k(Pe_0\, f_v^{OBL} + Pe_I\, f_v^{ICE}) \\
&\qquad + \sin^2\bar{\theta}_k(Pe_0\, f_h^{OBL} + Pe_I\, f_h^{ICE})\}.
\end{aligned} \tag{3.2-13}$$

The cross polarization scattering coefficients S_{xy} and S_{yx} represent the scattering of energy from one polarization component into its orthogonal component. This effect is directly related to the differential phase and differential attenuation ($f_v - f_h$) properties of the oblate raindrop and the ice crystal. The spherical raindrop on the other hand does not contribute to the depolarization process and when Pe_0 and Pe_I are zero, $S_{xy} = S_{yx} = 0$, and the rain slab does not depolarize the incident field.

Using Eqs. (3.2-1) and (3.2-11), the total field at point P now can be expressed in terms of the effective scattering coefficients as follows:

$$\begin{aligned} \dot{E}_x(P) &= \dot{E}_x^i(P) + \dot{E}_x^i(P)\, S_{xx} + \dot{E}_y^i(P)\, S_{yx} \\ \dot{E}_y(P) &= \dot{E}_x^i(P)\, S_{xy} + \dot{E}_y^i(P) + \dot{E}_y^i(P)\, S_{yy} \quad . \end{aligned} \tag{3.2-14}$$

In matrix form, Eq. (3.2-14) becomes

$$\begin{bmatrix} \dot{E}_x(P) \\ \dot{E}_y(P) \end{bmatrix} = \begin{bmatrix} (1 + S_{xx}) & S_{yx} \\ S_{xy} & (1 + S_{yy}) \end{bmatrix} \begin{bmatrix} \dot{E}_x^i(P) \\ \dot{E}_y^i(P) \end{bmatrix} . \tag{3.2-15}$$

The scattering properties of a single homogeneous thin rain slab of arbitrary particles now have been presented. Also an effective scattering coefficient has been formulated that includes the effects of arbitrary particles, a particle size distribution, and a particle orientation distribution. So now with an understanding of the scattering properties of a thin rain slab, the effect of a homogeneous

rain on a communications link can be investigated.

3.3 Electromagnetic Scattering by a Homogeneous Rain

The purpose of the scattering model is to predict the physical changes that an incident electromagnetic wave with a given polarization undergoes when all or part of the propagation path is filled with rain. Now that the scattering properties of this path are understood on a microscopic level, the entire rain extent can be modeled by extending the work in the previous two sections. In this section the assumption will be made that the rain is homogeneous in the direction of propagation. However, this restriction will be relaxed in the next section when a model for a piecewise homogeneous rain is developed.

Consider a propagation path with a homogeneous rain of extent ℓ meters in the direction of propagation. In the previous section the total electric field was determined at point P for a single thin rain slab. Since the rain volume is homogeneous in the direction of propagation, the rain extent ℓ can be modeled by a series of M_s thin rain slabs. If the incremental length $\Delta\ell$ of the thin rain slab is assumed to be one meter ($\Delta\ell$ = 1 m), M_s is a large number equal to the homogeneous rain extent length ℓ.

As a result of the assumption of a homogeneous rain in the direction of propagation, the M_s slabs have identical scattering properties as described by Eq. (3.2-15). The effect of M_s rain slabs on the incident field can be represented by the multiplication of the M_s matrices as follows:

$$\begin{bmatrix} \dot{E}_x \\ \dot{E}_y \end{bmatrix} = \begin{bmatrix} (1 + S_{xx}) & S_{yx} \\ S_{xy} & (1 + S_{yy}) \end{bmatrix}^{M_s} \begin{bmatrix} \dot{E}_x^i \\ \dot{E}_y^i \end{bmatrix} \tag{3.3-1}$$

The scattering matrix $[S]^{M_s}$ in Eq. (3.3-1) represents the changes that the incident field experiences as it propagates through a homogeneous rain medium of thickness ℓ. However, raising a matrix to the M_s^{th} power where M_s can be a large number (from 1000 to 10000 depending on the length ℓ) is numerically awkward. This problem can be solved by the use of the Cayley-Hamilton theorem [20]. The Cayley-Hamilton theorem allows the 2 x 2 matrix of Eq. (3.3-1) to be expressed in terms of the identity matrix and two unique constants as follows:

$$[S]^{M_s} = \alpha_0[I] + \alpha_1[S] \tag{3.3-2}$$

where,

$$\alpha_0 = \{\lambda_1^{M_s} \lambda_2 - \lambda_1 \lambda_2^{M_s}\}/(\lambda_2 - \lambda_1)$$

$$\alpha_1 = \{\lambda_2^{M_s} - \lambda_1^{M_s}\}/(\lambda_2 - \lambda_1) \tag{3.3-3}$$

$$\lambda_{1,2} = \{1 + \frac{(S_{xx}+S_{yy})}{2}\} \pm \sqrt{\{1 + \frac{(S_{xx}+S_{yy})}{2}\}^2 + S_{xy}^2 - (1 + S_{xx})(1 + S_{yy})} \; .$$

Thus, the electric field exiting the rain medium now can be represented by

$$\begin{bmatrix} \dot{E}_x \\ \dot{E}_y \end{bmatrix} = \begin{bmatrix} \{\alpha_0 + \alpha_1(1 + S_{xx})\} & \alpha_1 S_{yx} \\ \alpha_1 S_{xy} & \{\alpha_0 + \alpha_1(1 + S_{yy})\} \end{bmatrix} \begin{bmatrix} \dot{E}^i_x \\ \dot{E}^i_y \end{bmatrix} . \qquad (3.3\text{-}4)$$

In this section the scattering properties of a homogeneous rain have been modeled to predict the effect of this rain on an arbitrary incident field. Equation (3.3-1) provides a physical insight into the scattering properties of the medium while Eq. (3.3-4) provides an efficient method for computing the electric field exiting a homogeneous rain.

3.4 Electromagnetic Scattering by a Piecewise Homogeneous Rain

The development of the scattering model as presented in Sec. 3.2 considered a homogeneous mixture of particles with varying sizes, shapes, and orientations in a thin slab of rain. In the previous section a homogeneous rain was modeled as a series of identical thin rain slabs. In order to permit more accurate modeling of a real rain, the homogeneous rain restriction is removed in this section.

By discretizing the rain extent on a large scale basis as shown in Fig. 3.4-1, a piecewise homogeneous rain can be modeled with M discrete rain *cells*. Each rain cell can have arbitrary length and arbitrary rain conditions. The rain cells also can have different distributions of particle shape, particle size, and particle orientation. The scattering properties of each rain cell can be represented by a scattering matrix $[S_i]$ where the effect of the i^{th} rain cell on

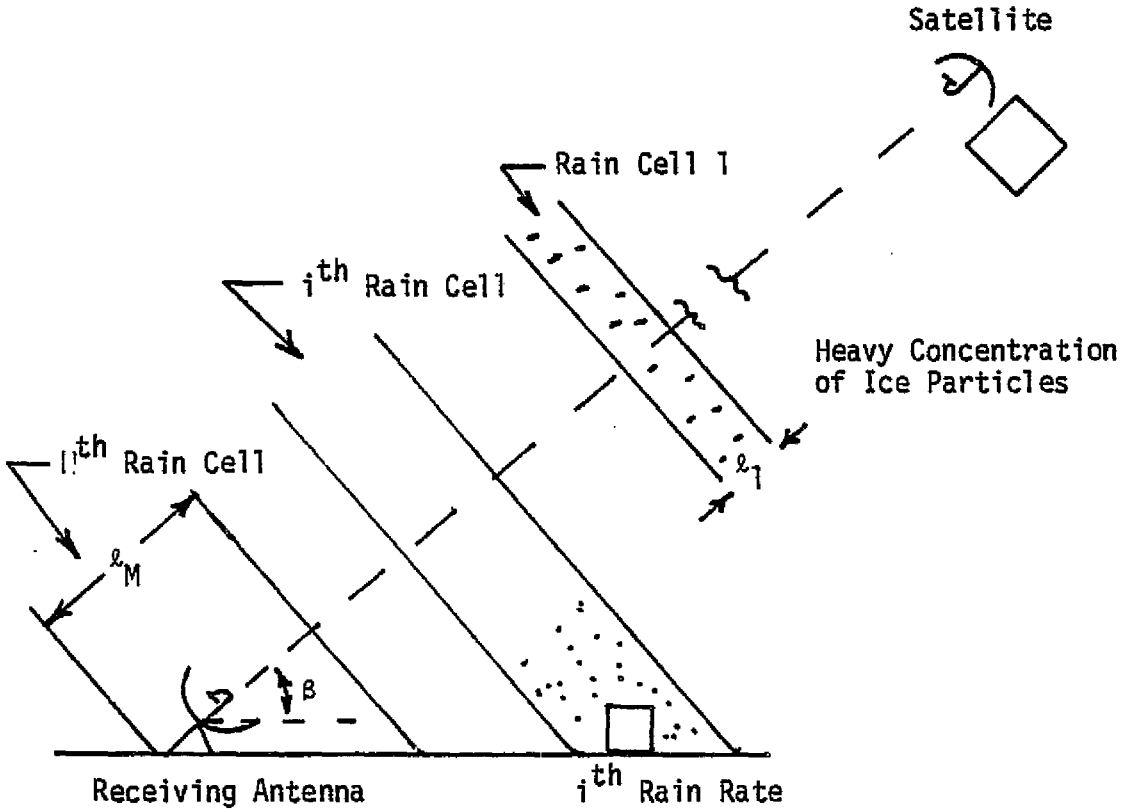

Figure 3.4-1. Rain cell division on a satellite communications link.

the electric field is determined by Eq. (3.3-4). The resulting fields after passing through the piecewise homogeneous rain then can be expressed by the multiplication of the rain cell matrices as follows:

$$\begin{bmatrix} \dot{E}_x \\ \\ \dot{E}_y \end{bmatrix} = [S_M]\,[S_{M-1}] \cdots [S_2]\,[S_1] \begin{bmatrix} \dot{E}_x^i \\ \\ \dot{E}_y^i \end{bmatrix} . \qquad (3.4\text{-}1)$$

Equation (3.4-1) is a very powerful tool in predicting the effects of an inhomogeneous rain on a millimeter wave communications link. However, data describing the true physical nature of a given rain extent are not readily available for most locations. To use this equation to its fullest extent, Sec. 3.6 presents a synthetic storm algorithm that can predict statistically rain effects for a variety of locations. Another use of this large scale discrete model is to allow only the first cell to contain ice particles. This is a physically meaningful situation because ice crystals usually exist only at the higher elevations of a storm. Physical situations of this nature are handled rather well by the above formulation and the generalized format of the scattering model has been achieved.

3.5 A Discussion of Rain Reciprocity

Now that a general model has been developed to predict the effects of an inhomogeneous rain on millimeter waves, the effects of nonreciprocity should be considered. Nonreciprocity as related to rain and millimeter wave propagation has received very little attention in the

literature; however, under certain rain conditions it may have important consequences on millimeter wave communications links. To describe the effects of an inhomogeneous rain on millimeter waves, the medium is modeled by the product of M homogeneous rain cell matrices. This section will show that an inhomogeneous rain may be nonreciprocal and then the order of matrix multiplication in Eq. (3.4-1) is important.

The reciprocity theorem [21] for electromagnetic fields states that the response of a medium to a source (transmitter) is unchanged when source and measurer (receiver) are interchanged. Consider two arbitrary homogeneous rain cells that are placed adjacent to one another to form an inhomogeneous rain cell as shown in Fig. 3.5-1. The measured electric field after passing through the piecewise homogeneous rain medium can be expressed in matrix form as follows:

$$\begin{bmatrix} \dot{E}_x \\ \dot{E}_y \end{bmatrix} = [S_2]\,[S_1] \begin{bmatrix} \dot{E}^i_x \\ \dot{E}^i_y \end{bmatrix} = \begin{bmatrix} A_2 & B_2 \\ B_2 & C_2 \end{bmatrix} \begin{bmatrix} A_1 & B_1 \\ B_1 & C_1 \end{bmatrix} \begin{bmatrix} \dot{E}^i_x \\ \dot{E}^i_y \end{bmatrix}$$

$$= \begin{bmatrix} A_2 & B_2 \\ B_2 & (A_2 + \varepsilon_2) \end{bmatrix} \begin{bmatrix} A_1 & B_1 \\ B_1 & (A_1 + \varepsilon_1) \end{bmatrix} \begin{bmatrix} \dot{E}^i_x \\ \dot{E}^i_y \end{bmatrix} . \qquad (3.5\text{-}1)$$

The symbols A_i, B_i, C_i, and ε_i represent the entries for the i^{th} rain cell matrix as defined by Eq. (3.3-1). For reciprocity as defined above to be satisfied, the matrices $[S_1]$ and $[S_2]$ must be cummutative. Using matrix algebra it can be shown that the two matrices are commuta-

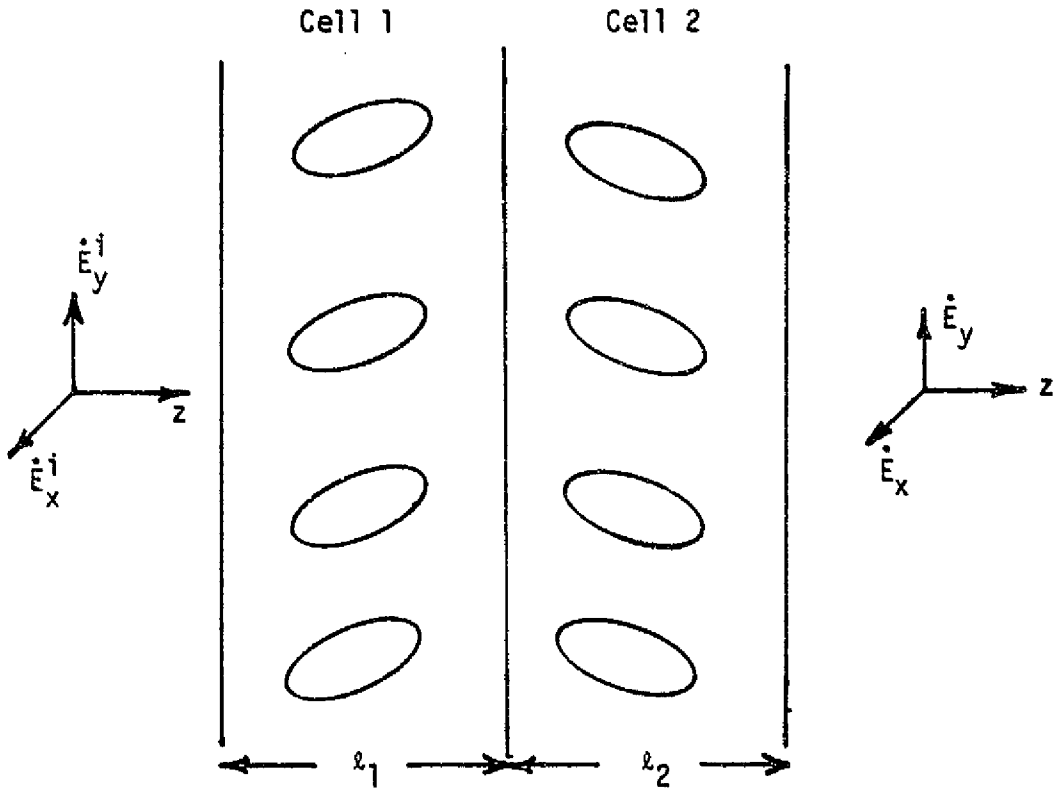

Figure 3.5-1. An inhomogeneous rain, two cells of dissimilar canting angles.

tive and the medium reciprocal if and only if

$$\Delta = \varepsilon_1 B_2 - \varepsilon_2 B_1 = 0 \ . \tag{3.5-2}$$

So that a more direct understanding of the nonreciprocal phenomenon can be achieved, a simplifying assumption will be made. Assume that all the particles within the respective rain cells are equioriented oblate spheroidal raindrops with equal drop size (the distributions are represented by unit impulse functions). With this assumption, the matrix formulation of Eq. (3.3-1) is equivalent to the classical propagation constant model formulation [22]. The matrix entries A_i, B_i, and C_i as defined by Uzunoglu, Evans, and Holt [5] are given below:

$$\begin{aligned} A_i &= d_{h_i} \cos^2 \theta_i + d_{v_i} \sin^2 \theta_i \\ B_i &= \gamma_i \sin \theta_i \cos \theta_i \\ C_i &= d_{h_i} \sin^2 \theta_i + d_{v_i} \cos^2 \theta_i \end{aligned} \tag{3.5-3}$$

where

$$\begin{aligned} \gamma_i &= d_{v_i} - d_{h_i} \\ d_{v_i} &= e^{-j\lambda \ell_i N_i f_{v_i}} \\ d_{h_i} &= e^{-j\lambda \ell_i N_i f_{h_i}} \ . \end{aligned} \tag{3.5-4}$$

Using Eq. (3.5-3) and the definition of ε_i as defined by Eq. (3.5-1),

$$\varepsilon_i = C_i - A_i = (d_{v_i} - d_{h_i})\{\cos^2 \theta_i - \sin^2 \theta_i\}$$
$$= \gamma_i \cos^2 2\theta_i \quad . \tag{3.5-5}$$

Now, Eq. (3.5-2) can be rewritten as

$$\Delta = \frac{\gamma_2\gamma_1}{2} \sin 2(\theta_2 - \theta_1) \tag{3.5-6}$$

where θ_2 and θ_1 represent the canting angles of the raindrops in the appropriate cells. The inhomogeneous rain medium of Fig. 3.5-1 is reciprocal only when $\Delta = 0$ or when

$$(\theta_2 - \theta_1) = \frac{n\pi}{2} \quad , \qquad n = 0,1,2,3 \ldots \quad . \tag{3.5-7}$$

Note that the conditions under which reciprocity fails are independent of the length and the rain rate of the two cells, but only depend on the difference of the respective canting angles.

By definition the classical propagation constant model requires that all drops in a giver thin, finite slab be equioriented. As a result, Eq. (3.5-7) indicates that the propagation constant model cannot deterministically model an arbitrary canting angle distribution without mathematically violating reciprocity. For this reason the *scattering model* accounts for the canting angle distribution within the finite slab with the use of the generalized single particle scattering coefficients discussed in Sec. 3.1.

Now the impact of nonreciprocity on communications link performance will be investigated. Although the assumptions of the classical propagation constant model lead to an exaggerated physical interpreta-

tion of the nonreciprocal phenomena, simple equations which explain the trends of nonreciprocity can be formulated. As a simple example consider the piecewise homogeneous medium of Fig. 3.5-1 with the incident field being vertically polarized ($\dot{E}_x^i = 0$). The exiting fields are found from Eqs. (3.5-1) and (3.5-3) with Case 1 having the incident field $\dot{E}_y^i$ incident on Cell 1 and Case 2 having $\dot{E}_y^i$ incident on Cell 2. The fields for the two cases are given below:

Case 1

$$\dot{E}_x^{(1,2)} = \{A_1B_2 + B_1A_2 + \varepsilon_1B_2\}\dot{E}_y^i$$

$$\dot{E}_y^{(1,2)} = \{B_1B_2 + (A_1 + \varepsilon_1)(A_2 + \varepsilon_2)\}\dot{E}_y^i$$

Case 2 (3.5-8)

$$\dot{E}_x^{(2,1)} = \{A_1B_2 + B_1A_2 + \varepsilon_2B_1\}\dot{E}_y^i$$

$$\dot{E}_y^{(2,1)} = \{B_1B_2 + (A_1 + \varepsilon_1)(A_2 + \varepsilon_2)\}\dot{E}_y^i \quad .$$

Clearly if ε_1B_2 equals ε_2B_1 ($\Delta = 0$), the fields of Case 1 equal the fields of Case 2 and the medium is reciprocal.

Define ΔA to be the difference in attenuation of the incident field for the two cases. The general expression for ΔA with any incident polarization is

$$\Delta A = 20 \log_{10} \frac{|\vec{E}^{(1,2)} \cdot E^{i*}|}{|\vec{E}^{(2,1)} \cdot E^{i*}|} \text{ dB} \quad . \tag{3.5-9}$$

For a vertically polarized incident field, ΔA is

$$\Delta A = 20 \log_{10} \left| \frac{\dot{E}_y(1,2)}{\dot{E}_y(2,1)} \right| = 0 \quad . \tag{3.5-10}$$

Independent of the rain conditions in either cell, attenuation is reciprocal. One can show, using Eq. (3.5-9), that attenuation is reciprocal for any arbitrary linear or circularly polarized incident field. Although it has not been proven for the general case of elliptical polarization, the same result is expected. Since attenuation should depend only on the volume of water present along the propagation path, the above conclusion seems reasonable.

Now define ΔI to be the difference in channel isolation on a dual polarized communications system for the two cases of Fig. 3.5-1. The general expression for any arbitrary incident polarization is

$$\Delta I = 20 \log_{10} \left| \frac{\vec{\dot{E}}(1,2) \cdot \vec{\dot{E}}'^*}{\vec{\dot{E}}(2,1) \cdot \vec{\dot{E}}'^*} \right| \text{ dB} \tag{3.5-11}$$

where $\vec{\dot{E}}'$ represents the polarization state orthogonal to the incident field. For a vertically polarized incident field $\vec{\dot{E}}' = \dot{E}_x \hat{x}$ and Eq. (3.5-11) reduces to

$$\Delta I = 20 \log_{10} \left| \frac{\dot{E}_x(1,2)}{\dot{E}_x(2,1)} \right| \text{ dB} \quad . \tag{3.5-12}$$

Using Eq. (3.5-8) in Eq. (3.5-12) yields

$$\Delta I = 20 \log_{10} \left| 1 + \frac{\Delta}{\{B_1 A_2 + A_1 B_2 + \varepsilon_2 B_1\}} \right| \text{ dB} \quad . \tag{3.5-13}$$

Examination of Eq. (3.5-13) yields only two conditions under which reciprocity holds for isolation:

1) $\Delta = 0$

2) $\dfrac{\Delta}{\{B_1A_2 + A_1B_2 + \varepsilon_2B_1\}} = -2$.

The first case is when the entire medium is reciprocal. The second is a special case and will be investigated shortly.

In general isolation is nonreciprocal. This is to be expected because it is the difference in the respective canting angles that makes the rain medium nonreciprocal. The magnitude of nonreciprocity depends on the difference of canting angles, input polarization, and other path rain conditions. The interdependence of the rain parameters {rain rate, rain extent, etc.} and their effect on the magnitude of ΔI will be presented through two special cases using the classical propagation constant model formulation. From these examples it will be evident that the magnitude of ΔI increases with frequency for a given input polarization and path rain conditions.

For the first special case allow the medium of Fig. 3.5-2 to have arbitrary rain rates in either cell. Allow the cells to have any length ℓ_1 and ℓ_2. The canting angle θ_2 is also arbitrary; however, let θ_1 equal zero. Under these conditions and using Eqs. (3.5-3) and (3.5-4) in Eq. (3.5-13) yield

$$\Delta I = 20 \log_{10} \left| e^{(\lambda \ell_1 N_1) \cdot \mathrm{Im}\{f_{v_1} - f_{h_1}\}} \right| \text{ dB} \qquad (3.5\text{-}14)$$

where

$$\theta_1 = 0$$

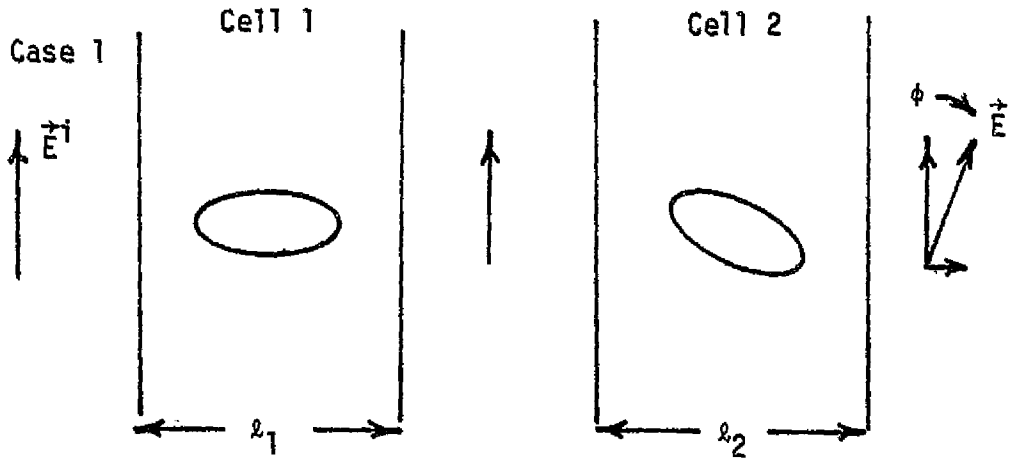

Figure 3.5-2a. Forward propagation.

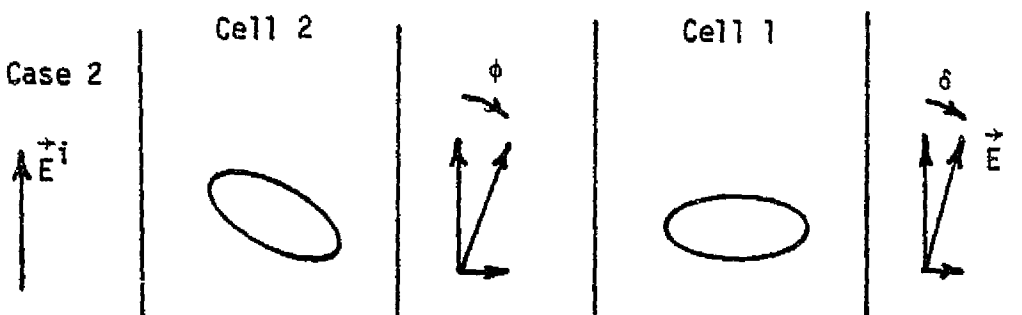

Figure 3.5-2b. Reverse propagation.

Figure 3.5-2. An example of nonreciprocity.

$$\theta_2 \neq n\pi/2 , \qquad n = 0,1,2,3 \ldots$$

$$RR_2 \neq 0$$

$$\ell_2 \neq 0 .$$

As long as θ_2 is not zero or ninety degrees (or a multiple thereof), the magnitude of nonreciprocity is independent of the rain conditions in the second cell. At first this result may seem surprising; however, it is explained easily with a physical example. Figure 3.5-2a illustrates Case 1. The incident field is not depolarized by Cell 1 and the drops of Cell 2 are oriented in such a manner that the field exiting Cell 2 is depolarized or rotated by ϕ degrees. Case 2 is illustrated in Fig. 3.5-2b. In this case the incident field is depolarized or rotated by ϕ degrees. The field incident upon Cell 1 is now oriented such that it will be depolarized. The depolarization by Cell 2 is the same in both cases since the input polarization is the same. However, the depolarizing properties of cell one are different for the two cases. Thus, the difference in isolation for the two cases depends only on the rain conditions of Cell 1. Equation (3.5-14) is plotted in Fig. 3.5-3 for three different frequencies as a function of rain rate.

The propagation constant model formulation predicts serious nonreciprocal crosstalk effects on a given communications link using frequency reuse techniques. Although it provides simple equations to predict the effects of various rain parameters of rain reciprocity,

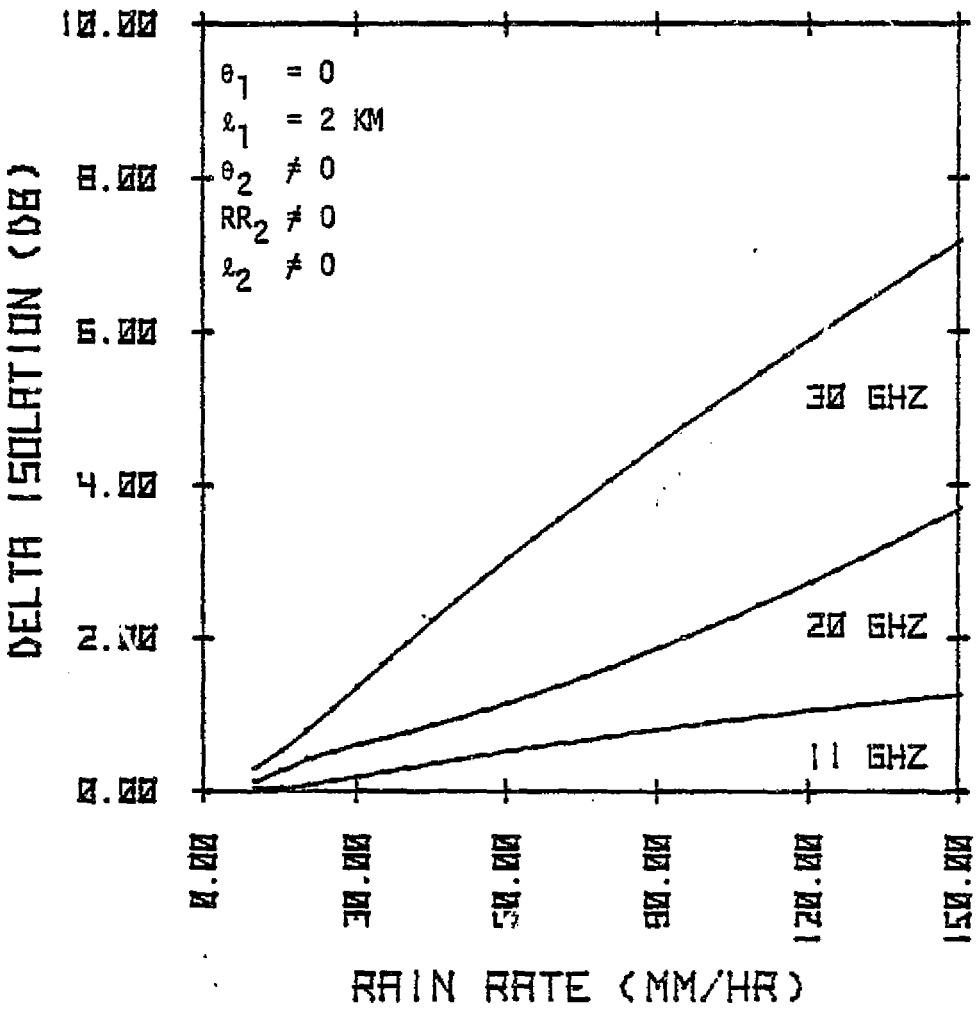

Figure 3.5-3. Theoretical predictions of the classical propagation constant model of the difference in isolation experienced on an uplink and a downlink of a millimeter wave satellite communications link.

the magnitude of the predicted results are exaggerated. The *scattering model* represents the rain in a more physically significant manner. With the inclusion of the spherical scatterer and the orientation and drop size distributions, the magnitude of ΔI is significantly decreased. Even for an operating frequency of 30 GHz, the scattering model indicates that ΔI is less than 0.5 dB. (The propagation constant model can also represent a drop size distribution.)

The second special case will illustrate the effect that the difference in the respective canting angles $(\theta_2 - \theta_1)$ has on the magnitude of ΔI. For this example, the rain rates and path lengths of both rain cells are equal, but the canting angles are allowed to be arbitrary. Under these assumptions γ_1 equals γ_2 and Eq. (3.5-13) reduces to

$$\Delta I = 20 \log_{10} \left| \frac{1 + g \tan \theta_1 \cot \theta_2}{g + \tan \theta_1 \cot \theta_2} \right| \qquad (3.5\text{-}15)$$

where

$$g = e^{-j\lambda N \ell (f_v - f_h)}$$

for both cells. Note for the special case of $\theta_2 = \pi - \theta_1$, ΔI equals zero. For any arbitrary linearly polarized incident field there is a certain special case of canting angle orientation that makes the medium reciprocal for isolation. This effect for vertical polarization is illustrated in Fig. 3.5-4. For a fixed value of θ_1, the isolation for each case and ΔI are plotted as a function of θ_2. Note that whenever $(\theta_2 - \theta_1) = n\pi/2$ where $n = 0,1,2 \ldots$, ΔI is zero. Again, the magnitude

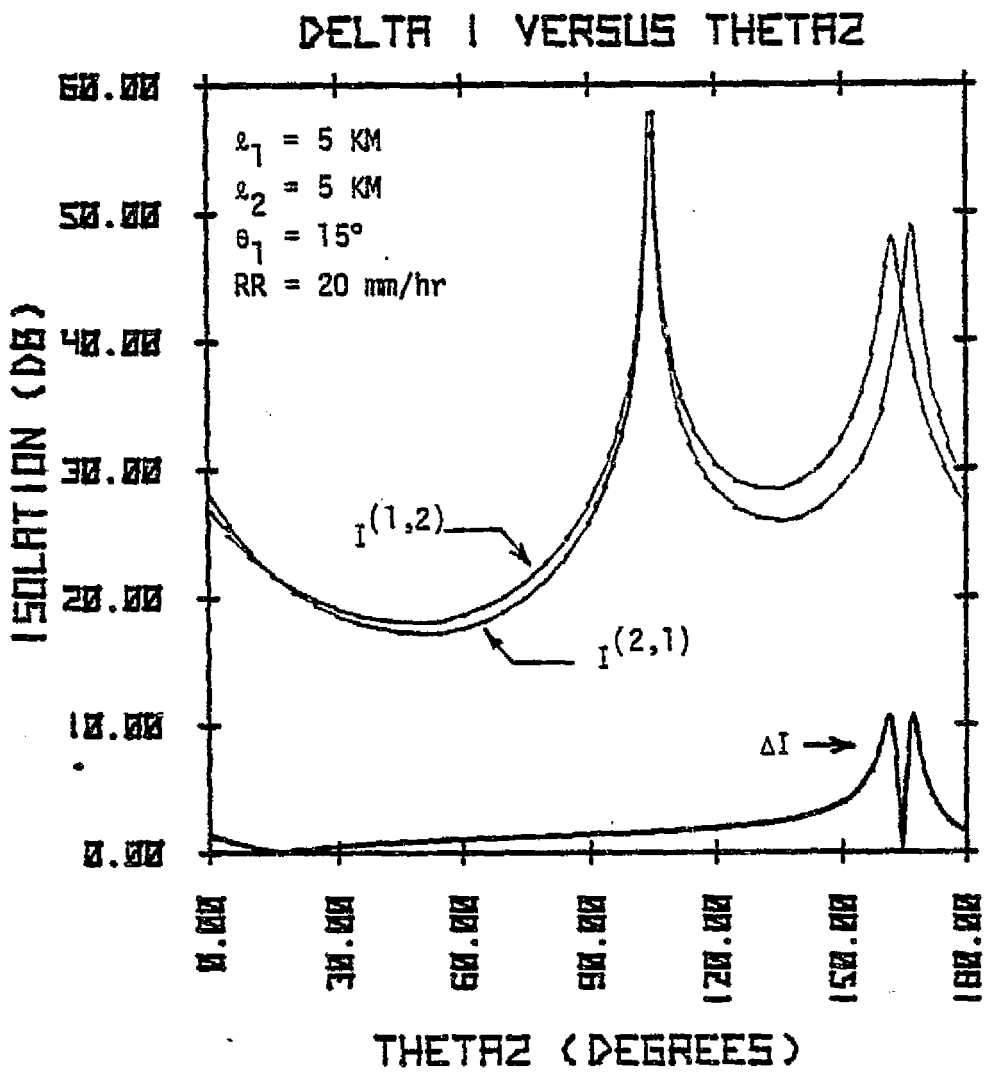

Figure 3.5-4. An example of the effect of canting angle on isolation nonreciprocity. (Classical propagation constant model, f = 30 GHz)

of ΔI is exaggerated. However, the peaks in ΔI for the special values of θ_2 suggest that certain physical conditions may exist that could affect the operation of an adaptive isolation correction system on a given satellite communications link.

The purpose of this section was to show that nonreciprocal conditions may exist on an uplink and a downlink of a given satellite communications system. The interdependence of the parameters attributing to the nonreciprocal phenomena have been investigated with the use of simple examples. In general the scattering model does not seem to predict any significant nonreciprocal effects for typical rain situations in the 10 to 30 GHz frequency band. Thus, the prediction of isolation nonreciprocity is exaggerated by models that do not include a canting angle or particle shape distribution. However, there still may be certain physical conditions that could have important consequences on millimeter wave communications links. Further investigation into the problem of rain reciprocity is necessary.

3.6 Model Implementation

Now that the scattering model has been presented formally and a word of caution has been noted about recip ocity, the practical implementation of the scattering model will be presented. The final goal of the scattering model is to predict signal attenuation, isolation, and phase shift for a variety of frequencies and site locations as a function of measured rain rate data. Before this goal can be achieved, a detailed analysis of particle shape, particle size, particle density,

and particle orientation as related to ground rain rate must be formulated. These topics will be discussed in this section. Also, the relationship of the single particle scattering coefficients to elevation angle β will be presented. The effect of non-ideal antennas on the predicted results will be investigated. Finally, this section presents a *Rain Propagation Prediction program (RPP)* that includes a *synthetic storm algorithm* that can predict the effects of rain on millimeter wave communications links for a range of frequencies, elevation angles, and locations.

It has been shown that spherical raindrops, oblate spheroidal raindrops, and ice crystals may be used to model an arbitrary rain path. In the practical application of the tools developed in Sec. 3.4, the assumption will be made that a given cell consists entirely of ice crystals or entirely of raindrops. The first cell will usually be modeled by ice crystals and the remaining cells will be modeled using an *effective* percentage of oblate spheroidal and spherical raindrops. The distributions associated with the rain cell and ice cell will be presented separately; however, the assumption is made that both particle density distributions are a function of ground rain rate. It should be noted that the scattering model can include a mixture of rain and ice in a given rain cell, but presently data are not available to describe accurately this physical distribution of particles. The scattering model also will allow varying distributions along the propagation path. However, based on existing physical data, each *rain* cell is assumed to have the same drop shape distribution, drop size distri-

bution, and drop orientation distribution. The drop density distribution is arbitrary for a given cell and is a function of rain rate.

3.6.1 Raindrop Shape Distribution

First consider the distribution of drop shapes. Jones [12] has found that the following distribution of shapes occur in an average rain for all radii greater than 0.9 mm:

Spherical	32%
Oblate Spheroidal	28%
Prolate Spheroidal	18.5%
Irregular	21.5%

Since the scattering model is limited by the availability of single particle scattering coefficients, the above distribution will be modeled by an effective percentage of oblate and spherical raindrops. About one-half of the prolate drops would be expected to be aligned with their elliptical cross section facing the incident field and therefore produce depolarization. On a satellite link, the elevation angles are such that a fraction of the remaining prolate drops would also depolarize the incident field. The prolate drop class may be modeled by assuming the class is made up of 70% oblate drops and 30% spherical drops. A large fraction of the irregular drop class would also depolarize the incident field. If the irregular drop class is modeled by 90% oblate drops and 10% spherical drops, the total *effective* percentage of oblate drops is approximately 60%. Based on

the above arguments and good correlation with measured data (see Sec. 4.2) a rain cell is assumed to have 60% oblate spheroidal raindrops and 40% spherical raindrops. This distribution is assumed not to be a function of rain rate.

3.6.2 Raindrop Size Distribution

For a given rain rate there will be a distribution of drop sizes. There are several drop size distributions published in the literature [8], [23], [24], [25]. A modification of the Laws and Parsons distribution will be used. The Laws and Parsons distribution as published is somewhat inconvenient in that it has no explicit functional form. However, real rains tend to deviate from any of the published distributions and an approximate functional representation of the Laws and Parsons distribution can be developed with little additional effect on the results. A simple approximation is that of a triangle. In Fig. 3.6-1, the Laws and Parsons distribution for a few rain rates is shown together with the triangular approximation where

$$s(\bar{a}) = \begin{cases} \dfrac{\bar{a}}{a_m^2} & a \le a_m \\ \dfrac{2}{a_m}\left(1 - \dfrac{\bar{a}}{2a_m}\right) & a_m \le \bar{a} \le 2a_m \\ 0 & \text{elsewhere} \end{cases} \qquad (3.6\text{-}1)$$

= fraction of drops in radius interval $\bar{a}$ to $\bar{a} + d\bar{a}$.

The symbol a_m represents the modal or most frequently occurring drop

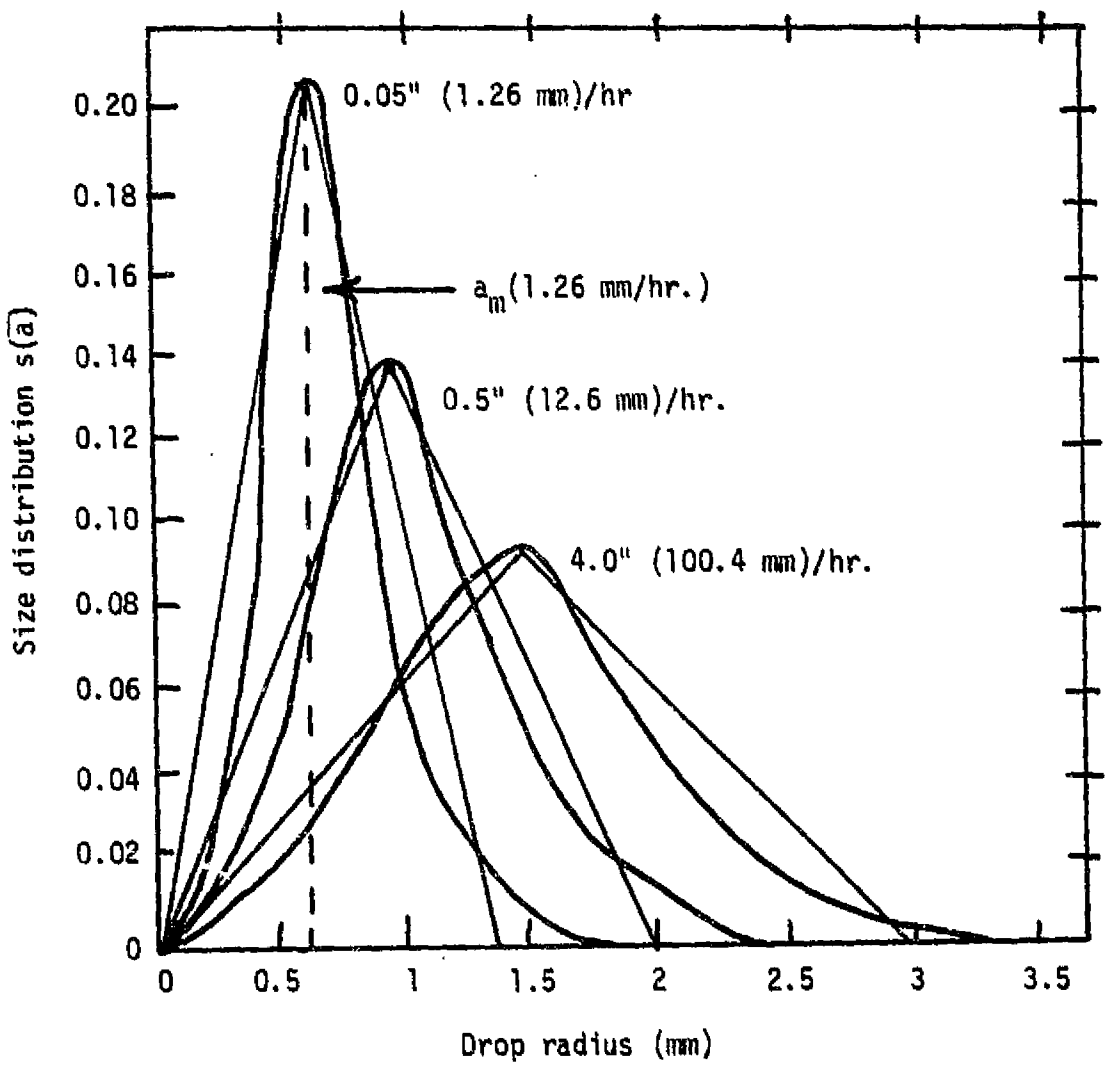

Figure 3.6-1. Triangular approximation to the Laws and Parsons size distribution.

radius and $\bar{a}$ is the equivolumetric drop radius. Both radii are in millimeters. The modal drop radius is a function of rain rate and is expressed by the relation [11]

$$a_m = 0.5 + 0.45 \log_{10} RR \qquad (3.6\text{-}2)$$

where RR is rain rate in mm/hr. The distribution of drop sizes can be represented by the relation

$$n(\bar{a}) = N_V \, s(\bar{a}) \qquad (3.6\text{-}3)$$

= number of drops per m^3 of space in the class $\bar{a}$ to $\bar{a} + d\bar{a}$.

The symbol N_V represents the particle density or the total number of drops per cubic meter of space. It can be shown (see Appendix 6.1.3) that N_V is a function of the modal drop size and thus is a function of rain rate,

$$N_V = 5.833 \, RR \, a_m^{-7/2} \quad . \qquad (3.6\text{-}4)$$

The calculation of the effective scattering coefficients (Eq. 3.2-13) include summations over the single drop scattering coefficients weighted by the number of drops in the appropriate finite drop size interval. Single drop scattering coefficients are available typically at 0.25 mm drop radius increments up to 3.25 mm or 3.50 mm, depending on the frequency. By using curve fitting routines, the scattering coefficients can be determined at any point over the interval 0.25 to 3.50 mm. This permits the selection of any convenient drop size

interval. In general define

M_i = number of drop size intervals over the range of drop sizes encountered

$\bar{a}_i$ = the equivolumetric drop radius value in mm at the midpoint of the i^{th} drop size interval

$\Delta\bar{a}$ = drop radius interval in mm .

Choose $M_i = 28$ intervals. This provides a very fine division and the corresponding drop radius interval is $\Delta\bar{a} = 0.125$ mm. The midpoints of these intervals are

$$\bar{a}_i = 0.0625 + 0.125(i - 1) \qquad 1 < i \leq 28 \ . \tag{3.6-5}$$

The number of drops per unit volume of space in the i^{th} drop size interval is

$$N_V(\bar{a}_i) = \int_{\bar{a}_i - \frac{\Delta\bar{a}}{2}}^{\bar{a}_i + \frac{\Delta\bar{a}}{2}} n(a)\, da \ . \tag{3.6-6}$$

Using Eqs. (3.6-1) and (3.6-3) in Eq. (3.6-6) yield

$$N_V(\bar{a}_i) = \begin{cases} N_V \dfrac{\Delta\bar{a}}{a_m^2}\, a_i & 0.25 \leq \bar{a} \leq a_m \\ N_V \dfrac{2\Delta\bar{a}}{a_m}\left(1 - \dfrac{a_m}{2}\, a_i\right) & a_m \leq \bar{a}_i \leq 2a_m \\ 0 & \bar{a}_i > 2a_m \ . \end{cases} \tag{3.6-7}$$

A rough estimate of usable rain rates for this drop size distri-

bution can be formulated. For a_m less than 0.4 mm the lack of small drop size contributions would become significant. From Eq. (3.6-2) this modal drop radius corresponds to a rain rate of 0.60 mm/hr. For high rain rates the large drop contributions become more important. Drop radii out to $2a_m$ are included in the triangular distribution. Since scattering coefficients are not complete beyond $\bar{a}$ = 3.25 mm, a_m = 3.25/2 = 1.625 mm. From Eq. (3.6-2) this corresponds to a rain rate of 316 mm/hr. Thus, the above drop size distribution is reliable for rain rates between 1 mm/hr and 300 mm/hr.

3.6.3 Raindrop Orientation Distribution

The drop orientation distribution is very important to the prediction of cross-polarization. Although Brussaard [19] has shown that wind gradients affect the orientation of falling raindrops, little is known about the nature of the distribution itself. The work of Saunders [26] indicates that the distribution is Gaussian; however, researchers disagree on the range of the mean and the standard deviation. Most have assumed an *effective* drop orientation and modeled the distribution with a unit impulse function. Although the unit impulse assumption leads to simple formulations, it does not adequately describe the true physical situation. Uzunoglu, Evans, and Holt [5], using the distribution of Saunders, employ a stochastic method of *averaging* the effects of a canting angle distribution; however, this is not internal to the model and does not consider the effects of arbitrary orientation in the rain cell. Further experimental investiga-

tion into the problem of canting angle distributions is needed; however, until this is accomplished some sort of assumption must be formulated. Experimental measurements of cross-polarization at three frequencies over approximately the same propagation path (see Sec. 4.2) indicate that there is good correlation between theory and measurement with a Gaussian distribution whose mean ranges from -10° to 10° and with a standard deviation of 12°.

The drop orientation distribution *within* a finite slab can be discretized in the same manner as the drop size distribution. Define

M_k = number of drop orientation intervals over the canting angles encountered

$\bar{\theta}_k$ = the canting angle in radians at the midpoint of the k^{th} orientation interval

$\Delta\bar{\theta}$ = canting angle interval in radians

$\bar{\theta}_\mu$ = mean canting angle in radians

σ = standard deviation in radians .

Saunders indicates that canting angles ranging from -100° to 100° can be found in an average rain. Over this range choose M_k to be 20 intervals. Thus, $\Delta\bar{\theta}$ is $\pi/18$ or 10 degrees. The midpoints of these intervals are given by the following equation:

$$\bar{\theta}_k = -1.6581 + 0.1745\ k \quad \text{radians} \quad (1 \leq k \leq 20) \ . \qquad (3.6\text{-}8)$$

The number of drops per unit volume of space in the k^{th} orientation interval is

$$N_V(\bar{\theta}_k) = \frac{N_V}{\sigma\sqrt{2\pi}} \int_{\theta_1}^{\theta_2} e^{-\{\frac{(\theta - \bar{\theta}_\mu)^2}{2\sigma^2}\}} d\theta \qquad (3.6\text{-}9)$$

where

$$\theta_1 = \{\bar{\theta}_k - \frac{\Delta\bar{\theta}}{2}\}$$

$$\theta_2 = \{\bar{\theta}_k + \frac{\Delta\bar{\theta}}{2}\} \quad .$$

To evaluate the effective scattering coefficients of Eq. (3.2-13), the joint distribution of drop size and drop orientation must be known. Since the assumption has been made that the drop orientation is independent of drop size, the joint distribution is simply the product of the two distributions.

$$N_V(\bar{a}_i, \bar{\theta}_k) = N_V(\bar{a}_i)\ N_V(\bar{\theta}_k) \ . \qquad (3.6\text{-}10)$$

3.6.4 Single Particle Scattering Coefficients and Elevation Angle

It was indicated in Sec. 3.1 that the single particle scattering coefficients are a function of particle size, frequency and elevation angle. Coefficients are available for many frequencies and sizes; however, the selection of coefficients over the spectrum of elevation angles is limited. Uzunoglu, Evans, and Holt [5] have shown that a simple trigonometric relation can be used to evaluate the scattering coefficients for any arbitrary elevation angle. The relation is given below:

$$f_v(\beta) = f^{SPH} \sin^2 \beta + f_v(0°) \cos^2 \beta$$

$$f_h(\beta) = f^{SPH} \sin^2 \beta + f_h(0°) \cos^2 \beta \qquad (3.6\text{-}11)$$

$$f_v(\beta) - f_h(\beta) = \{f_v(0°) - f_h(0°)\} \cos^2 \beta$$

where $f_{v,h}(0°)$ is the scattering coefficient evaluated for an elevation angle of zero degrees. This approximation is accurate to within 1% for elevation angles ranging from 0° to 90° and provides a simple formulation to evaluate scattering coefficients for a range of elevation angles.

3.6.5 Ice Crystal Distribution

Ice effects on satellite communications links have drawn considerable attention since experimenters recently have observed cross-polarization without a significant fade in the co-polarized signal [27], [28], [29]. This so-called "anomalous" depolarization is attributed to a collection of ice crystals at high altitudes. Although the effect is not as severe, ice crystals also affect the isolation of a given communications system when followed by a series of rain cells.

Haworth, McEwan, and Watson [30] have shown that the scattering coefficients for ice particles can be derived using Rayleigh scattering for frequencies up to 30 GHz. The derivation depends on the assumption that the particle eccentricity is very close to one. This physically models the ice particles as ice plates (oblate spheroidal) and ice needles (prolate spheroidal) as shown in Fig. 3.6-2 (see Appendix

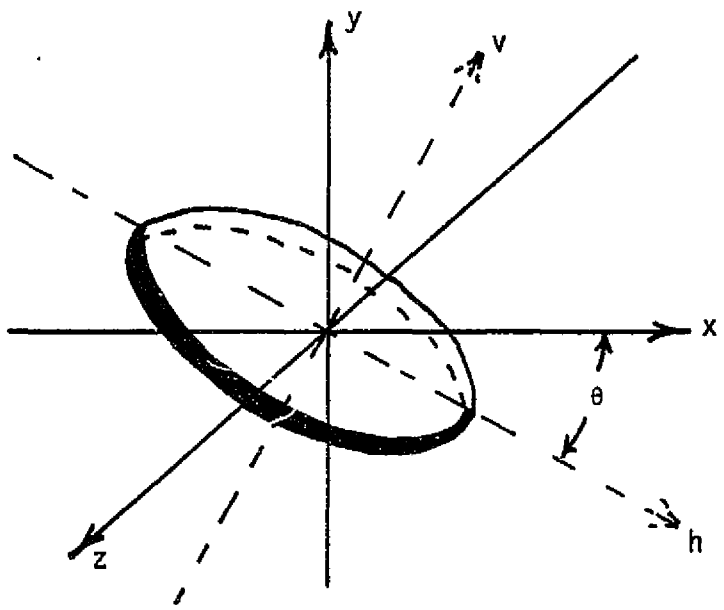

Ice Plate

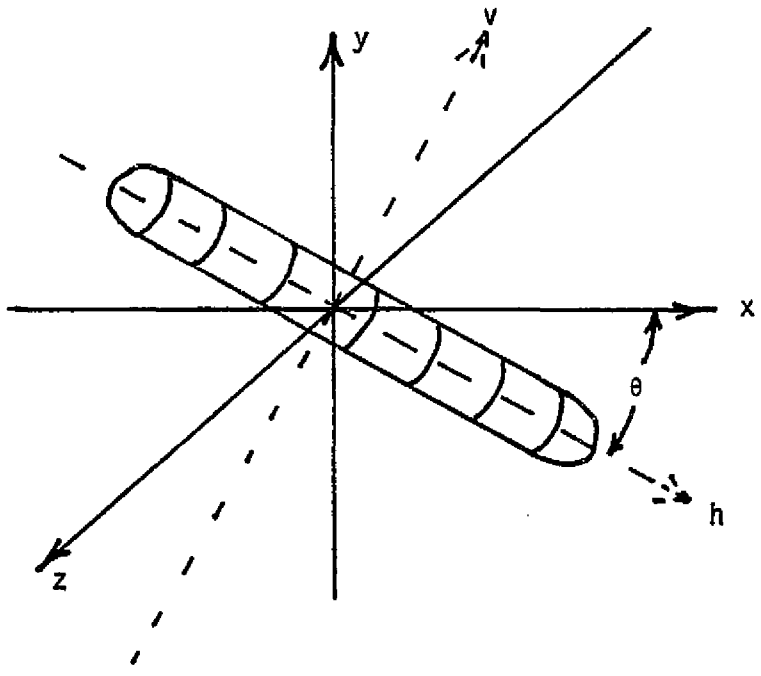

Ice Needle

Figure 3.6-2. Ice particle shapes.

6.1.4). One disadvantage of this formulation is that it does not lend itself to a distribution of particle orientation. The assumption is made that all particles are equioriented at an effective canting angle. It has been observed by radar that lightning [31] and wind shear [32] align the particles in a given orientation. Since the ice cell is relatively thin, the assumption of an effective canting angle is not necessarily restrictive. The Haworth - McEwan - Watson formulation does include a particle size distribution.

Using the Haworth - McEwan - Watson formulation in Eq. (3.2-13) along with the elevation angle formulation previously mentioned, the effective scattering coefficients of a thin finite slab of ice particles are given below:

$$S_{xx} = -j \frac{V}{2\lambda} \Delta\ell \{\sin^2\theta(A_v^{PRO} + A_v^{OBL'}) + \cos^2\theta(A_h^{PRO} + A_h^{OBL'})\}$$

$$S_{xy} = S_{yx} = -j \frac{V}{2\lambda} \Delta\ell \{(A_v^{PRO} + A_v^{OBL'}) - (A_h + A_h^{OBL'})\} \sin\theta \cos\theta$$

$$S_{yy} = -j \frac{V}{2\lambda} \Delta\ell \{\cos^2\theta(A_v^{PRO} + A_v^{OBL'}) + \sin^2\theta(A_h^{PRO} + A_h^{OBL'})\} \quad (3.6\text{-}12)$$

where

$$A_v^{OBL'} = \sin^2\beta\, A^{SPH} + \cos^2\beta\, A_v^{OBL}$$

$$A_h^{OBL'} = \sin^2\beta\, A^{SPH} + \cos^2\beta\, A_h^{OBL} \quad (3.6\text{-}13)$$

and A_v^{PRO}, A_v^{OBL}, A_h^{PRO}, A_h^{OBL} and A^{SPH} are complex constants independent of frequency and are given in Table 3.6-1 (see Appendix 6.1-4). Note that the scattering coefficients describing the prolate particle are independent of the elevation angle β. The symbol V represents the

Table 3.6-1. Ice scattering coefficients.

$A_h^{PRO} = \{6.812211 - j\ 0.026842\}$
$A_v^{PRO} = \{3.268519 - j\ 0.006179\}$
$A_h^{OBL} = \{6.812211 - j\ 0.026842\}$
$A_v^{OBL} = \{2.150047 - j\ 0.002674\}$
$A^{SPH} = \{3.95417 - j\ 0.009044\}$

total volume of ice in a cubic meter of air. In Eq. (3.6-12) the assumption has been made that the ice slab has 50% ice needles and 50% ice plates.

Haworth, McEwan, and Watson [30] use a value of $V = 10^{-6}$ in their predictions of anomalous depolarization. However, when a ice cell is followed by a series of rain cells, the volume of ice should have some dependence on ground rainfall. *The hypothesis is made that the volume of ice per cubic meter of air in the freezing layer of a storm is equal to the volume of rain per cubic meter of air near the ground.* The total volume of ice in a cubic meter of air is then a function of rain rate and is expressed by the relation

$$V = (24.43 \times 10^{-9}) \frac{RR}{\sqrt{a_m}} \quad . \tag{3.6-14}$$

One should note that there still can be ice particles present without ground rainfall thus producing anomalous depolarization.

3.6.6 Antenna Effects

The development of the scattering model thus far has not included the interaction of the wave exiting the rain medium with the receive antenna. Even in clear weather conditions, a polarization mismatch is observed with non-ideal antennas. This polarization mismatch is modeled easily and for low rain rates has significant effects in the prediction of attenuation, isolation, and phase shift.

The co-polarized (main) and the cross-polarized (orthogonal) antenna polarization states can be described by a complex vector repre-

sentation. The symbol $\hat{e}_a$ represents the respective antenna state and is defined below:

$$\dot{e}_a = \dot{e}_x \hat{x} + \dot{e}_y \hat{y} \tag{3.6-15}$$

where for the co-polarized state

$$\begin{aligned} \dot{e}_x^{co} &= \cos\{\gamma_{co}\} \\ \dot{e}_y^{co} &= \sin\{\gamma_{co}\} e^{j\,\delta_{co}} \end{aligned} \tag{3.6-16}$$

and for the cross-polarized state

$$\begin{aligned} \dot{e}_x^{cross} &= \cos\{\gamma_{cross}\} \\ \dot{e}_y^{cross} &= \sin\{\gamma_{cross}\} e^{j\,\delta_{cross}} \quad . \end{aligned}$$

The symbols γ and δ define the polarization ellipses of the respective antenna states as shown in Fig. 3.6-3.

The wave-antenna interaction can be modeled by the use of a phasor voltage. Define a phasor voltage V(w, a) which describes the interaction of a wave polarization state w and an antenna polarization state as

$$V(w, a) = \vec{E}_w \cdot \hat{e}_a^* \quad . \tag{3.6-17}$$

The wave state exiting the rain medium is found from Eq. (3.4-1) and the antenna states from Eq. (3.6-15).

To evaluate attenuation, isolation, and phase referenced to the antenna ports, the clear weather wave state must be known. The attenu-

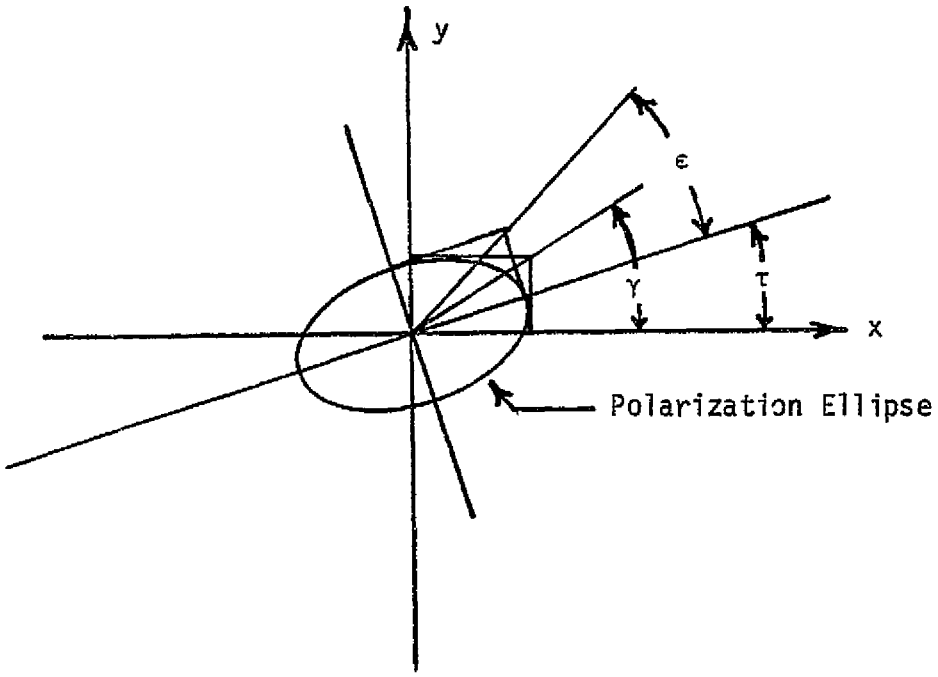

$$\delta = \tan^{-1}\left\{\frac{\tan 2\varepsilon}{\sin 2\tau}\right\}$$

$$\gamma = \frac{1}{2}\cos^{-1}\{\cos 2\varepsilon \cos 2\tau\}$$

$$\varepsilon = \cot^{-1}\{\text{axial ratio}\}$$

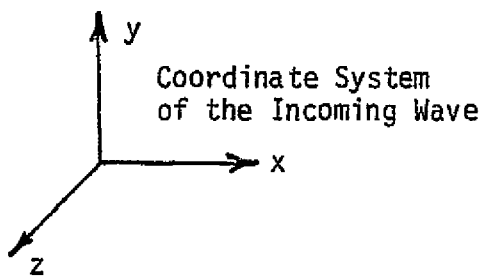

Direction of Propagation

Figure 3.6-3. Polarization ellipse.

ation of the co-polarized component is

$$A = 20 \log_{10} \left| \frac{V(w, a_{co})}{V(w', a_{co})} \right| = 20 \log_{10} \frac{|\vec{E}_w \cdot \hat{e}_a^{co*}|}{|\vec{E}_w' \cdot \hat{e}^{co*}|} \text{ dB} \qquad (3.6\text{-}18)$$

where $\vec{E}_w$ is the clear weather wave and $\vec{E}_w'$ is the wave exiting the rain medium. The isolation between the two receive channels is

$$I = 20 \log_{10} \left| \frac{V(w', a_{co})}{V(w', a_{cross})} \right| = 20 \log_{10} \frac{|\vec{E}_w' \cdot \hat{e}_a^{co*}|}{|\vec{E}_w' \cdot \hat{e}^{cross*}|} \text{ dB} \quad . \quad (3.6\text{-}19)$$

Also of interest is the phase difference between the phasor voltages of the two receive polarization states co and cross. Define

$$\begin{aligned} \Phi &= \text{Cross Phase - Co Phase} \\ &= \angle\{\vec{E}_w' \cdot \hat{e}^{cross*}\} - \angle\{\vec{E}_w' \cdot \hat{e}^{co*}\} \text{ radians} \quad . \end{aligned} \qquad (3.6\text{-}20)$$

The terms attenuation, isolation, and phase appear frequently in the remaining sections of this text and unless otherwise specified, the definitions of Eqs. (3.6-18), (3.6-19), and (3.6-20) will be assumed.

3.6.7 A Synthetic Storm Algorithm

Rain is not usually uniform over the extent of a storm and for increasing rain rates rain cells of higher rain rate tend to decrease in size. However, most researchers assume uniform rains and account for this phenomenon with an effective rain extent referred to in the literature as effective path length. As rain rate increases, effective path length decreases. The effective path length formulation is based

on experimental measurements and theoretical predictions for uniform rain conditions. The intention is to formulate an effective path length based on statistical data that can be used for a variety of locations to predict rain effects on millimeter wave propagation. There is one major disadvantage to this approach: effective path lengths are frequency dependent. Thus, experimental data is required for all frequencies of interest and this is overly restrictive. The frequency dependence of effective path length is investigated in this section and a *frequency independent synthetic storm algorithm* that models nonuniform rain rates is presented.

The actual or measured attenuation on a given propagation path with physical rain extent L can be expressed as

$$A_m = \int_0^L A_1\{RR(\ell),\ f\}\, d\ell \qquad (3.6\text{-}21)$$

where $A_1\{RR(\ell),\ f\}$ is attenuation per meter and is a function of rain rate and frequency. Note that rain rate is also a function of length ℓ. Effective path length in km is defined as

$$L_e(RR_{AVG},\ f) = \frac{A_m}{A_{AVG}(RR_{AVG},\ f)} \qquad (3.6\text{-}22)$$

where $A_{AVG}(RR_{AVG},\ f)$ is a theoretically predicted attenuation per kilometer assuming a uniform *average* rain rate. The average rain rate is based on rain rate measurements taken over a long period of time. The measured attenuation is also indirectly a function of average rain rate. Measured attenuation and measured rain rate data are compared on an equal probability of occurrence basis over a long time base (see

Sec. 4.1). This removes the instantaneous time dependence of the measurements. Note that if rain rate is not a function of length ℓ, $A_m = A_{AVG}(RR_{AVG}, f)\, L$, and the effective path length would equal the physical rain extent L.

To investigate the frequency dependence of effective path length, consider the ratio of two effective path lengths for two frequencies f_1 and f_2:

$$\frac{L_e(RR_{AVG}, f_1)}{L_e(RR_{AVG}, f_2)} = \frac{A_{AVG}(RR_{AVG}, f_2)}{A_{AVG}(RR_{AVG}, f_1)} \frac{\int_0^{\bar{L}} A_1\{RR(\ell), f_1\}d\ell}{\int_0^{\bar{L}} A_1\{RR(\ell), f_2\}d\ell} \qquad (3.6\text{-}22)$$

$$= R_p R_m \ .$$

Ratio R_m is the ratio of measured attenuation for the two frequencies. Ratio R_p is a theoretical prediction of the ratio of attenuation assuming uniform rain conditions. For effective path length to be independent of frequency, R_p must equal R_m inverse. The effective path lengths for two frequencies (19.04 GHz and 28.56 GHz) are plotted as a function of statistical (average) rain rate in Fig. 3.6-4. Effective path length data for these curves were calculated from three months (July, August and September, 1977) measured attenuation and rain rate data. The data were collected at the VPI&SU earth station using the COMSTAR D2 satellite. It is obvious from Fig. 3.6-4 that effective path length is frequency dependent. Other researchers have also observed this frequency dependence [33]. This indicates that for higher rain rates a theoretical model should not assume uniform rain conditions, but model the nonuniform rain with a synthetic storm

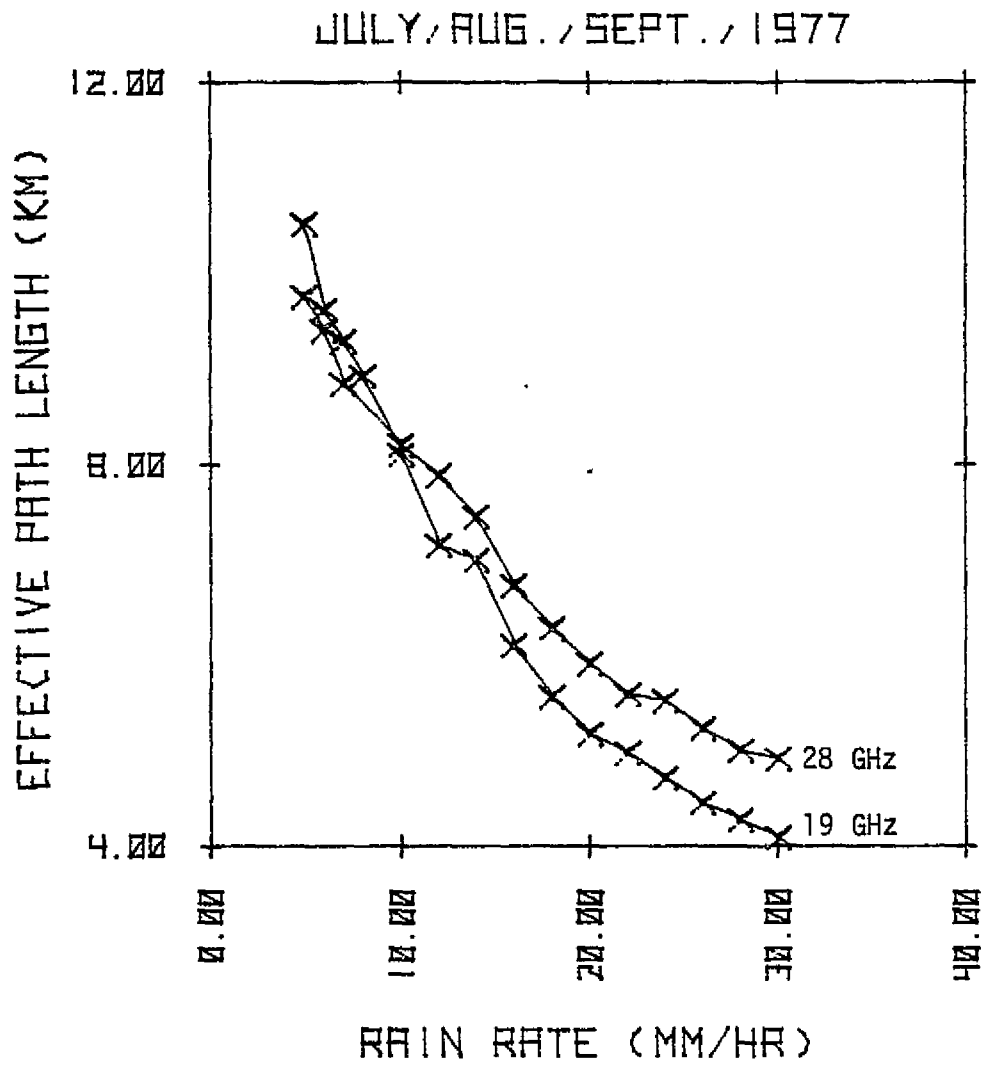

Figure 3.6-4. Effective path lengths for the VPI&SU COMSTAR 19 and 28 systems based on measured data collected during the months of July, August, and September, 1977.

algorithm.

The scattering model, because of its ability to represent a piecewise homogeneous rain, can accomodate easily a synthetic storm algorithm. The storm algorithm will model rain rate as a function of position along the path and storm extent as a function of elevation angle. Based on the data of Fig. 3.6-4, two physical assumptions will be made:

1) the rain is uniform for low rain rates
2) as rain rate increases, the rain becomes nonuniform.

The first step in the development of a synthetic storm algorithm is to obtain a functional relationship between effective storm extent and elevation angle. Define effective storm height as

$$H_e = L_e(10 \text{ mm/hr}) \sin \beta \qquad (3.6\text{-}23)$$

where L_e is the effective path length calculated for a *rain rate of 10 mm/hr*, and β is the elevation angle. Since for low rain rates the rain is nearly uniform, effective path length at 10 mm/hr is frequency independent ($R_p = R_m^{-1}$) and equal to the physical rain extent L. As a result, Eq. (3.6-23) can be rewritten as

$$H_e = L \sin \beta \quad \text{km} \qquad (3.6\text{-}24)$$

or the physical rain extent is

$$L = H_e / \sin \beta \quad \text{km} \quad (\beta \neq 0) \ . \qquad (3.6\text{-}25)$$

Note that effective storm height approaches zero as elevation angle approaches zero. The effective storm height formulation provides a limit to the storm extent both in height and ground extent. Using the data of various experimenters [17], [34], [35] at various locations, elevation angles, and frequencies, the functional relationship between elevation angle and effective storm extent can be obtained. Valid statistical attenuation data are very limited over the spectrum of frequencies and elevation angles; however, enough data are available to provide a *first order approximation* for an effective storm model. The available data at a rain rate of 10 mm/hr are used to calculate effective storm heights and these are tabulated in Table 3.6-2. Using the data of Table 3.6-2, an effective storm model is presented in Fig. 3.6-5. From this figure given an elevation angle, the physical rain extent L can be calculated where L is not a function of rain rate.

To model the nonuniform rain rate along the physical rain extent, assume that the maximum rain rate occurs in the rain cell closest to the receive antenna or cell M of Fig. 3.4-1. This is a valid assumption over long periods of time since it has been shown that statistical rain rate is independent of the measurement location [35]. The rain rates of all other rain cells will be a function of the M^{th} cell. This functional relationship is the storm algorithm.

To obtain the functional relationship, another comparison to measured attenuation data is necessary. However, for this comparison only data for a *single* frequency and a *single* location are needed. Figure 3.6-6 is a plot of measured attenuation data at 28.56 GHz as a

Table 3.6-2. Effective storm heights obtained from measured attenuation and rain rate statistics from various locations.

Data Point	β	f	H_e	Location
1)	54°	30 GHz	5.4 km	University of Texas
2)	44°	28 GHz	5.7 km	VPI&SU
3)	44°	19 GHz	5.6 km	VPI&SU
4)	23°	28 GHz	4.4 km	Comsat Labs
5)	23°	19 GHz	4.4 km	Comsat Labs

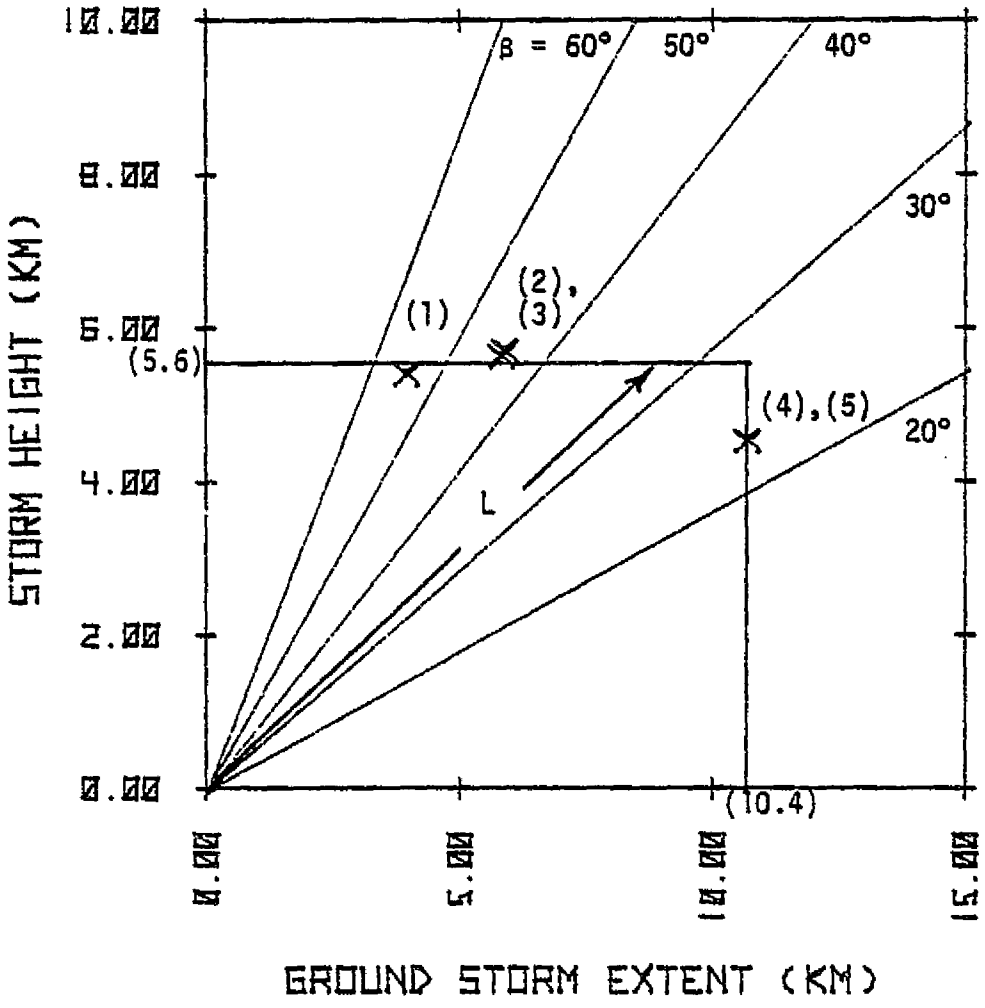

Figure 3.6-5. Effective storm model based on data from Table 3.6-2. (Rain extent versus elevation angle.)

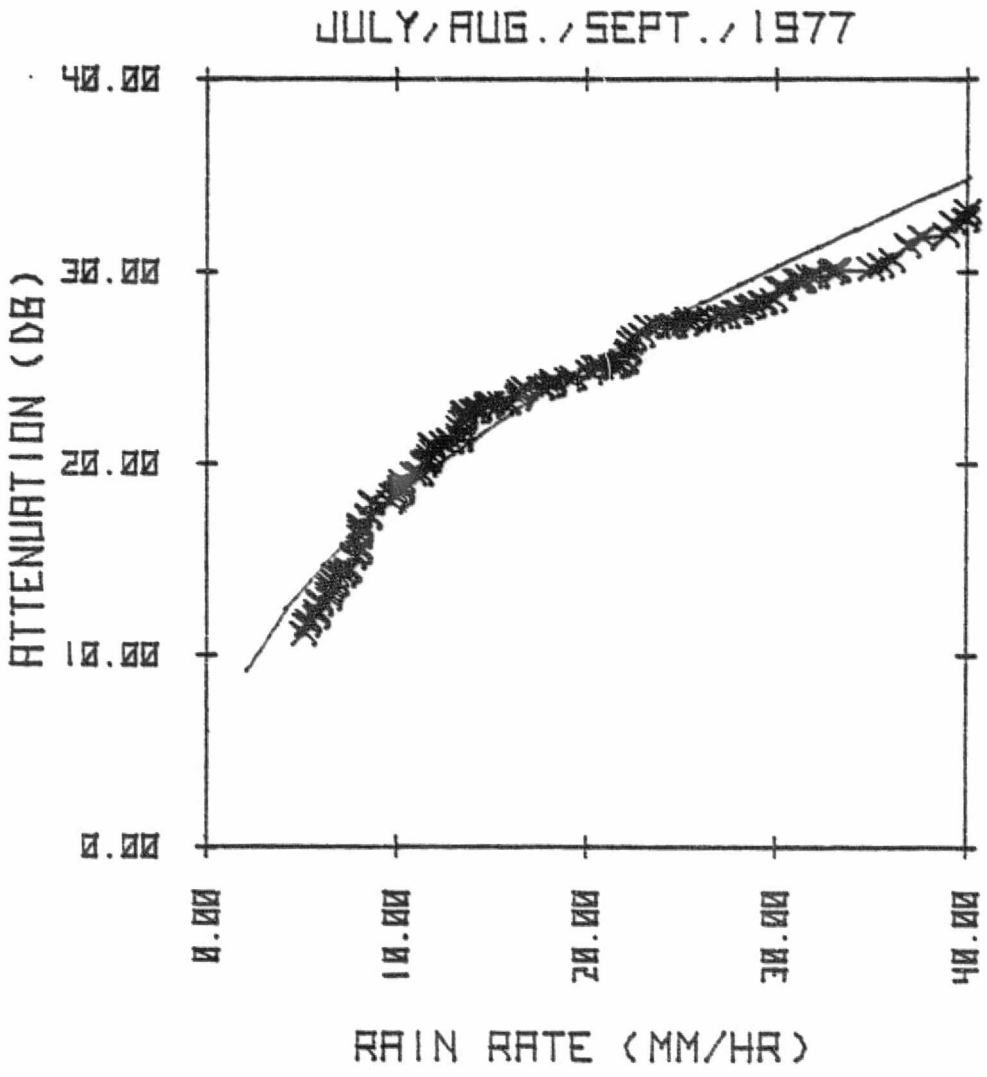

Figure 3.6-6. Measured 28 GHz attenuation compared to the theoretical prediction of the scattering model using the synthetic storm algorithm. (28.56 GHz)

function of statistical rain rate. The data were taken over a three month period (July, August and September, 1977) at the VPI&SU earth station. To remove the instantaneous time dependence, the curve is plotted using equal probability techniques. For an elevation angle of 44°, using Fig. 3.6-2 along with Eq. (3.6-25) the rain extent L is 8.2 km.

Assume that the rain extent can be modeled by ten rain cells as shown in Fig. 3.6-7. The rain rate of cells nine and ten equals the statistical rain rate of Fig. 3.6-6. Rain cells one through eight are equal and are related to cell ten by the following relation:

$$RR_i = \{\frac{RR_{10}}{10}\}^{x_i} RR_{10} \text{ mm/hr} \quad . \tag{3.6-26}$$

This relation models the nonuniform rain rate over the rain extent. The value of x_i can be obatined by trial and error until the attenuation corresponding to a rain rate of 40 mm/hr is predicted by the scattering model. The value of $x_{9,10}$ by definition is zero. The value of $x_{1\to8}$ is found to be

$$x_{1\to8} = -.66 \quad . \tag{3.6-27}$$

Although the value of $x_{1\to8}$ was obtained from one set of attenuation data, it models the nonuniformity of a rain medium as rain rate increases and is completely general for a variety of frequencies, elevation angles, and locations.

The theoretical prediction for 28 GHz attenuation over the entire spectrum of rain rate is shown in Fig. 3.6-6. Other comparisons to

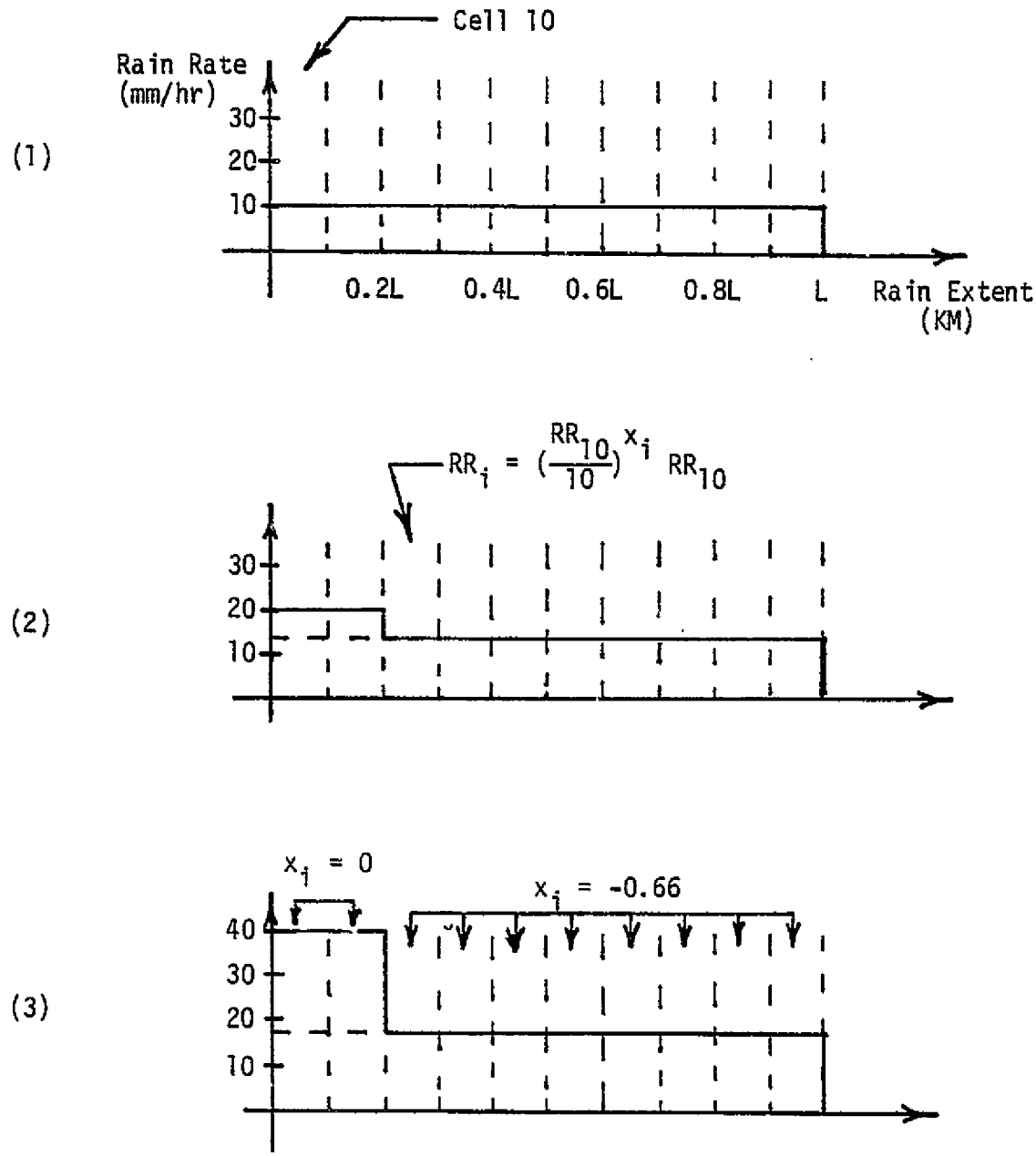

Figure 3.6-7. Synthetic storm algorithm, rain rate versus physical rain extent.

measured data using the above formulation are presented in Chapter IV. Given an elevation angle, the synthetic storm algorithm models non-uniform rain rates and effective storm extent and reliably predicts rain effects on communications links regardless of site location.

3.6.8 Rain Propagation Prediction Program

The Rain Propagation Prediction program (RPP) uses the scattering model and the synthetic storm algorithm of the previous section to predict attenuation, isolation, and phase as a function of rain rate. The input format allows changes in system parameters so that the effects of rain on millimeter wave propagation as a function of frequency, location and elevation angle can be predicted. The program is written in FORTRAN and its operational format is explained in Appendix 6.2. The program listing is found in Appendix 6.2.3. The RPP program is computationally efficient and it accurately predicts measured experimental data.

CHAPTER IV

EXPERIMENTAL VERIFICATION

In this chapter the theoretical predictions of the scattering model are compared to measured data obtained from three different site locations: (1) VPI&SU, Blacksburg, Virginia; (2) Comsat Labs, Clarksburg, Maryland; and (3) University of Texas, Austin, Texas. The data obtained from these sites cover the existing frequency range of interest for millimeter wave communications links (11 to 30 GHz) and provide a good comparison of theoretical predictions to measured data for a variety of system parameters. Before the data comparison is made a system description of the VPI&SU experiment is presented with an emphasis on general data reduction techniques. Then measured attenuation, isolation, and phase data for three frequencies (11.7 GHz, 19.04 GHz, and 28.56 GHz) collected by the VPI&SU experiment are compared with theory. The scattering model predictions are then compared to attenuation data measured by Comsat Labs and the University of Texas to demonstrate the flexibility of the synthetic storm algorithm. The chapter concludes with an investigation of frequency scaling techniques and the frequency dependence of attenuation and isolation.

4.1 The VPI&SU Experiment

4.1.1 General System Description

The Virginia Polytechnic Institute and State University (VPI&SU) millimeter wave propagation experiment is sponsored by NASA with

important additive support from the Defense Communications Agency and the U.S. Army Research Office. The experiment monitors continuous transmissions from the Communications Technology Satellite (CTS) at 11.7 GHz and the COMSTAR D2 satellite at 19.04 GHz and 28.56 GHz. The VPI&SU experiment is designed to measure attenuation, isolation, and phase shift and correlate these quantities with rain rate and other weather data. The experiment has been described in considerable detail in previous publications [36], [37], [17] and will be reviewed here only briefly with an emphasis on data reduction techniques.

A block diagram of the VPI&SU system is presented in Fig. 4.1-1. The experiment is controlled by a PDP-11/10 mini computer which monitors the experiment through a digital controller and analog to digital converter interface. The three different frequency systems are monitored simultaneously and the PDP 11/10 stores receiver data along with weather and time reference data on a storage disk for later transfer to an IBM/370 for data reduction. The CTS (11.7 GHz) satellite transmits a right hand circularly polarized wave and the CTS ground antenna receives both the co-polarized and cross-polarized signals. The COMSTAR receive antennas are both dual-linearly polarized. The COMSTAR satellite transmits vertical polarization at 28.56 GHz; however, the COMSTAR 19.04 GHz beacon switches between vertical and horizontal polarization at a 1 KHz rate. This feature was incorporated into the propagation experiment to provide information on the differential attenuation and differential phase properties of the rain medium. As a result of this switching polarization, there are four

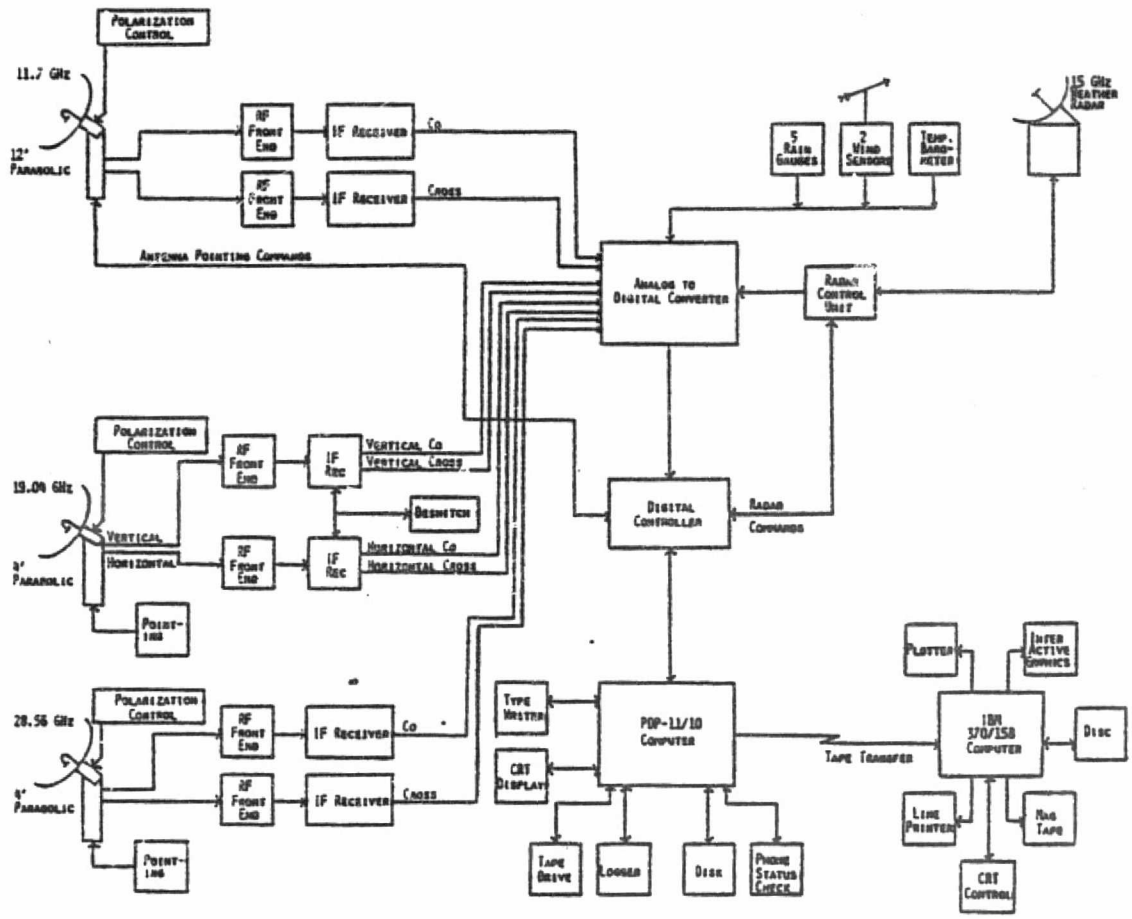

Figure 4.1-1. VPI&SU system block diagram.

receive channels (Vertical Co, Vertical Cross, Horizontal Co, and Horizontal Cross) for the 19 GHz system. The 19 GHz IF signal processor has a deswitching control unit that provides a switching signal to monitor the various polarization states. The 28 GHz system is also a dual-polarized system and monitors the co-polarized and cross-polarized signals. From these eight channels, attenuation, isolation, and phase data are recorded for the different frequencies and polarizations. The dynamic range of each system and other system parameters are tabulated in Table 4.1-1. The polarization parameters describing the polarization ellipses of the incoming waves and antenna states are tabulated in Table 4.1-2.

4.1.2 Preliminary Data Processing

As indicated in the previous section, on-line data acquisition is controlled by the PDP 11/10 mini computer. Each data channel has an identifying number that is used throughout the data reduction process. The PDP 11/10 also monitors various status indicators that indicate the validity of the data and whether it should be stored on the PDP 11/10 storage disk. Data are stored only when the status indicators indicate valid data and when the specific data input has changed by a predetermined amount. Data are stored with a time flag and other identifiers for later off-line processing.

During periods of low experimental activity, accumulated experimental data can be transferred to the main IBM 370 computer for subsequent data reduction. Before each data transfer all data are

Table 4.1-1. VPI&SU system parameters.

System Parameter	CTS (11.7 GHz)	COMSTAR (19.04 GHz)	COMSTAR (28.56 GHz)
Antenna			
Reflector size:	12'	4'	4'
Gain:	50.9 dBi	44.7 dBi	44.7 dBi
Polarization:	RHCP, LHCP	LV, LH	LV, LH
Look angle			
Azimuth:	240°	213°	213°
Elevation:	33°	44°	44°
RF Front Ends			
Co {Gain/Noise Temp}:	41.5 dB/962° K	34.8 dB/1540° K	37.5 dB/1716° K
Cross {Gain/Noise Temp}:	79 dB/184° K	32.8 dB/1450° K	34.5 dB/1716° K
IF Signal Processors			
Dynamic Range {Co/Cross}	39 dB/39 dB	30 dB/30 dB	39 dB/39 dB
Clear Weather Input Power: {Co/Cross}	-78 dBm/-75 dBm	-90 dBm/-125 dBm	-86 dBm/-121 dBm
Clear Weather Isolation:	37 dB	35 dB	35 dB

Table 4.1-2. VPI&SU polarization parameters.

Polarization Parameters	CTS (11.7 GHz)	COMSTAR (19.04 GHz)	COMSTAR (19.04 GHz)	COMSTAR (28.56 GHz)
Co-Polarized Wave				
ε:	-44.34°	0.82°	0.82°	1.02°
τ:	0°	52.5°	142.5°	52.5°
Co-Polarized Antenna				
ε:	-43.68	0°	0°	0°
τ:	0°	52.5°	142.5°	52.5°
Cross-Polarized Antenna				
ε:	43.68	0°	0°	0°
τ:	90°	142.5°	52.5°	142.5°

Note: See Fig. 3.6-3 for definition of ε and τ.

checked for time sequence and any required calibration is performed at this time. The data are transferred from the PDP-11/10 storage disk to magnetic tape and then read by the IBM 370 onto a system data base tape. The data base tape is a *complete time history* record of the VPI&SU experiment. A data exception tape is stored also in the IBM 370. This tape records time markers of any system failure that cannot be determined by the status indicators such as a complete power failure and any other special cases in which erroneous data may have been stored. For a particular data reduction time interval, these two tapes are merged to form a process file. This process file can be accessed through an IBM time sharing system that allows efficient data reduction over the specified time interval. An inter-active graphics system is also available to aid the data reduction process.

4.1.3 Data Reduction

The data reduction software [38] is capable of processing data in a wide range of data reduction formats. A few of these formats will be illustrated in this section. Figures 4.1-2a through 4.1-2e illustrate rain rate and signal behavior during a storm observed on August 9, 1977. These figures are time history plots and illustrate the instantaneous time dependence of signal level and rain rate. Note that the rain began to fall after significant fading had occurred at all three frequencies. The storm was severe enough (125 mm/hr) to cause the 19 GHz and 28 GHz systems to lose phase lock. Note that the peak fades occurred approximately at the same time and the severity of the fades

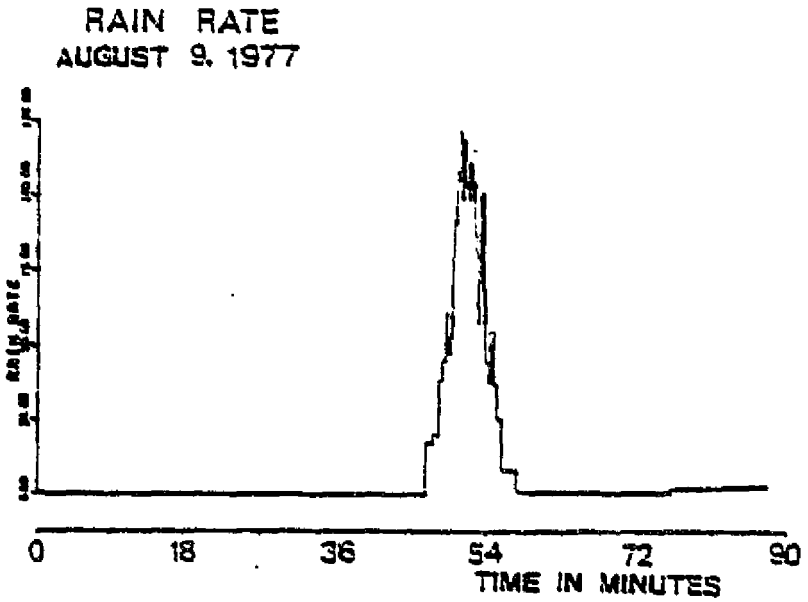

Figure 4.1-2a. Ground rainfall rate on August 9, 1977. (The rain gauge is located beside the receiving antennas.)

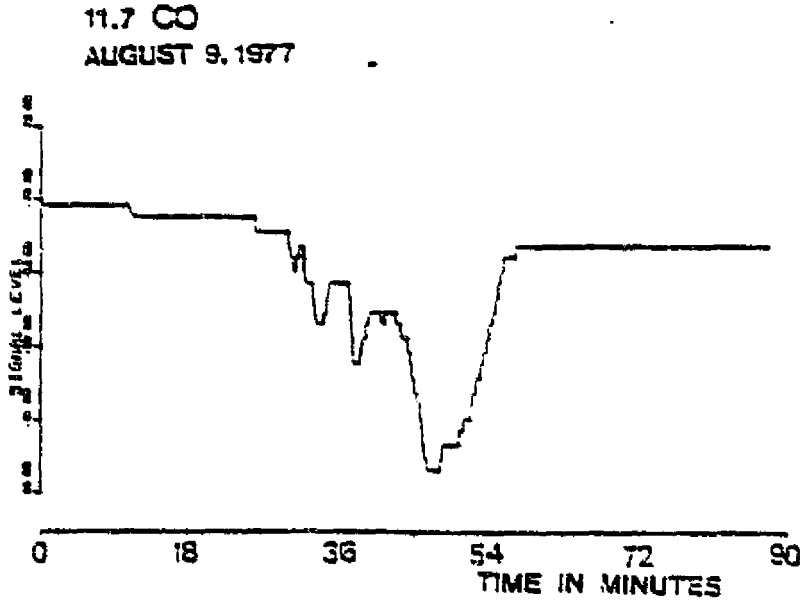

Figure 4.1-2b. CTS 11.7 GHz co-polarized signal behavior on August 9, 1977. (Measured fade 15 dB)

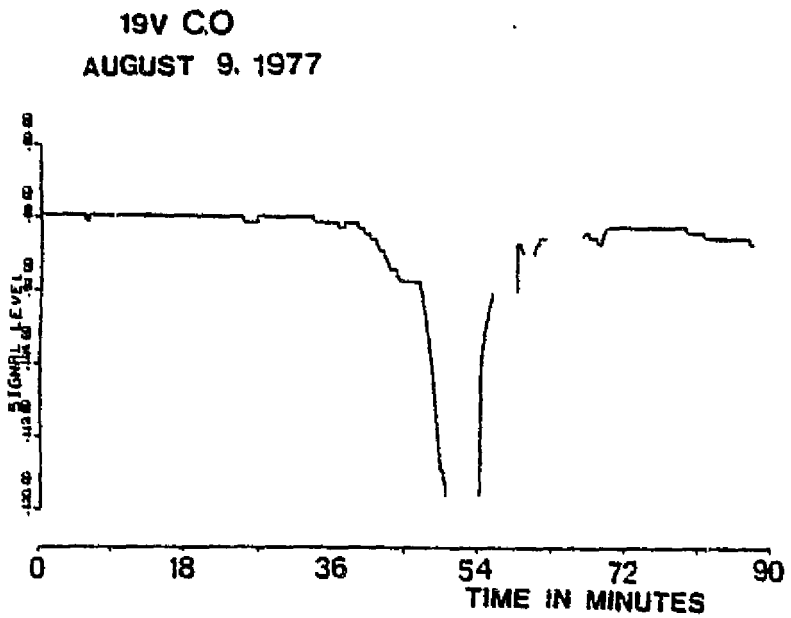

Figure 4.1-2c. 19 GHz vertical co-polarized signal behavior on August 9, 1977. (Measured fade 32 dB)

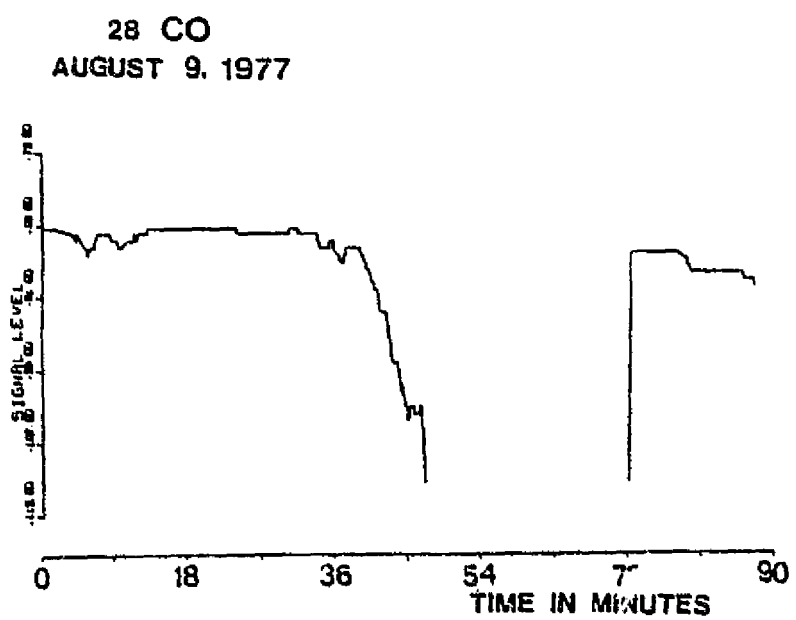

Figure 4.1-2d. COMSTAR 28 GHz co-polarized signal behavior on August 9, 1977. (Measured fade 32 dB)

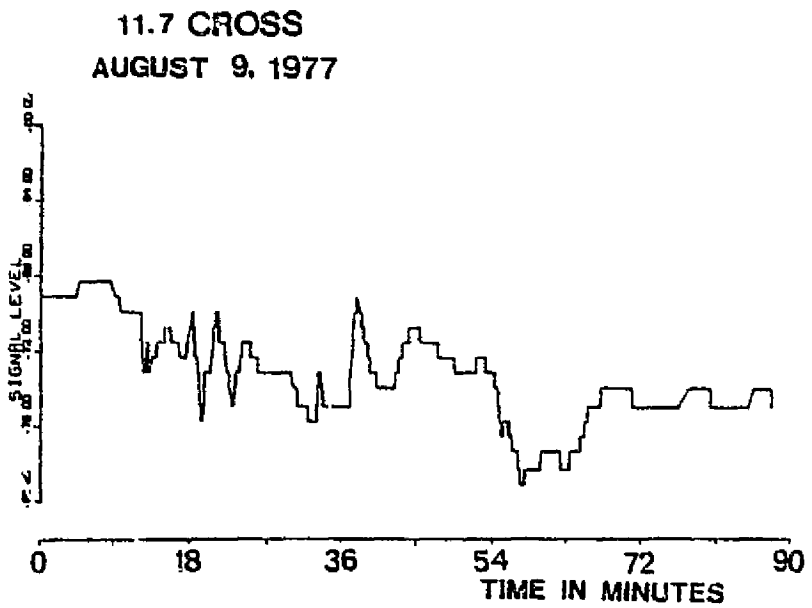

Figure 4.1-2e. 11.7 GHz cross-polarized signal behavior on August 9, 1977.

Figure 4.1-2. VPI&SU system time history plots.

increased with frequency.

Figures 4.1-3a and 4.1-3b are scatter plots which provide an insight into the instantaneous interdependence of attenuation and isolation at different frequencies. Figure 4.1-3a is a plot of isolation verses attenuation at 11.7 GHz for the storm of August 9, 1977. Figure 4.1-3b is a comparison of attenuation of the 19 GHz vertical and the 28 GHz COMSTAR channels during the storm of August 9, 1977. The attenuation ratio for these two frequencies is approximately 2 to 1. Attenuation ratios will be discussed in more detail in Sec. 4.4.

The data reduction process used in Figures 4.1-2 and 4.1-3 did not include any statistical techniques. However, for the prediction of rain effects on millimeter wave signals the removal of the instantaneous time dependence from measured data is necessary. This is accomplished by using the VPI&SU reduction software coupled with a statistical analysis system called SAS [39]. System engineers designing communications links operating in the millimeter wave band are interested in the percent of time that attenuation, isolation, and rain rate will equal or exceed a given value. Such "exceedence" plots are presented in Fig. 4.1-4 and 4.1-5. Figure 4.1-4 is a plot of the attenuation statistics for July, August, and September, 1977. Figure 4.1-5 is a plot of the rain rate statistics over the same time base. The theoretical prediction of the Rice-Holmberg rain rate model [40] is also plotted in Fig. 4.1-5 and agrees rather well with the measured data. The Rice-Holmberg model will be discussed in more detail in Sec. 4.2.

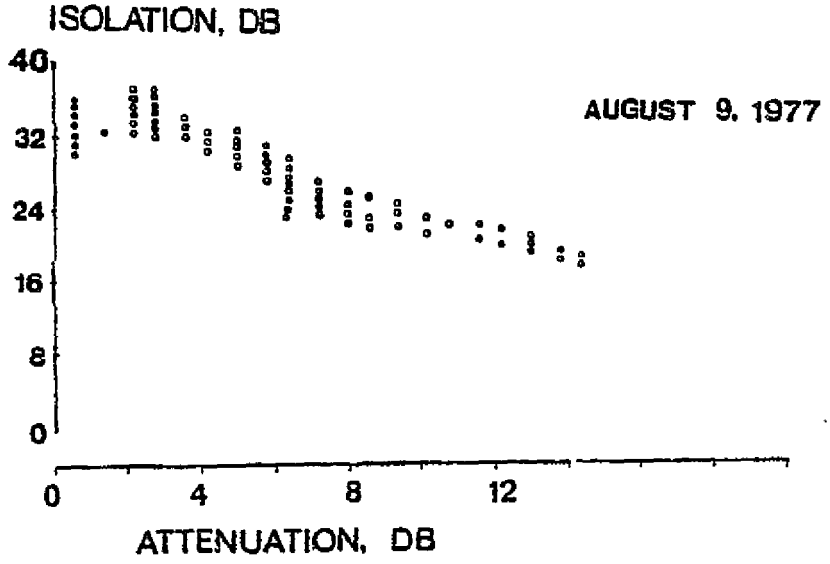

Figure 4.1-3a. 11.7 GHz isolation versus attenuation for the storm of August 9, 1977.

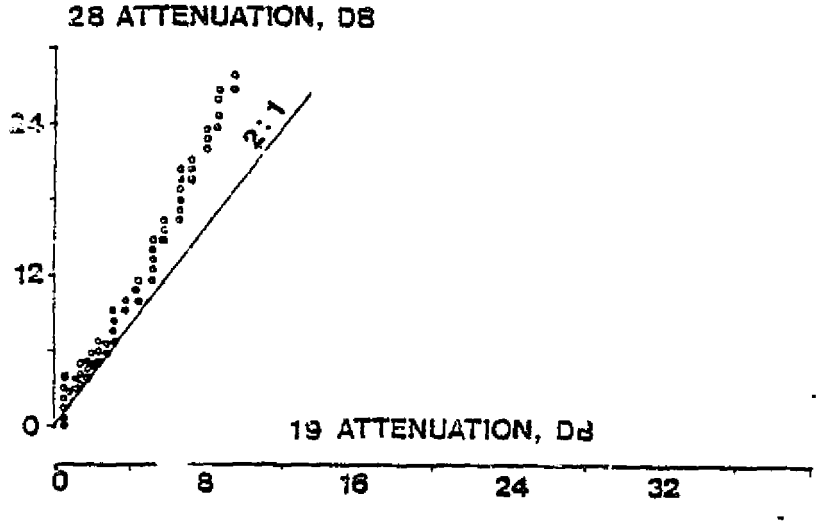

Figure 4.1-3b. A comparison of attenuation on the 19 GHz vertical and the 28 GHz COMSTAR channels during the storm of August 9, 1977.

Figure 4.1-3. VPI&SU system scatter plots.

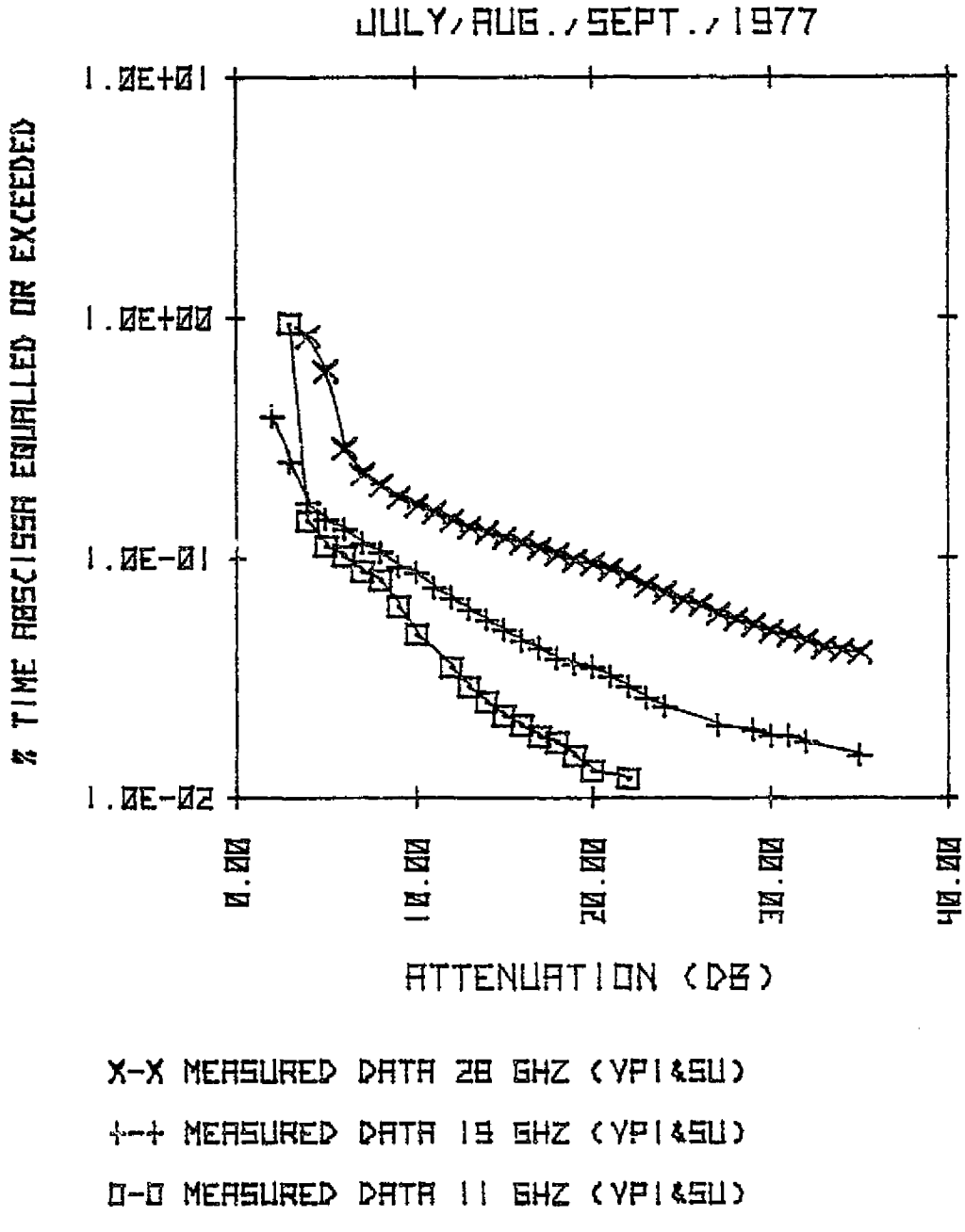

Figure 4.1-4. Measured attenuation statistics for July, August, and September, 1977.

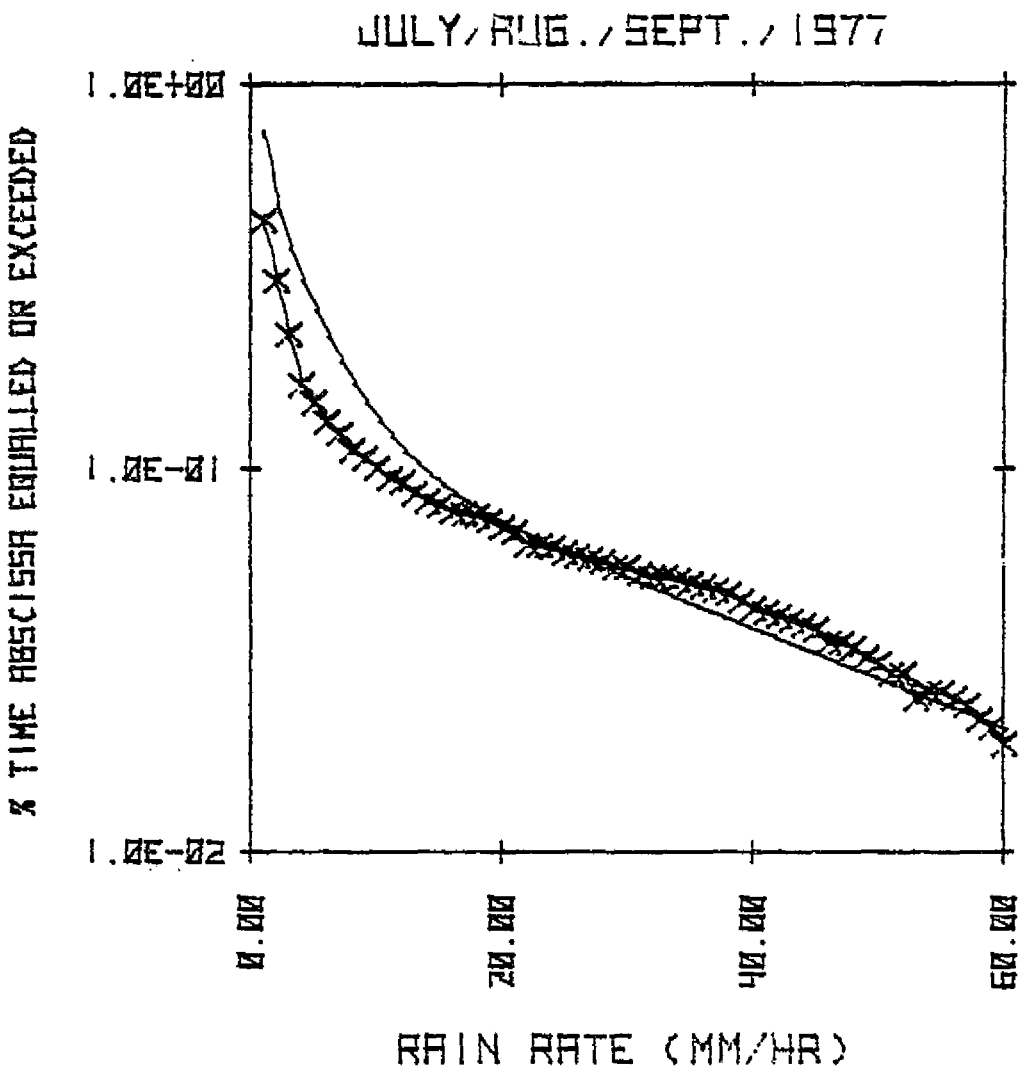

Figure 4.1-5. Rain rate statistics for July, August, and September, 1977.

In Fig. 3.6-6 a plot of attenuation versus rain rate was presented using equal probability techniques. This plot was obtained by comparing attenuation data and rain rate data of Figs. 4.1-4 and 4.1-5 for a given percent of time. This process removes the instantaneous time dependence as seen in Fig. 4.1-2 and represents the data on an equal probability of occurrence basis. Figure 3.6-6 is duplicated in Fig. 4.1-6 for comparison to Figs. 4.1-4 and 4.1-5.

4.2 Comparison of Theory with Measured Data from the VPI&SU Experiment

This section demonstrates the ability of the *scattering model* to predict the effects of rain on a dual-polarized satellite communications link. Theoretical predictions of the scattering model will be compared to measured attenuation, isolation, and phase data collected by the VPI&SU earth station during the months of July, August, and September, 1977. Experimental results are presented using graphs which also contain theoretical predictions of the rain propagation prediction program (RPP). These graphs make the comparison between theory and experiment evident at a glance. The frequency range of the VPI&SU data and the polarization diversity of the VPI&SU experiment provide an excellent opportunity to test the scattering model with a variety of system parameters.

Before theoretical predictions can be formulated for the three systems of the VPI&SU earth station, the input parameters for the RPP program must be determined. The only input parameters needed are the operating frequency, the elevation angle, the effective physical rain

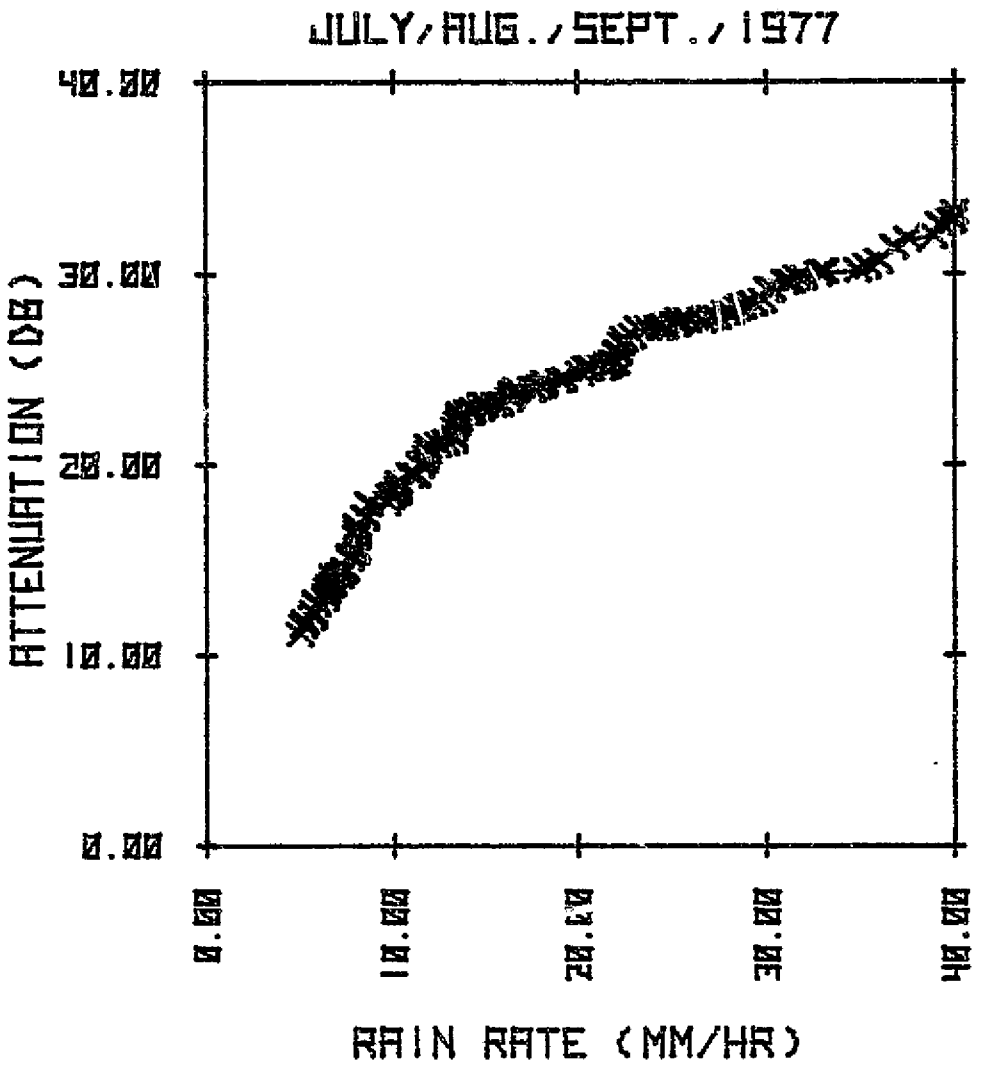

Figure 4.1-6. Measured 28 GHz attenuation versus rain rate. (Plotted using equal probability of occurrence techniques.)

C-2

extent, and the system polarization parameters. The polarization parameters and the elevation angles for the three systems are given in Tables 4.1-2 and 4.1-1, respectively. Knowing the system elevation angle, the physical rain extent L can be determined using Fig. 3.6-5 and Eq. (3.6-25). The effective rain extents for the CTS and COMSTAR systems are 10 km and 8.2 km, respectively. The RPP program is currently limited to the discrete frequency values of 11.0, 14.0, 20.0, and 30.0 GHz. In the following figures the frequencies given are those of the measurement frequency and the particular frequency used in the associated theoretical prediction is the closest available value.

4.2.1 Attenuation

Engineers designing satellite communications links are faced with the problem of determining rain fade margins to provide a reliable communications link during periods of inclement weather. As the operating frequency increases, rain fading becomes more severe. As a result, fade margins have to increase or ground station site diversity must be employed. Either of these solutions is expensive. Data are being collected to help determine the best solution to rain fade problems; however, for satellite links this collection of data is also expensive. For this reason, the development of a reliable theoretical model is necessary. The purpose of this section is to demonstrate the effectiveness of the scattering model in predicting the attenuation experienced on a satellite communications link for a given frequency and ground rain rate.

The relationship between attenuation and ground rain rate as measured by one tipping bucket rain gauge near the VPI&SU antennas is illustrated in Fig. 4.2-1. Measured data are presented using equal probability data reduction techniques. The theoretical predictions are those of the RPP program where the nonuniform rain rates present on a satellite link have been modeled using the *synthetic storm algorithm* presented in Sec. 3.6. As can be seen, the agreement between theory and experiment is very good over the entire rain rate spectrum for all three frequencies. The severe fading at the higher frequencies (19.04 and 28.56 GHz) indicate that site diversity may be the only solution for communications links operating at these frequencies and requiring a high degree of reliability.

Simple equations relating attenuation to rain rate can be written in the form

$$A = a\, RR^b \text{ dB} \tag{4.2-1}$$

where A is attenuation in dB and RR is rain rate in mm/hr. Using power curve regression techniques on both the measured and theoretical data presented in Fig. 4.2-1, the constants a and b of Eq. (4.2-1) can be determined and are given in Table 4.2-1. These values include the effects of the synthetic storm algorithm and are valid for rain rates up to 60 mm/hr.

Ground station site selection is aided by the knowledge of the percent of time that a given value of attenuation will be exceeded during a particular time interval. Thus, the percent of time that the

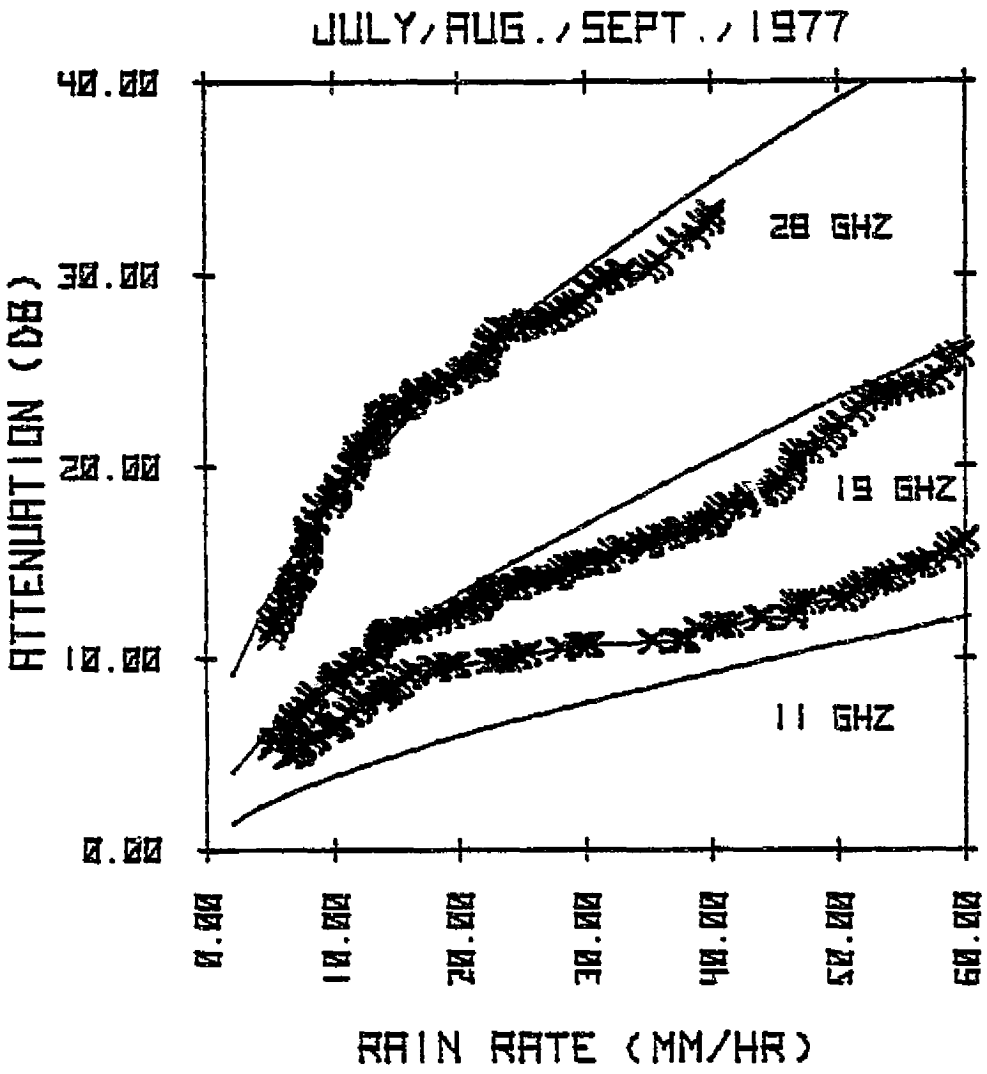

Figure 4.2-1. Attenuation versus rain rate for July, August, and September, 1977. (11.7, 19.04, 28.56 GHz)

Table 4.2-1. Power curve fits to attenuation versus rain rate data presented in Fig. (4.2-1). (RR $\leq$ 60 mm/hr)

Frequency	Theory (RPP)			Measured(VPI&SU)		
	a	b	r^2	a	b	r^2
11 GHz	0.9646	0.6158	1.00	1.9446	0.5195	0.92
19 GHz	2.5878	0.5598	1.00	2.327	0.5615	0.98
28 GHz	6.4779	0.4569	1.00	5.8033	0.4828	0.96

link performance is degraded beyond acceptable system specifications can be determined. Using the scattering model coupled with the Rice-Holmberg rain rate model [40], attenuation statistics can be predicted that agree rather well with the measured attenuation statistics of the VPI&SU earth station. The Rice-Holmberg rain rate model is an empirical fit to a very large data base of measured rain rate data. The model predicts the percent of time that a given rain rate was exceeded based on the total rain accumulation over the time period in question. The Rice-Holmberg equation is given below:

$$\%T(RR) = A_{RH}\{0.03\beta_{RH}\, e^{-0.03RR} + 0.2(1 - \beta_{RH})\{e^{-0.258RR} + 1.86\, e^{-1.63RR}\}\} \qquad (4.2\text{-}2)$$

where A_{RH} is the total rain accumulation in mm times 100 divided by the number of hours in the accumulation period, β_{RH} is the ratio of accumulation of "thunder storm rain" to the total accumulation of rain, and RR is rain rate in mm/hr. The total accumulation of rain measured by the VPI&SU earth station was 153 mm for the months of July, August, and September, 1977 (2208 hours). As a result,

$$A_{RH} = 6.93 \quad \text{mm/hr} \quad . \qquad (4.2\text{-}3)$$

Since the time period in question is the thunder storm season,

$$\beta_{RH} = 0.6 \quad . \qquad (4.2\text{-}4)$$

The Rice-Holmberg prediction is compared to measured rain rate statis-

tics in Fig. 4.2-2. The United States Weather Service observer (located within 8 km of the VPI&SU rain gauge) measured an accumulation of 418 mm for the same time period. This indicates that over short statistical time periods (less than a year), the local terrain may bias the observed statistics, particularly in mountainous regions. However, over long statistical time periods the design engineer should be able to use rain accumulation data from the USWS and predict rain rate and attenuation statistics for a given location [41].

Attenuation statistics for the months of July, August, and September, 1977 can be predicted using the theoretical power curve regressions in Table 4.2-1 and the Rice-Holmberg rain rate equation. Given a value of attenuation, the associated value of rain rate can be determined using the inverse of Eq. (4.2-1) given below:

$$RR = e^{\frac{1}{b}\ln\left(\frac{A}{a}\right)} \text{ mm/hr} \quad . \tag{4.2-5}$$

Using Eq. (4.2-5) in Eq. (4.2-2), the percent of time that a given value of attenuation is exceeded can be determined. Figure 4.2-3 compares the theoretical attenuation exceedence plots to those measured at the VPI&SU earth station. As can be seen for rain rates above 10 mm/hr (.1%), experiment and theory agree rather well for all three frequencies.

4.2.2 Isolation

As the channel capacity of single-polarized satellite communications systems become saturated, dual-polarized communications system[5]

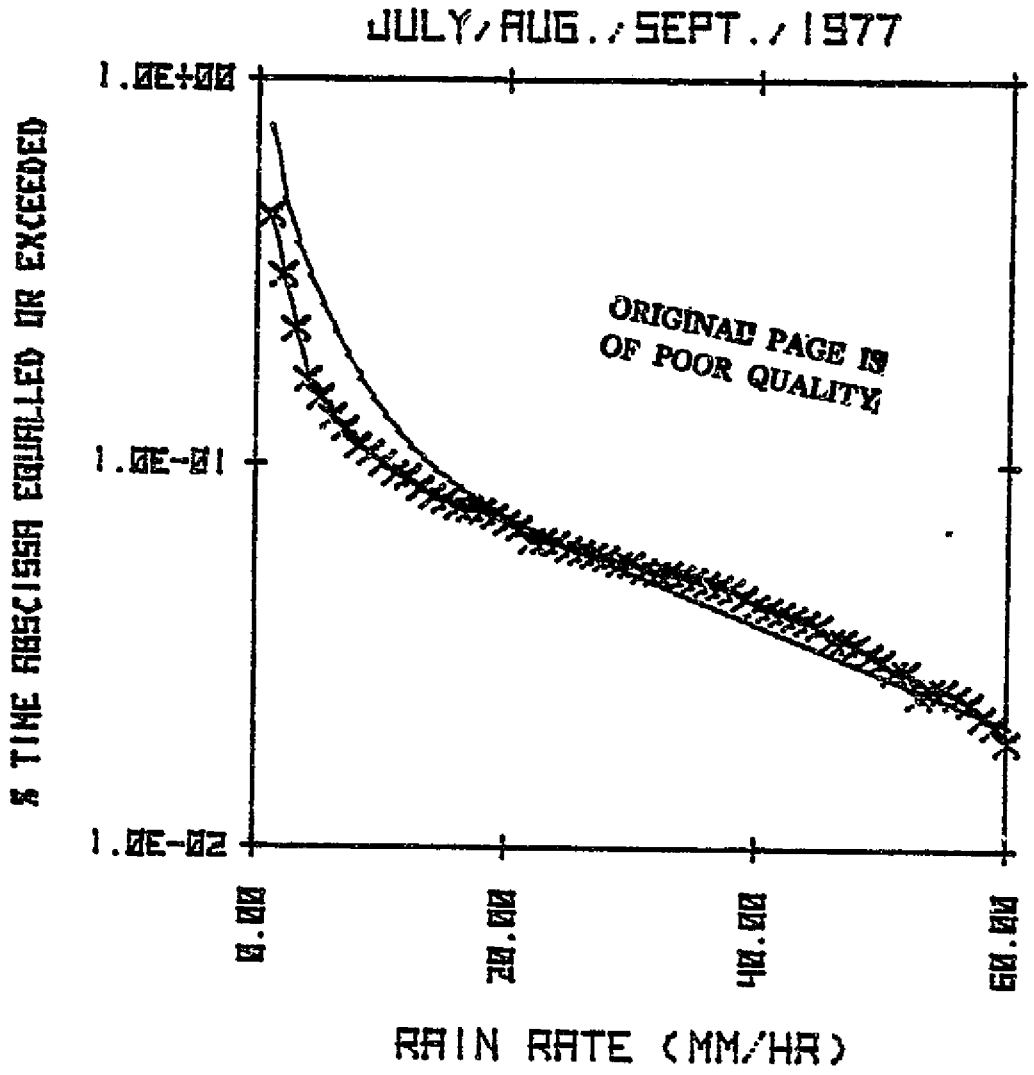

Figure 4.2-2. Measured rain rate statistics for July, August, and September, 1977 compared to the Rice and Holmberg rain rate model.

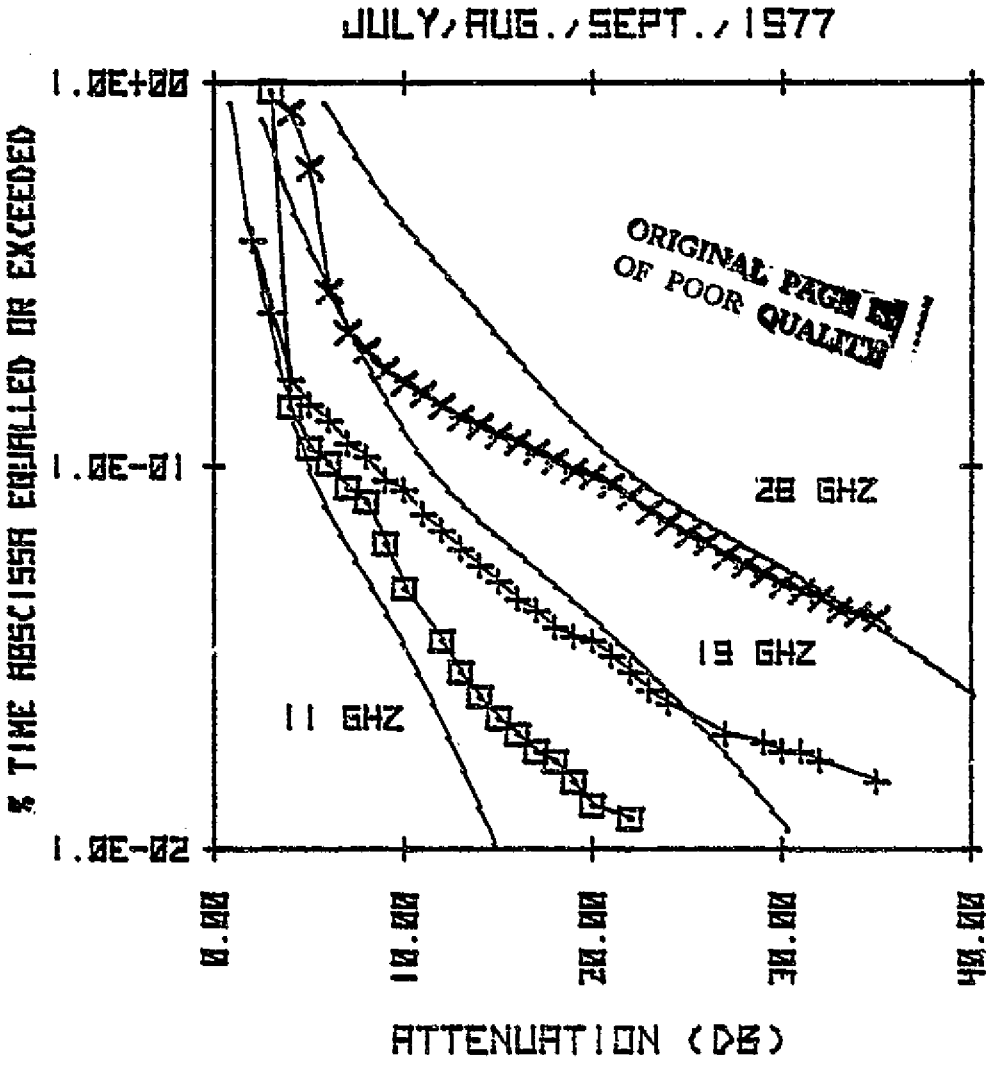

Figure 4.2-3. Measured attenuation statistics for July, August, and September, 1977 compared to the theoretical predictions using the Rice and Holmberg rain rate model and the scattering model.

have been suggested [1] to increase channel capacity without significantly increasing the system cost. However, for operating frequencies above 10 GHz the isolation between the dual-polarized channels is affected significantly by rain. In this section theoretical predictions of isolation as related to attenuation are compared to measured data taken by the VPI&SU earth station during the month of August, 1977. Theoretical predictions of isolation statistics for the months of July, August, and September, 1977 are also presented along with the effects of ice on the isolation of a dual-polarized communications link.

In the previous section measured data were presented using equal probability data reduction techniques. However, multiple frequency isolation statistics are not presently available because of data reduction difficulties. Since hard rains often cause the COMSTAR 19 and 28 systems to lose phase lock, uncertainties have developed in how best to handle these periods when computing isolation statistics. This problem was overcome in the evaluation of attenuation statistics by frequency scaling from lower frequencies where the receiver remained phase locked. However, as of this writing no standard format has been decided upon to scale isolation. Frequency scaling is discussed in more detail in Sec. 4.4. Measured isolation data presented in this section were reduced using instantaneous data reduction techniques. For a given value of attenuation, all of the corresponding values of isolation are averaged and a standard deviation computed. For a given value of attenuation, the scatter in the associated isolation values is significant and can be explained by examining the physical scatter-

ing properties of the rain medium.

The scatter in measured isolation data can be accounted for by three physical properties of the rain medium: 1) the oscillation of the mean canting angle with wind gusts [42], 2) the presence or the absence of a freezing layer, and 3) the movement of inhomogeneous rain cells along the propagation path. The assumption is made that wind gusts can cause the mean canting angle to range between -10° and 10°. However, for a prevailing wind direction, the mean canting angle is predominately negative or positive [42]. Attenuation is relatively insensitive to changing canting angle; however, isolation can vary up to 3 or 4 dB depending on the canting angle and rain intensity. The presence of an ice layer during a rain storm has no significant effect on signal attenuation; however, channel isolation degrades with an increase in ice particle concentration. The effects of canting angle oscillation and the presence of an ice layer on the isolation of a dual-polarized communications link can be predicted by the scattering model. Figures 4.2-4, 4.2-5, and 4.2-6 compare the predictions of the RPP program to measured isolation and attenuation data during the month of August, 1977. In each of the fore-mentioned figures there are four theoretical curves a, b, c, and d with the following mean canting angle and ice content:

a: $\bar{\theta}_\mu = 10°$, no ice

b: $\bar{\theta}_\mu = -10°$, no ice

c: $\bar{\theta}_\mu = 10°$, ice layer present

d: $\bar{\theta}_\mu = -10°$, ice layer present .

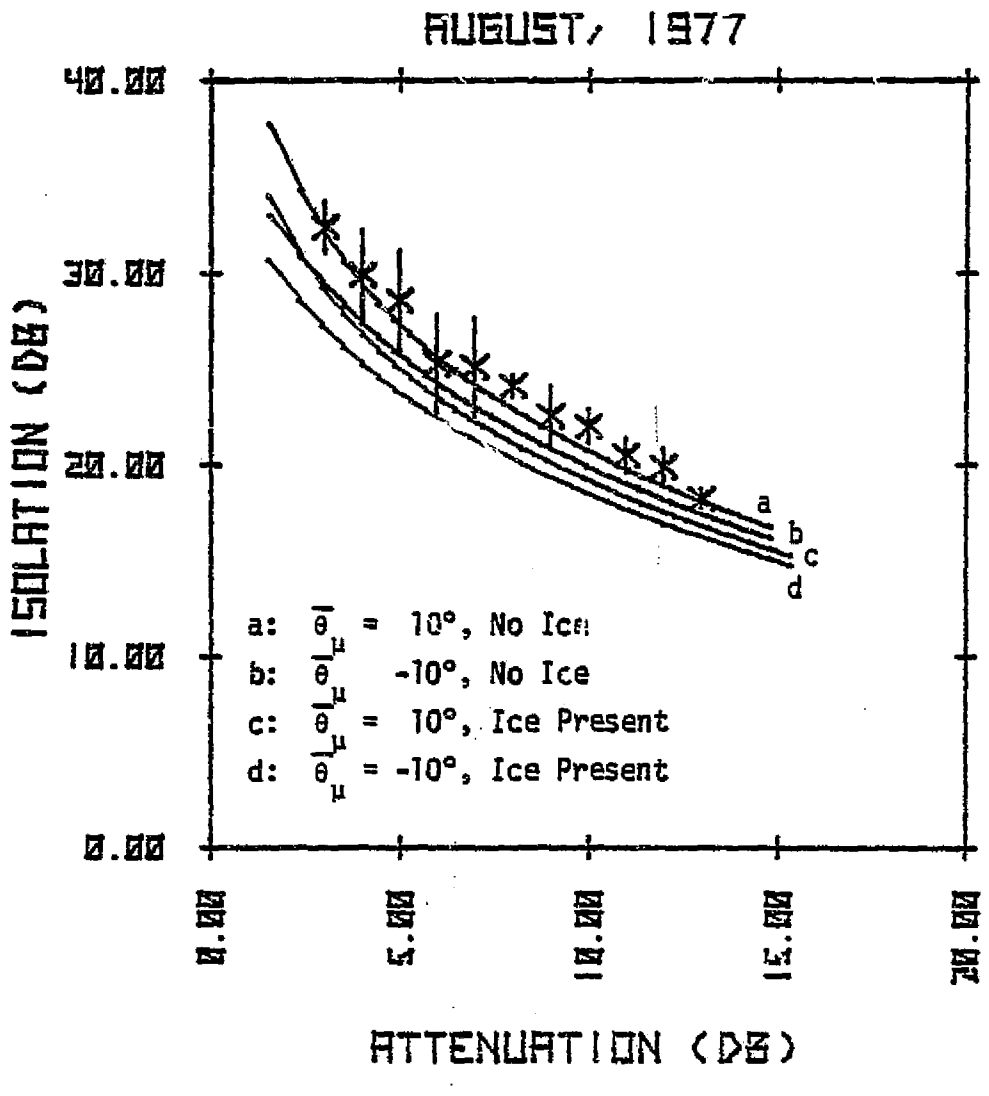

Figure 4.2-4. Isolation versus attenuation for the VPI&SU CTS system for August, 1977. (11.7 GHz)

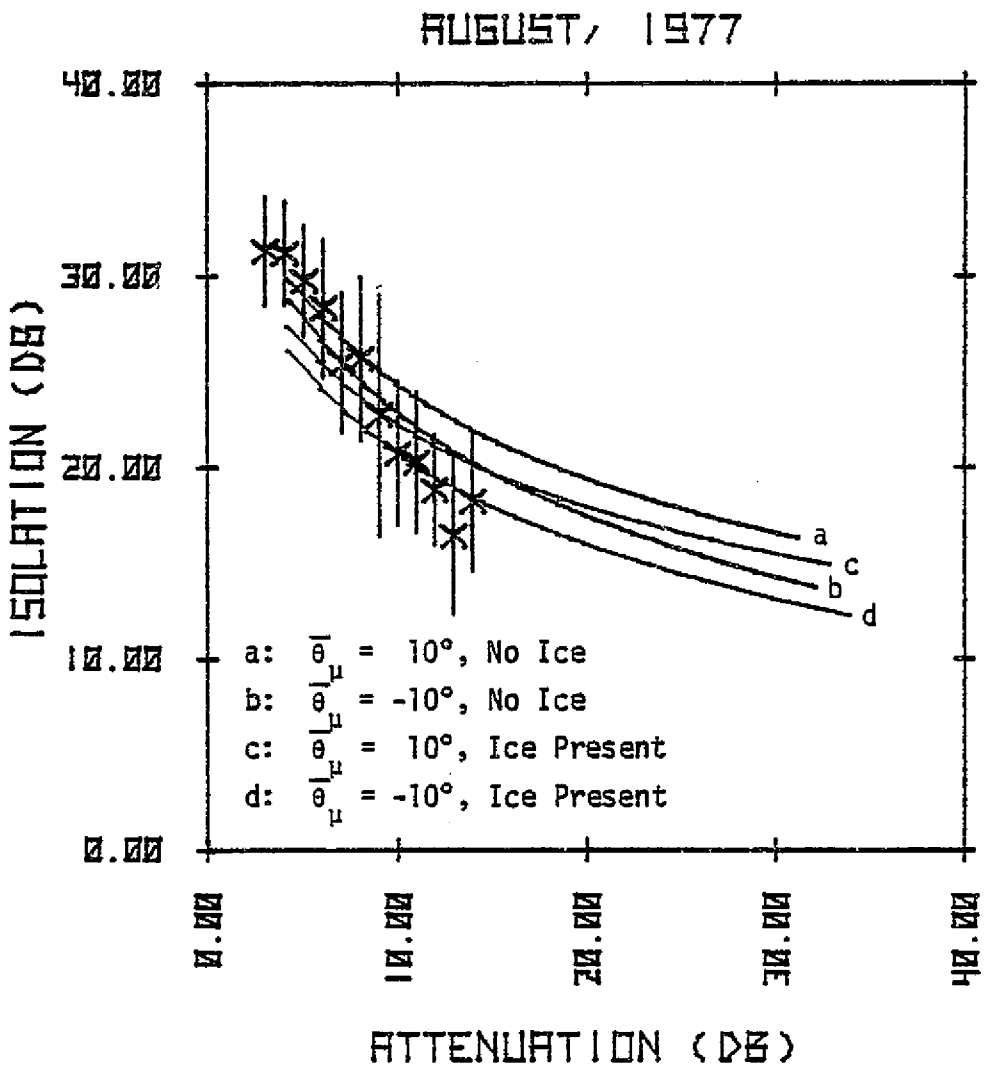

Figure 4.2-5. Isolation versus attenuation for the VPI&SU COMSTAR 19 system for August, 1977. (19.04 GHz)

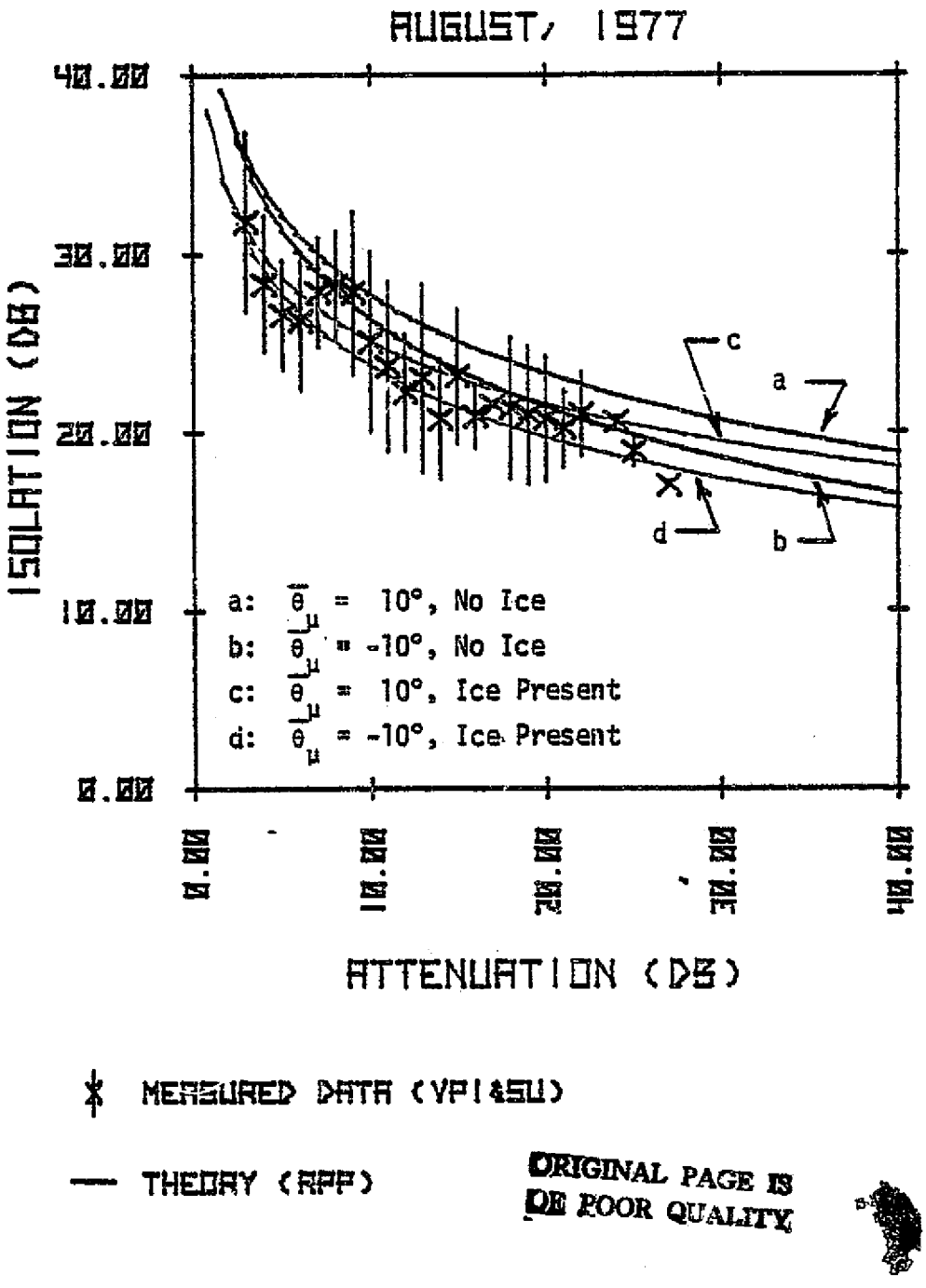

ORIGINAL PAGE IS
OF POOR QUALITY

Figure 4.2-6. Isolation versus attenuation for the VPI&SU COMSTAR 28 system for August, 1977. (28.56 GHz)

The ice layer is assumed to be 1 km thick and since the ice layer does not affect signal attenuation significantly, the effective physical *rain* extent L remains the same. Theory and experiment agree rather well for all three frequencies. However, close examination of the three figures indicates that the scatter in isolation increases with frequency. This is not completely accounted for by the oscillation of the canting angles or the presence of an ice layer. Because the data presented in the three figures are well within the system dynamic range, the scatter should not be a result of receiver error. One possible explanation is the movement of inhomogeneous rain cells along the propagation path. As indicated in Sec. 3.5, isolation may be nonreciprocal under inhomogeneous rain conditions and the magnitude of this nonreciprocity increases with frequency. So for a given value of attenuation (attenuation is reciprocal), there could be a range of varying isolation values depending on the inhomogeneous rain conditions.

Mean isolation can be calculated from attenuation through equations of the form

$$I_m = U + V \ln (A) \text{ dB} \qquad (4.2\text{-}6)$$

where I_m is the mean isolation and A is attenuation in dB. If reliable values of U and V can be determined for arbitrary earth station locations, then Eq. (4.2-6) could be used to calculate isolation statistics from existing attenuation statistics. This would enable communications engineers to predict the performance that would be available if an existing single-polarized link were replaced by a

dual-polarized link. The theoretical prediction assuming no ice and a canting angle of -10° appears to best describe mean isolation as a function of attenuation for all three frequencies. With this assumption and using logarithmic curve regression techniques, the constants U and V of Eq. (4.2-6) can be determined for the mean isolation data presented in Figs. 4.2-4, 4.2-5, and 4.2-6 and are given in Table 4.2-2. The logarithmic curve fits for this case for all three frequencies (11.0, 20.0, and 30.0 GHz) are presented in Fig. 4.2-7 to illustrate the frequency dependence of isolation and attenuation. For a given value of attenuation, channel isolation improves with frequency. It should be noted that the 11 GHz system is circularly polarized and as a result isolation is slightly worse than if the system were linearly polarized.

Isolation statistics can also be predicted without a prior knowledge of attenuation statistics. Using the scattering model coupled with the Rice-Holmberg equation, isolation statistics can be predicted for arbitrary site locations based on total rain accumulation. Mean isolation can be calculated from ground rain rate through equations of the form

$$I_m = T + W \ln (RR) \text{ dB} \qquad (4.2\text{-}7)$$

where I_m is the mean isolation in dB and RR is rain rate in mm/hr. The constants T and W again can be determined using logarithmic curve fitting techniques and are given in Table 4.2-3. For the theoretical assumptions of Fig. 4.2-7 (no ice, $\bar{\theta}_\mu = -10°$), given a value of isolation the associated value of rain rate can be determined using the

Table 4.2-2. Logarithmic curve fits to mean isolation versus attenuation for August, 1977. (For theory, A < 40 dB; for measured CTS and COMSTAR 19, A < 15 dB; and for measured COMSTAR 28, A < 30 dB)

	Theory RPP θ_μ - 10° No Ice			Measured (VPI&SU)		
Frequency	U	V	r^2	U	V	r^2
11 GHz	42.2507	-9.4005	1.00	44.74	-9.8	0.76
19 GHz	40.1418	-7.6020	1.00	46.56	-10.63	0.7087
28 GHz	42.6301	-7.0897	0.99	39.38	-6.67	0.2469*

* r^2 is low because of the scatter in the data.

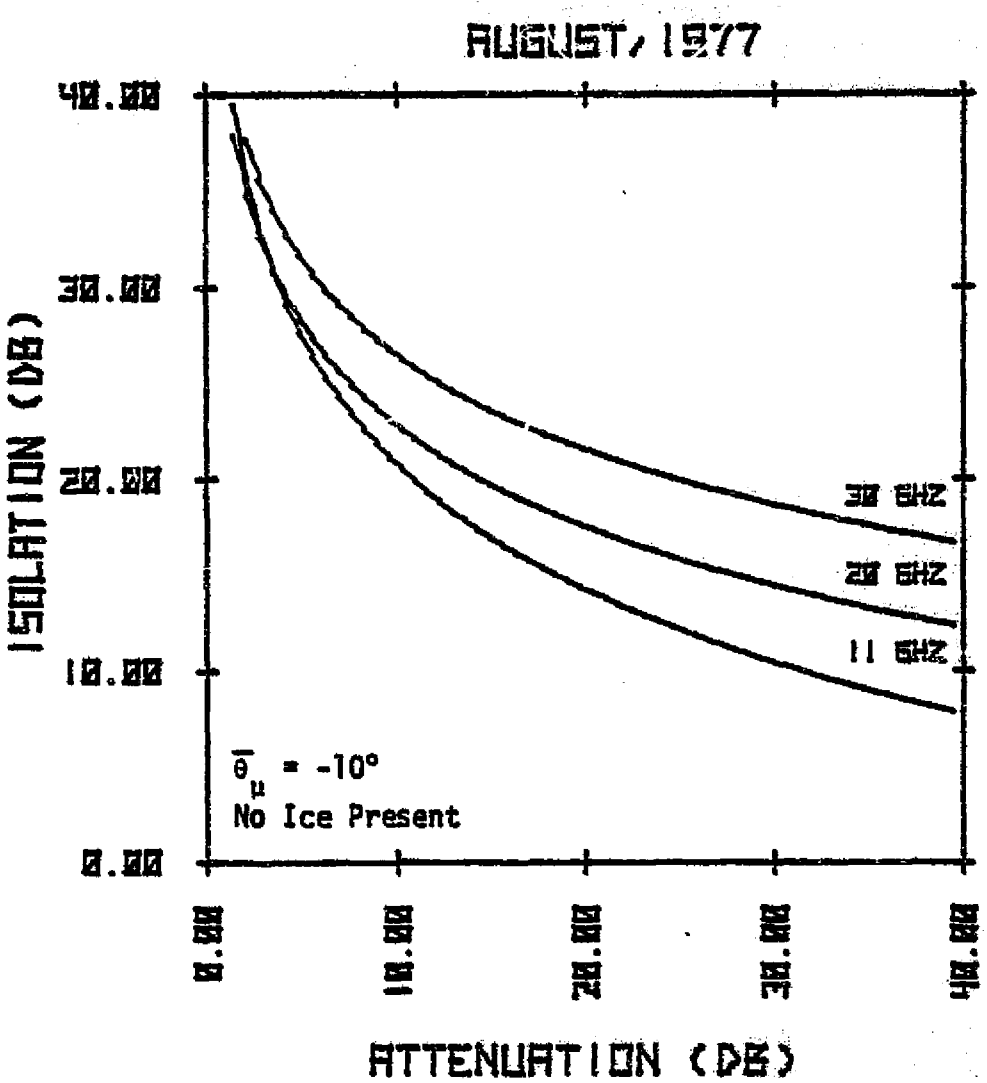

Figure 4.2-7. Logarithmic curve fits of theoretical isolation versus attenuation. (August, 1977)

Table 4.2-3. Logarithmic curve fits to theoretical isolation versus rain rate data. (Rain rate < 60 mm/hr, $\overline{\theta}_{\mu}$ = -10°, no ice)

Frequency	T	W	r^2
11 GHz	42.7801	-5.8524	1.00
20 GHz	32.7645	-6.2008	0.99
30 GHz	29.0694	-3.1824	0.98

ORIGINAL PAGE IS
OF POOR QUALITY

inverse of Eq. (4.2-7) given below:

$$RR = \exp\{(I_m - T)/W\} \quad \text{mm/hr} . \tag{4.2-8}$$

Using Eq. (4.2-8) in Eq. (4.2-2), the percent of time that isolation is less than a given value can be determined. Theoretical isolation statistics are presented in Fig. 4.2-8 without validation by experiment for all three frequencies. Isolation statistics are affected by parameters other than rain such as tracking error and antenna polarization sensitivity. Figure 4.2-8 only accounts for rainfall degradation.

A decrease in channel isolation also can be observed without an associated rain event. This phenomenon is due to ice crystals which can depolarize incident fields without significantly affecting the co-polarized signal. Assuming that a 1 km freezing layer can exist without ground rainfall, Fig. 4.2-9 illustrates the effect this freezing layer would have on the VPI&SU earth station for various particle canting angles. Although these effects have not been observed by the VPI&SU facility, ice depolarization has been observed in other climatic zones [29]. The theoretical data in Fig. 4.2-9 is presented to illustrate the ice depolarization phenomenon and to demonstrate the flexibility of the RPP program. Note that the isolation of the circularly polarized 11 GHz system is relatively constant over the ice crystal canting angle range.

4.2.3 Phase

To improve the channel isolation of a dual-polarized communica-

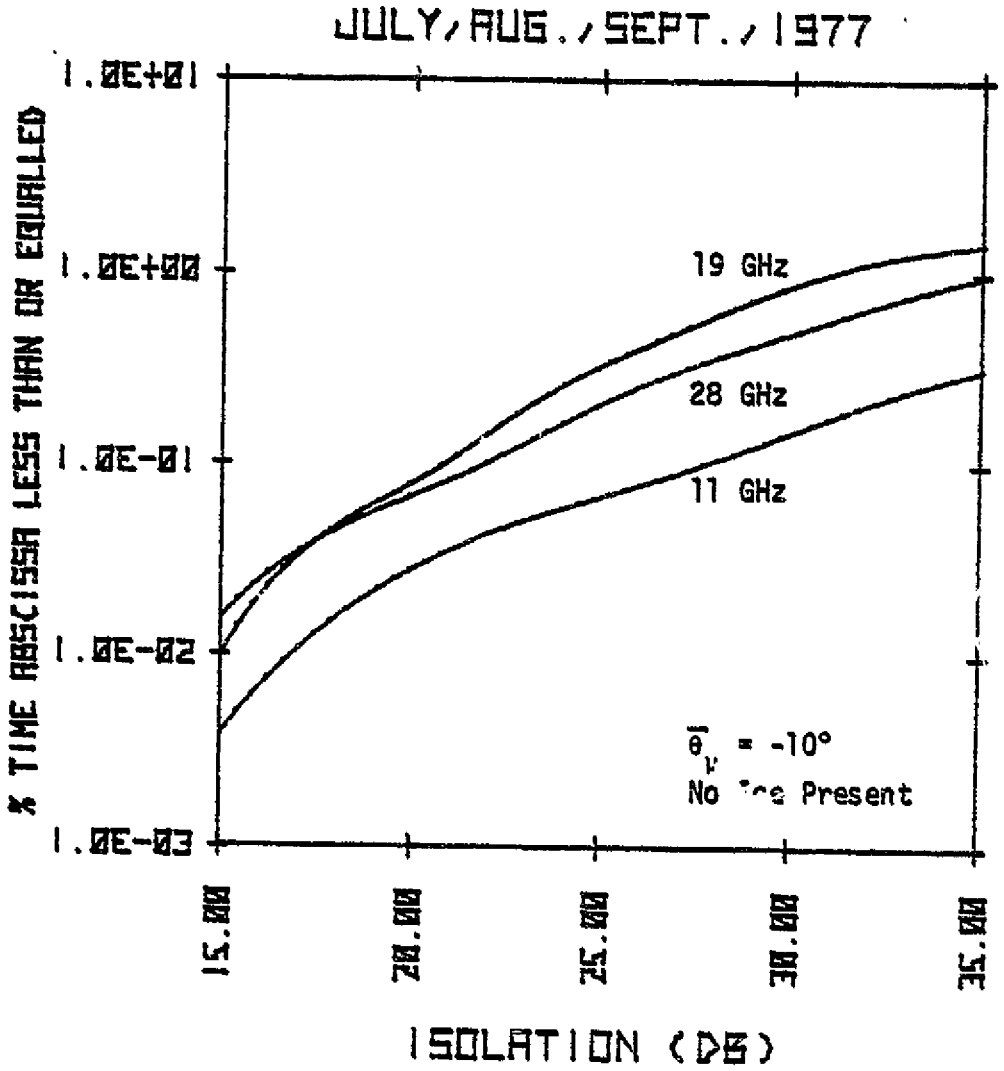

ORIGINAL PAGE IS
OF POOR QUALITY

Figure 4.2-8. Theoretical prediction of the isolation statistics for the VPI&SU system. (July, August, and September, 1977)

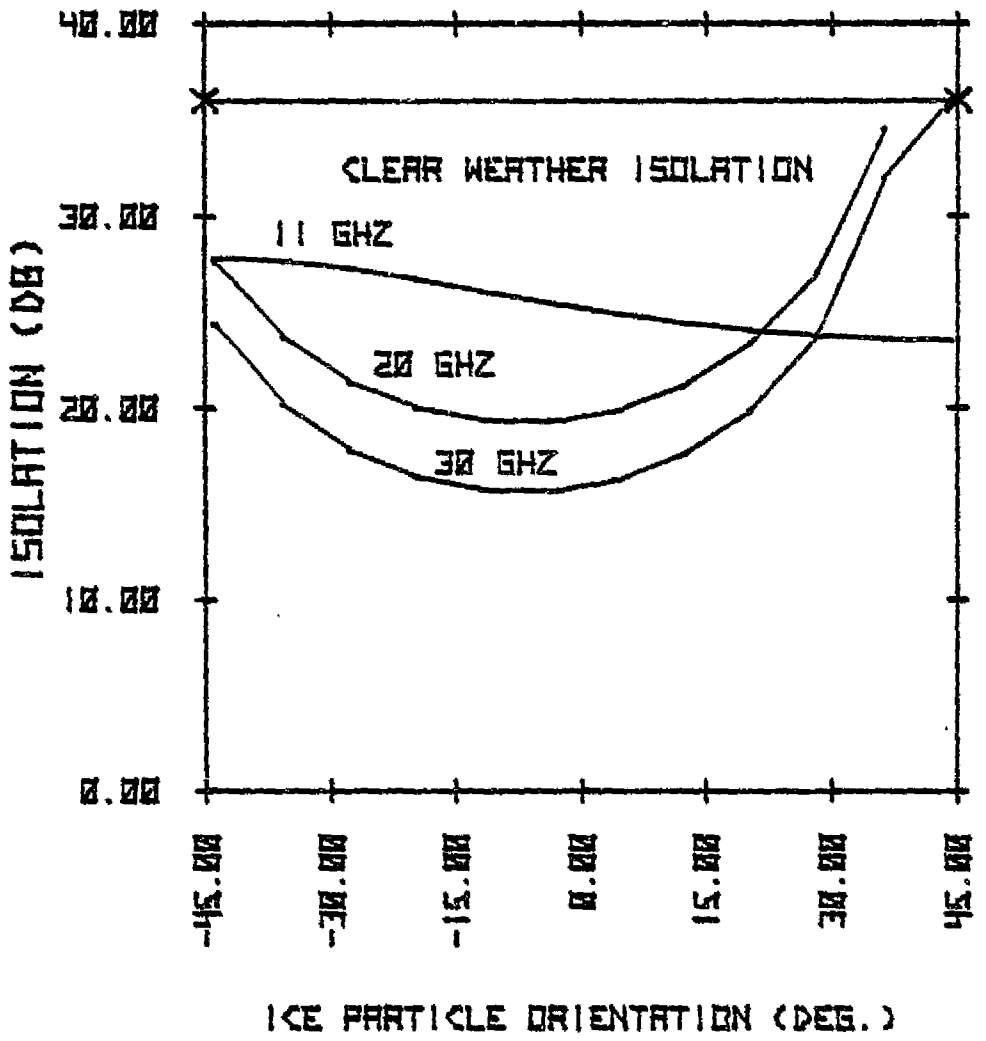

50% Oblate, 50% Prolate Particles

1 KM of Ice, No Rain

Volume of Ice/M^3 = 10^{-6}

Figure 4.2-9. Theoretical predictions of the scattering model of ice depolarization in the absence of rain for different particle orientations.

tions link during precipitation events, static or adaptive cancellation systems are being considered. These systems adaptively change the polarization state of the receive antenna to improve system isolation. To design adaptive cancellation systems, a prior knowledge of the relative phase of the dual-polarized channels is often helpful. For convenience the term "phase", represented by the symbol Φ, is defined as the cross-polarized channel phase minus the co-polarized channel phase. By controlling the relative phase Φ between the two channels and the differential channel attenuation, system isolation can be improved. This section illustrates the sensitivity of phase changes to changes in antenna polarization parameters and the ability of the scattering model to predict these changes as system isolation degrades with an increase in ground rain rate.

Theoretical phase data versus isolation data are compared to measured data in Figs. 4.2-10 and 4.2-12. The theoretical predictions assume that an ice layer is not present along the propagation path and that the mean canting angle ($\bar{\theta}_\mu$) ranges between -10° and 10° as a result of wind gusts. Since adaptive cancellation systems correct for relatively fast changes in phase, measured data are presented on an *instantaneous time* basis for a particular rain storm. This eliminates slow phase variations over longer periods of time and more accurately describes the requirements of an isolation enhancement system.

Figure 4.2-10 represents a typical response of the CTS (11.7 GHz) system during the storm of August 9, 1977. Note that the scatter in

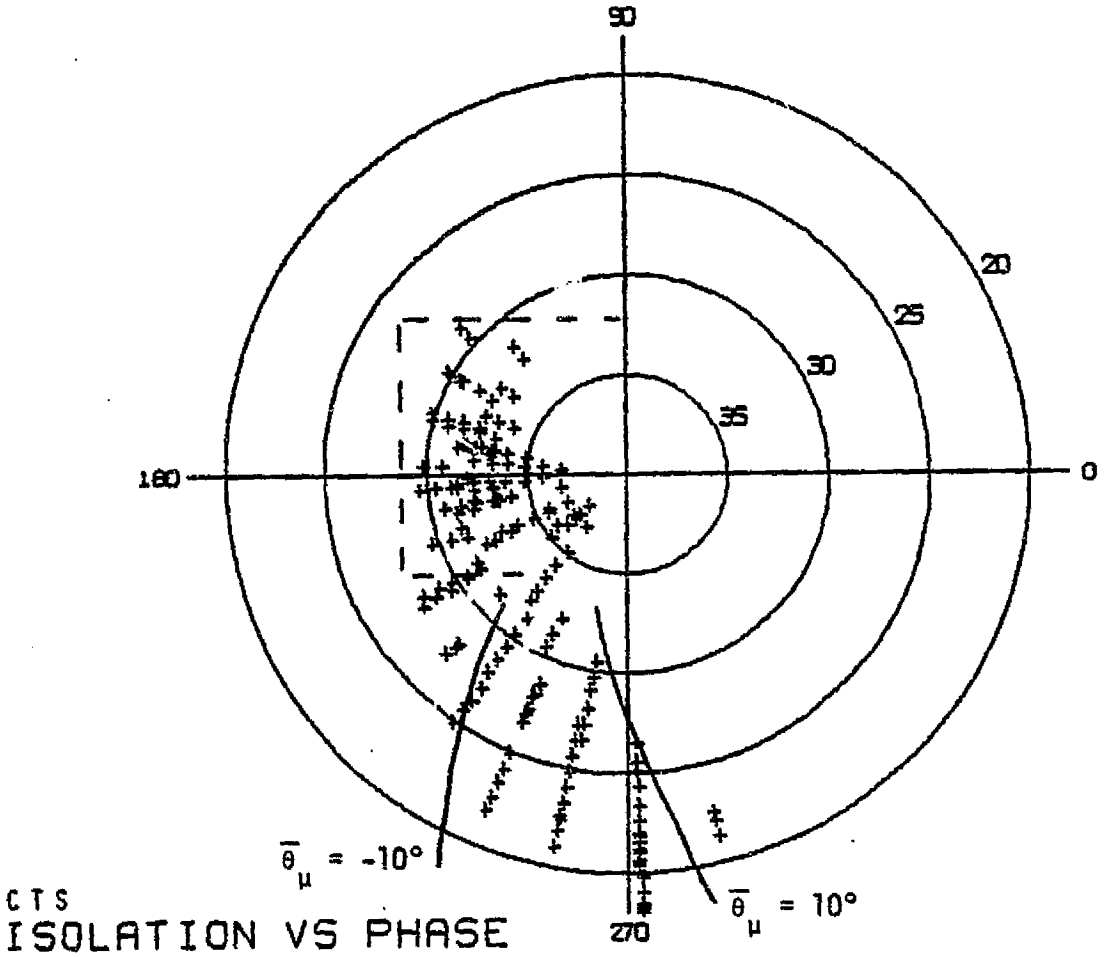

ORIGINAL PAGE IS
OF POOR QUALITY

Figure 4.2-10. CTS isolation versus phase for the storm of August 9, 1977. (CTS is circularly polarized)

isolation and phase supports the assumption of a 20° range in canting angle. The boxed-in area of Fig. 4.2-10 represents the system behavior before the actual rain event. This enhancement of isolation before the onset of a storm is seen often and is attributed to the special characteristics of the system polarization parameters. The circular polarization of the CTS system also accounts for the relatively large phase scatter for a given value of isolation. For circular polarization, Overstreet [43] has shown that phase scatter is usually twice that of the mean canting angle range and this is verified in Fig. 4.2-10.

Phase changes during precipitation events for a dual circularly polarized communications system are very sensitive to changes in antenna polarization parameters. If the satellite and ground station antenna polarization parameters are changed *slightly* from those found in Table 4.1-2 (the new epsilon's and tau's are given in Table 4.2-4), the phase retardation of Fig. 4.2-10 can change direction and advance as seen in Fig. 4.2-11. Note that for high values of isolation or for low rain rates, the phase has changed by a significant amount (61°) relative to Fig. 4.2-10; however, for higher rain rates the change is relatively minor (7°). For high rain rates, changes in the polarization parameters of the spacecraft antenna are masked because of the large cross-polarized component generated by the rain. Changes in the ground station antenna are then minor for small polarization parameter deviations. However, for low rain rates the interaction of the spacecraft and ground station antennas becomes significant. The co-polar-

Table 4.2-4. Epsilon's and Tau's used in Fig. 4.2-11. (Clear weather isolation is 38 dB)

Polarization Parameters	CTS
ϵ_w:	-43.35
τ_w:	0°
ϵ_{co}:	-44.01
τ_{co}:	0°
ϵ_{cross}:	-44.11
τ_{cross}:	90°

ORIGINAL PAGE IS
OF POOR QUALITY

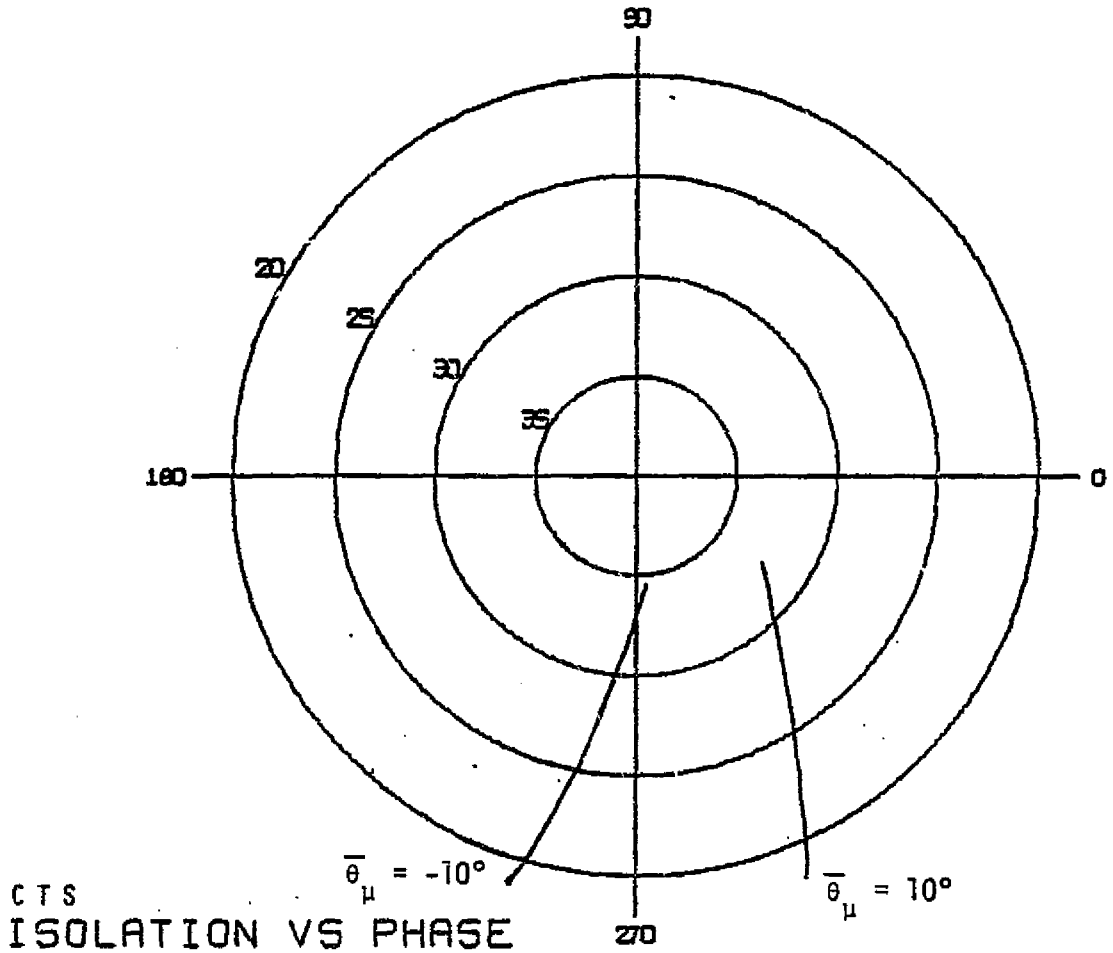

Figure 4.2-11. Theoretical prediction of isolation versus phase for the polarization parameters of Table 4.2-4.

ized phase is relatively insensitive to changes in the antenna polarization parameters; however, for low rain rates the cross-polarized phase is very sensitive to polarization parameter deviations. During low rain rate conditions, the cross-polarized component generated by the satellite is approximately equivalent to the cross-polarized component generated by the rain. Thus, the phase of the resultant wave is very sensitive to the cross-polarized phase of the wave transmitted by the satellite. Because phase (ϕ) is insensitive to antenna polarization changes during high rain rate conditions, phase for a circularly polarized system can advance or retard depending on the antenna polarization parameters and the associated effect on the cross-polarized phase for low rain rates.

Although the same arguments apply for a dual linearly polarized communications system as for the circularly polarized antenna system, the uniqueness of the polarization parameters for a linear system reduce the dependence of phase on polarization parameter deviations. Also, the associated phase scatter of a linearly polarized system is significantly reduced as seen in Fig. 4.2-12. This figure represents a typical response of the COMSTAR 28 (28.56 GHz) system during a storm on August 30, 1977. From the data presented in this section, a linearly polarized system is recommended over a circularly polarized system when an adaptive polarization system is being considered [43].

4.3 Comparison of Theory to Measured Data from Other Experiments

In the previous section the theoretical predictions of the

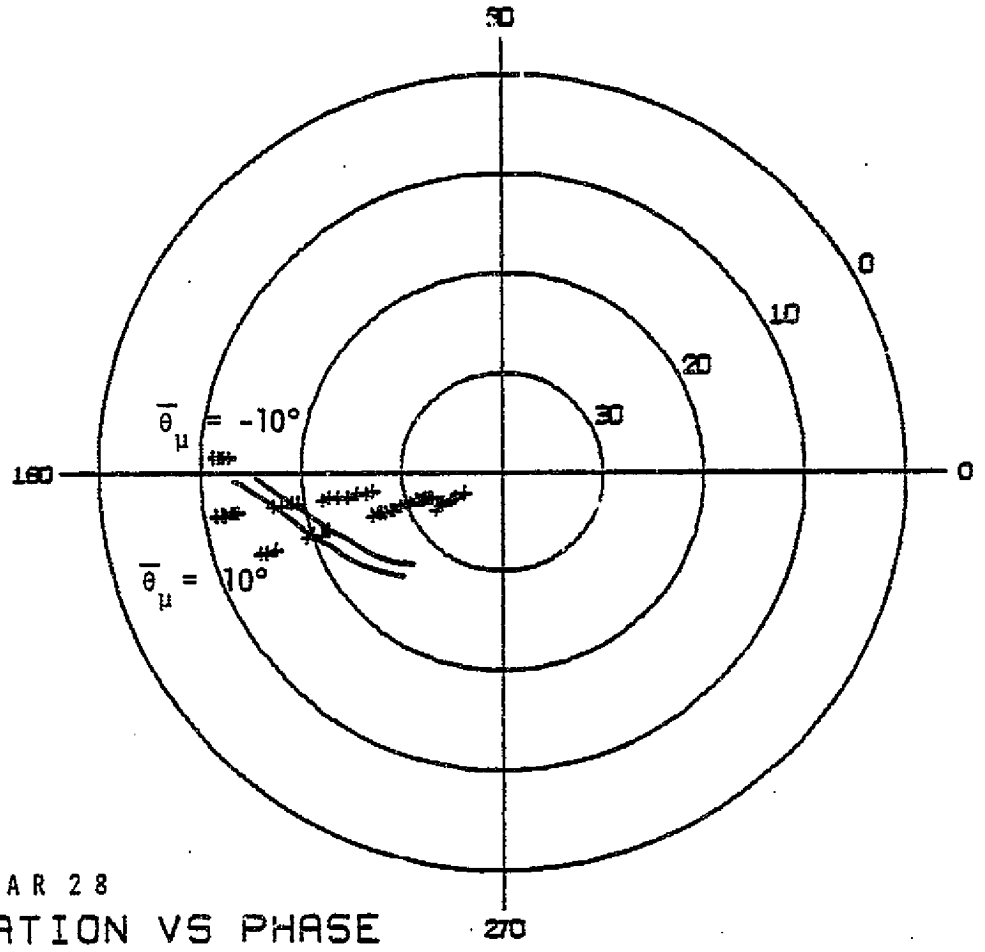

Figure 4.2-12. COMSTAR 28 isolation versus phase for the storm of August 30, 1977. (COMSTAR 28 is linearly polarized)

scattering model were compared to measured data from the VPI&SU earth station for a variety of system parameters. Excellent correlation between measurement and theory was seen. However, the true test of a theoretical propagation model is the ability to predict the effects of rain on dual-polarized communications links for different frequencies, elevation angles, and locations. Using the first order approximation of the synthetic storm model (Fig. 3.6-5) and the respective system parameters of the Comsat Labs COMSTAR experiment and the University of Texas ATS-6 experiment, theoretical attenuation predictions of the scattering model are presented in this section that agree rather well with published measured data from those experiments.

Since attenuation is relatively insensitive to changes in polarization parameters and the exact polarization parameters for the experiments of Comsat Labs and the University of Texas are not known by the authors, the polarization parameters of the VPI&SU COMSTAR system will be assumed in the theoretical predictions of this section. Comsat Labs monitors continuous transmissions from the COMSTAR D1 satellite at an elevation angle of 23°. As a result, using Fig. 3.6-5 and Eq. (3.6-25) the effective rain extent is 11.2 km for the 19.04 GHz and 28.56 GHz COMSTAR D1 beacons. Putting this data into the RPP program yields the theoretical attenuation predictions in Fig. 4.3-1 for the 19 GHz and 28 GHz systems of Comsat Labs. The associated measured data were taken from published rain rate and attenuation statistics for July, 1976 through January, 1977 [34]. As can be seen, the agreement between theory and measurement is very good. Since no

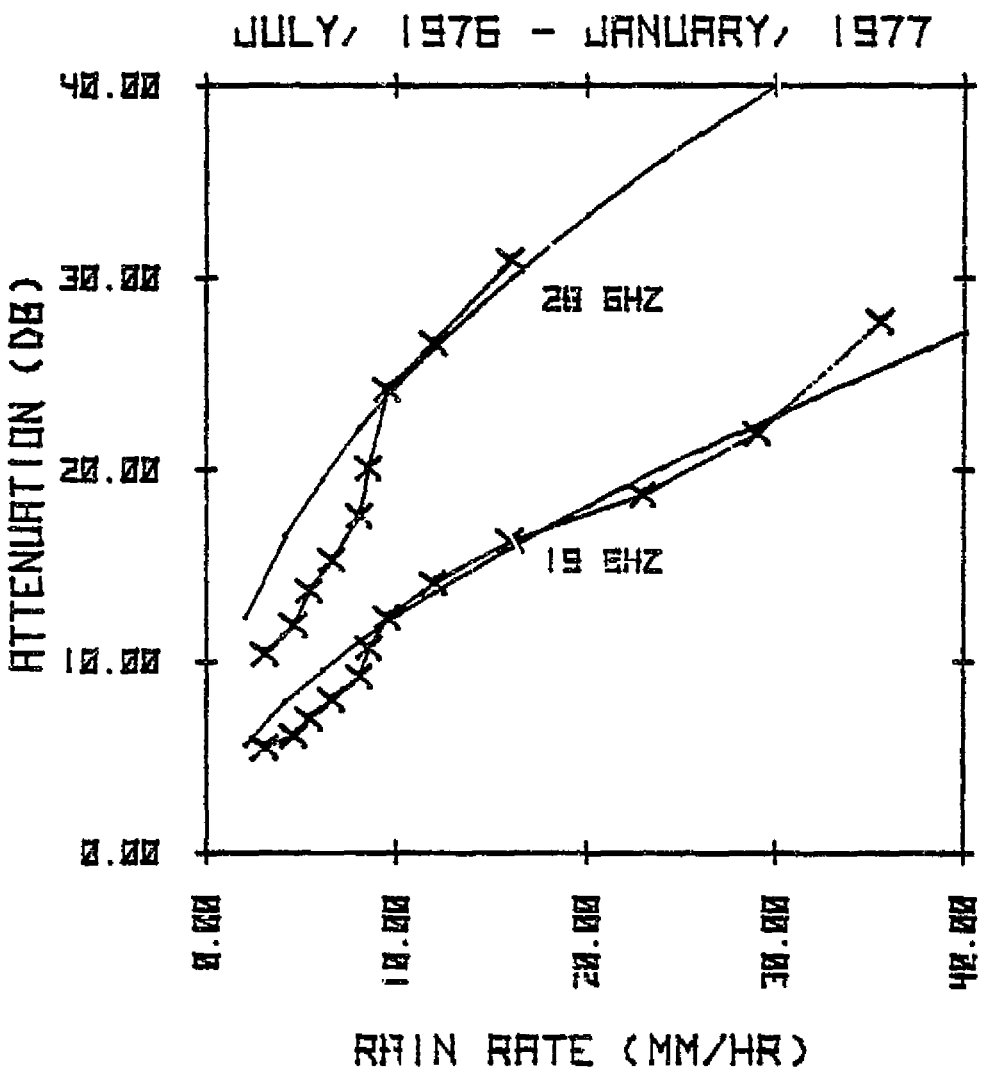

ORIGINAL PAGE IS
OF POOR QUALITY

Figure 4.3-1. Attenuation versus rain rate, theoretical predictions of the scattering model compared to measured data of Comsat Labs. (19.04, 28.56 GHz)

isolation data are available, no theoretical predictions are presented. The University of Texas monitored transmissions from the ATS-6 satellite on a time-available basis from July, 1974, to May, 1975. Measured attenuation data from the NASA Technical Note [35] along with the theoretical predictions of the scattering model are presented in Fig. 4.3-2. The ATS-6 propagation frequency was 30 GHz and the elevation angle from the University of Texas experiment site was 54°. As a result, the effective rain extent was 6.7 km. Again there is good agreement between theory and measurement.

Figures 4.3-1 and 4.3-2 demonstrate the flexibility of the synthetic storm algorithm of Sec. 3.6 and the scattering model in predicting rain effects on millimeter wave communications links. However, before the scattering model can be used to predict the effect of rain on *any arbitrary* earth station, more data must be collected to improve the synthetic storm model of Fig. 3.6-5. An effective storm height of 6 km and a ground rain extent of 10 km seems reasonable; however, these values may change for different climatic zones. Before the full potential of the synthetic storm algorithm can be achieved, more data are needed.

4.4 Frequency Scaling

4.4.1 Attenuation

It is often very useful to scale measured attenuation data at one frequency in order to estimate system performance at another frequency. The frequency dependence of attenuation and the relation-

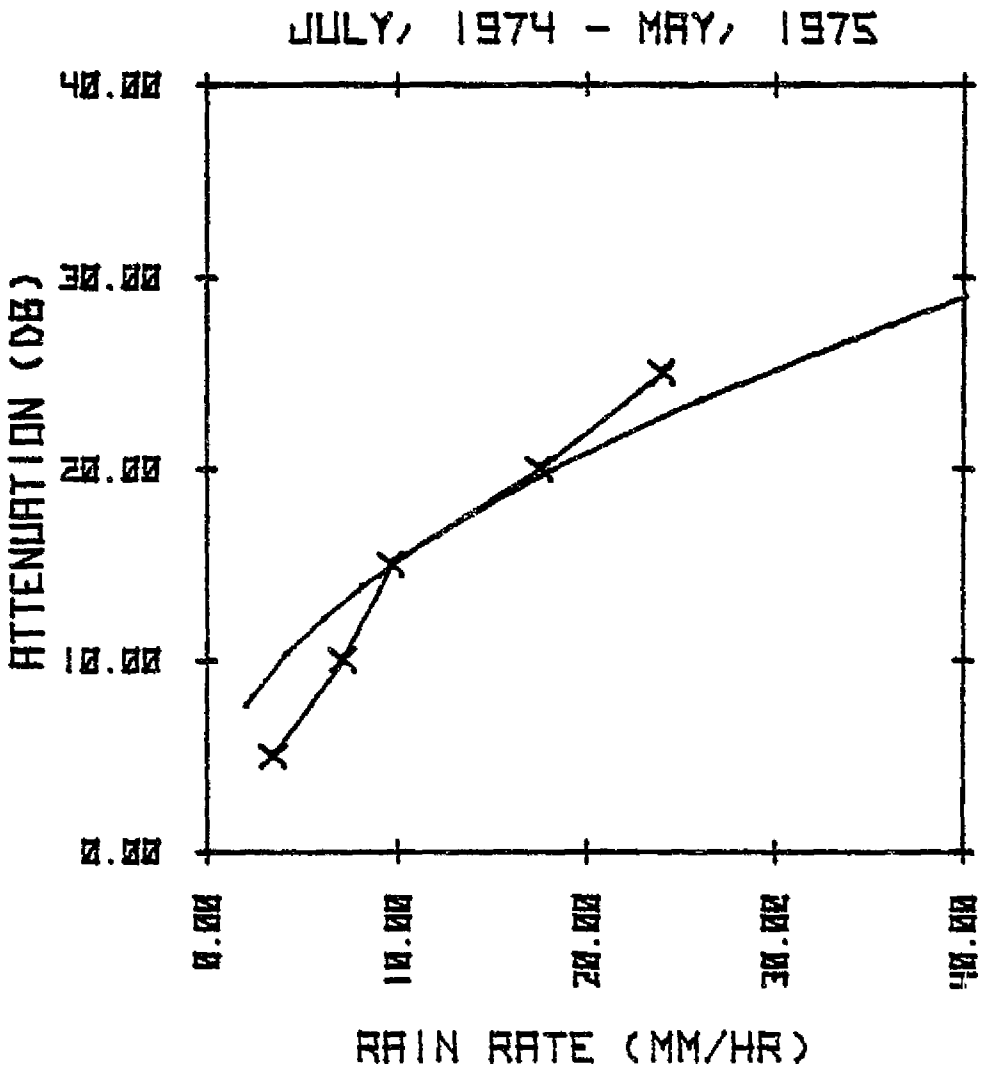

Figure 4.3-2. Attenuation versus rain rate, theoretical predictions of the scattering model compared to measured data of the University of Texas. (30 GHz)

ship to ground rain rate is predicted easily by the scattering model. In this section theoretical predictions of the scattering model are compared to measured data and to the recent frequency scaling algorithm of Hodge [44].

Figures 4.4-1, 4.4-2, and 4.4-3 illustrate the frequency dependence of attenuation measured at the VPI&SU earth station and the corresponding predictions of the scattering model. Measured and theoretical data are plotted using equal probability of occurrence techniques. Figure 4.4-4 presents the measured attenuation data of Comsat Labs along with the associated prediction of the scattering model. Although the rain extent and the elevation angles are different for the two sites, the ratio of the 28 GHz attenuation to the 19 GHz attenuation is the same.

For a given value of attenuation at a particular frequency, the corresponding scaled value of attenuation at a second frequency can be determined using equations of the form

$$A_2 = u\, A_1^v \quad \text{dB} \tag{4.4-1}$$

where A_i represents the attenuation of the i^{th} frequency in dB. Using power regression techniques the constants u and v in Eq. (4.4-1) can be determined and are given in Table 4.4-1 for both the theoretical and measured data presented in Figs. 4.4-1, 4.4-2, 4.4-3, and 4.4-4.

Another way of describing the frequency dependence of attenuation is through equations of the form

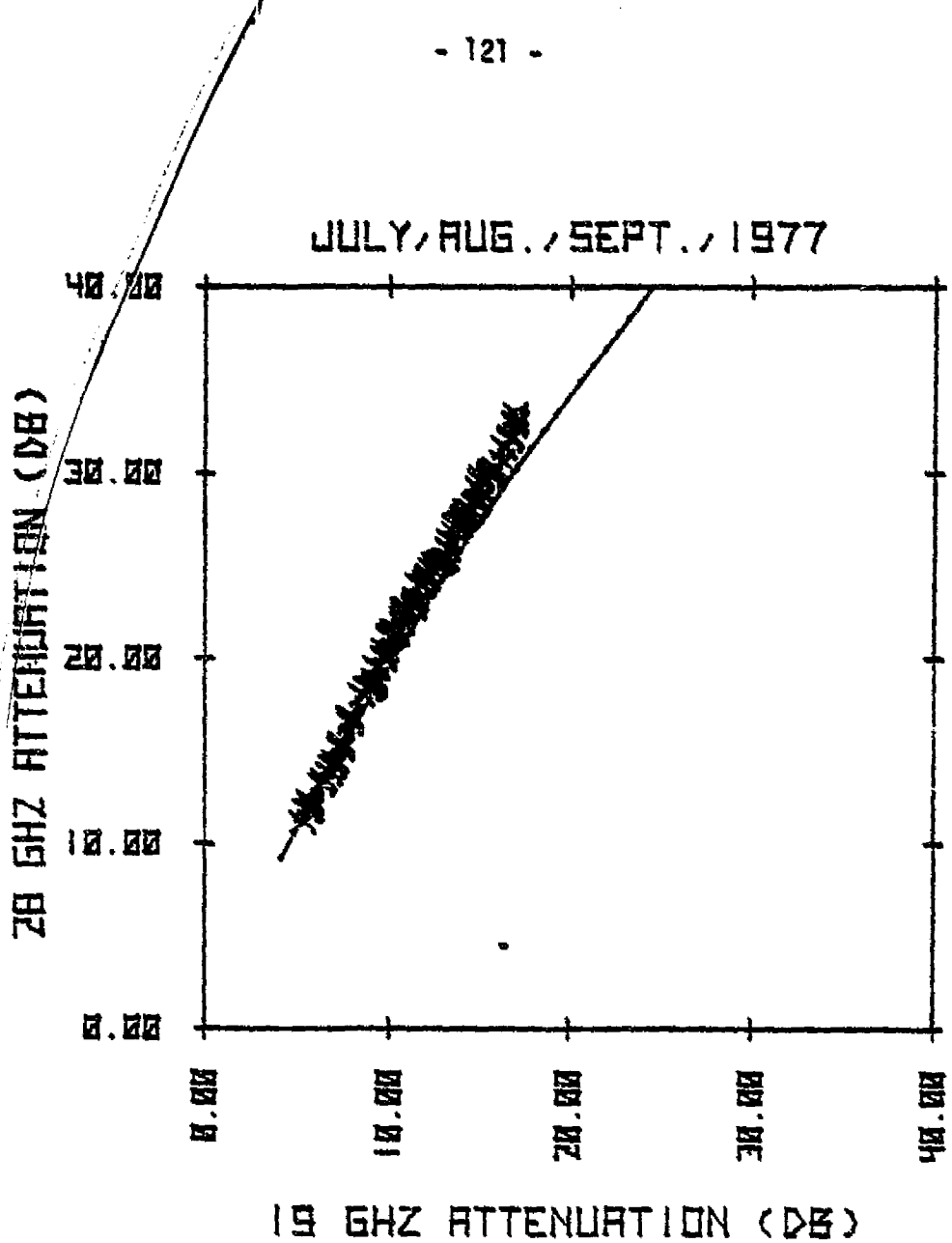

Figure 4.4-1. 28 GHz attenuation versus 19 GHz attenuation (VPI&SU).

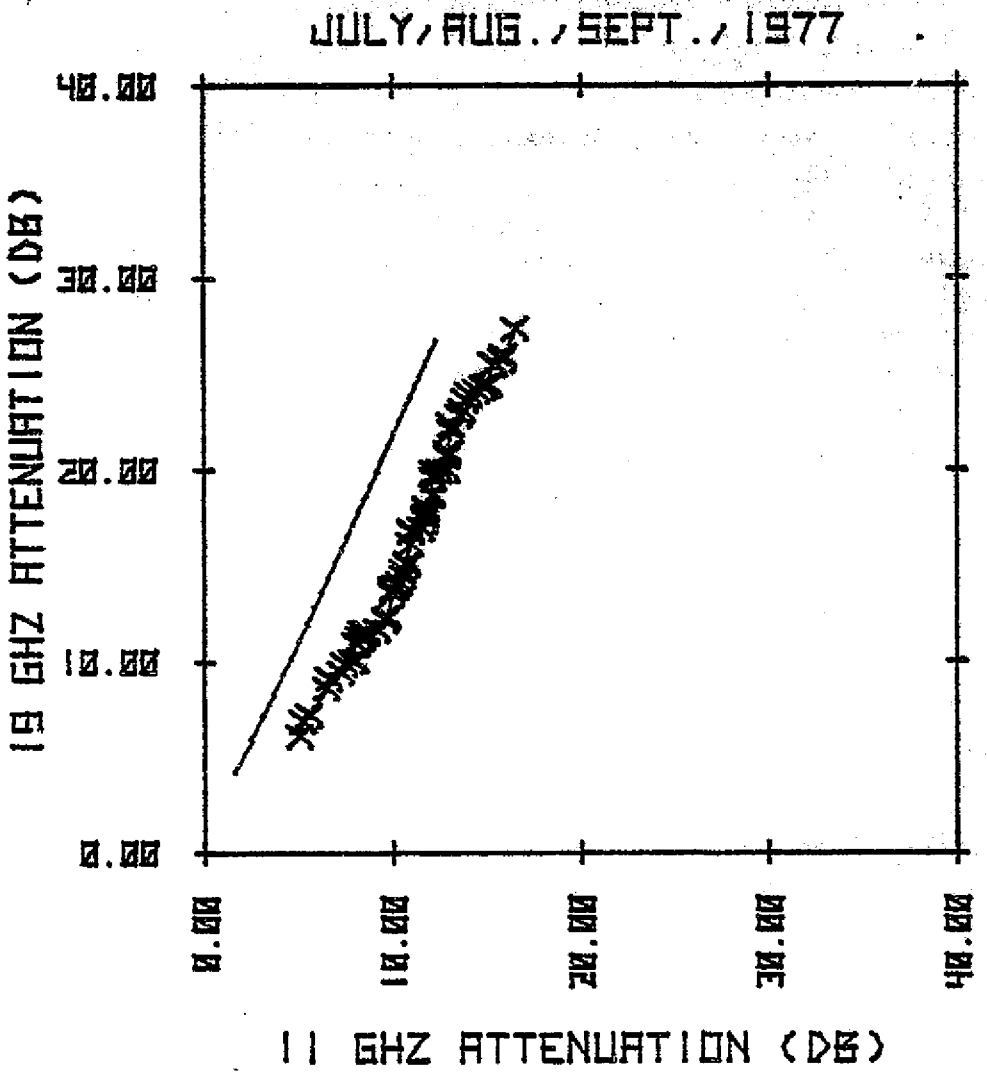

ORIGINAL PAGE IS
OF POOR QUALITY

Figure 4.4-2. 19 GHz attenuation versus
11 GHz attenuation (VPI&SU).

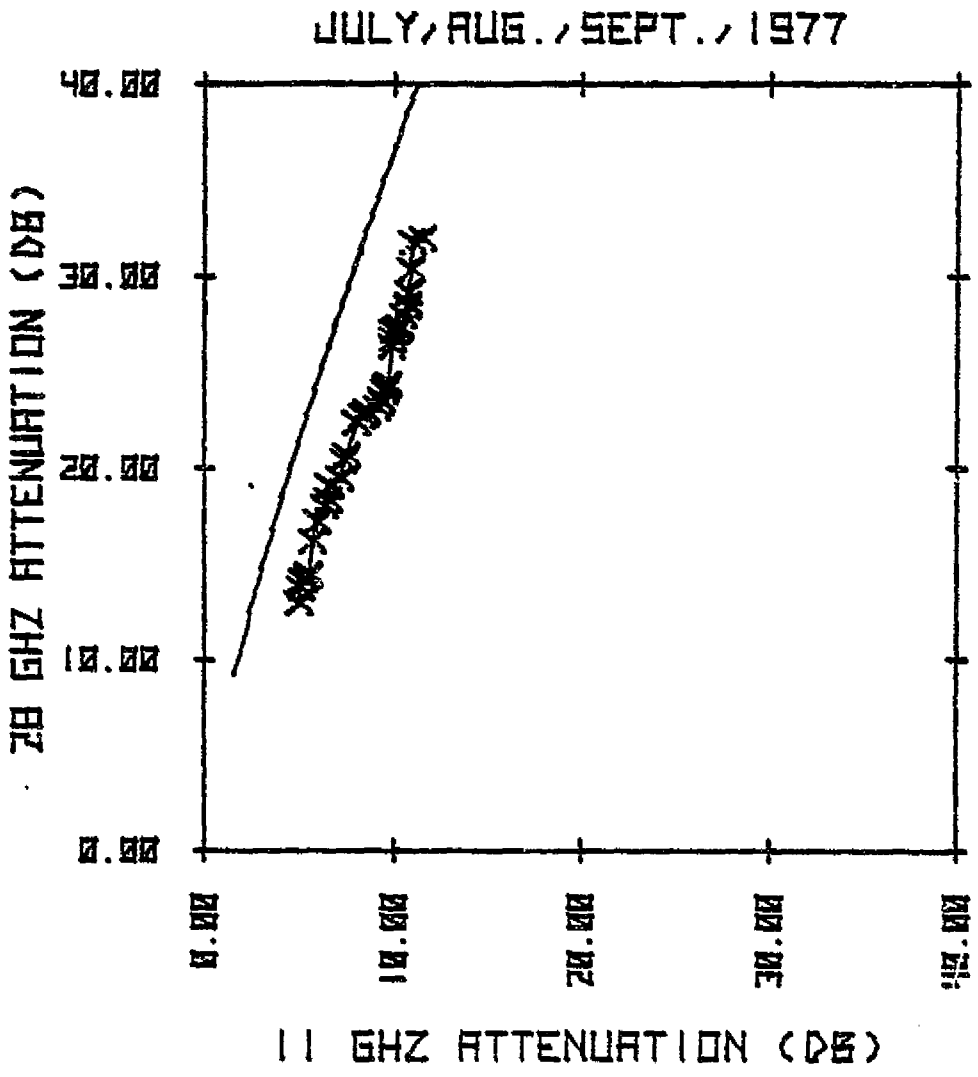

Figure 4.4-3. 28 GHz attenuation versus 11 GHz attenuation (VPI&SU).

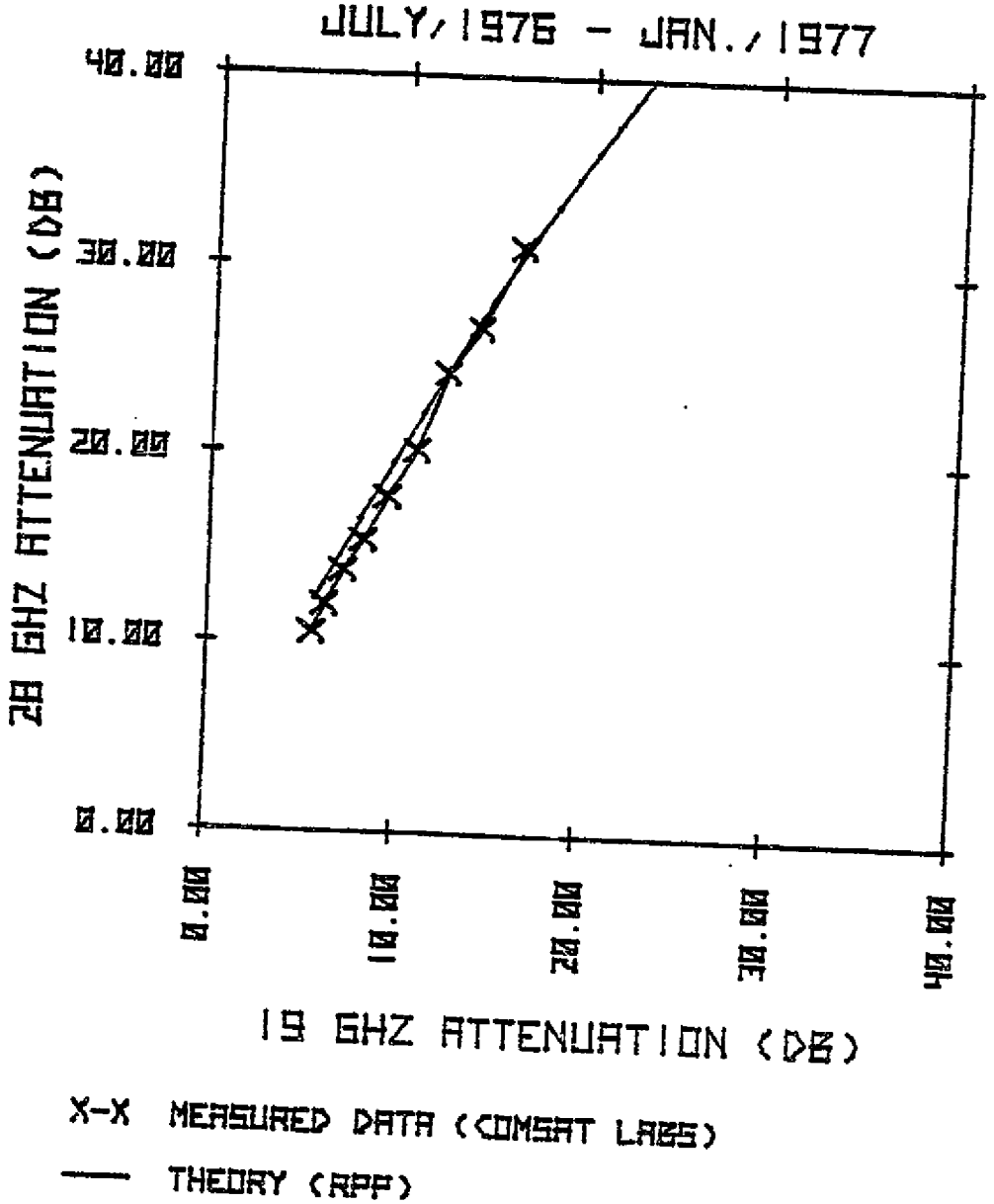

Figure 4.4-4. 28 GHz attenuation versus 19 GHz attenuation (Comsat Labs).

Table 4.4-1. Power curve fits to attenuation versus attenuation data presented in Figs. 4.4-1, 4.4-2, 4.4-3, and 4.4-4. (A_i < 40 dB) See Eq. (4.4-1).

	VPI&SU						Comsat Labs					
	Measured			Theory			Measured			Theory		
Frequency Ratio	u	v	r^2	u	v	r^2	u	v	r^2	u	v	r^2
28/19	2.4902	0.9106	0.99	2.9919	0.8148	1.00	1.9377	0.9927	1.00	3.0778	0.8148	1.00
28/11	2.9722	0.9552	0.98	6.6514	0.7421	1.00	------	------	----	------	------	----
19/11	0.8019	1.2501	0.97	2.6708	0.9099	1.00	------	------	----	------	------	----

ORIGINAL PAGE IS
OF POOR QUALITY

$$\frac{A_2}{A_1} = \frac{a_2}{a_1} RR^{(b_2 - b_1)} \tag{4.4-2}$$

where RR is rain rate in mm/hr and a_i and b_i are found in Table 4.2-1 for the VPI&SU experimental system. It is obvious from Eq. (4.4-2) that the frequency dependence of attenuation is also dependent on ground rainfall.

Hodge [44] also has considered the dependence of attenuation scaling on rain rate. Assuming that rainfall along the propagation path is a Gaussian function of position on the path, the ratio of attenuations at two different frequencies is expressed by the relation

$$\frac{A_2}{A_1} = \frac{\alpha_2}{\alpha_1} \sqrt{\xi_1/\xi_2}\, RR^{(\xi_2 - \xi_1)} \tag{4.4-3}$$

where α_i and ξ_i are constants associated with power curve fits to attenuation per kilometer (specific attenuation) as a function of a uniform rain for the i^{th} frequency. These constants are given in Table 4.4-2. The scattering model prediction, the theory of Hodge, and a curve fit to measured data for the ratio of 28 GHz attenuation to 19 GHz attenuation are illustrated in Fig. 4.4-5. The theory of the scattering model and the theory of Hodge both employ a nonuniform distribution of rain rate along the propagation path. As a result both models agree rather well with measured data. However, unlike the Hodge formulation, the synthetic storm algorithm is internal to the scattering model and can be used also to scale isolation (the Hodge formulation can predict only the ratio of two attenuations).

Table 4.4-2. Power curve fits to theoretical attenuation per kilometer versus rain rate assuming uniform rain conditions.

Frequency	α	ξ	r^2
11	0.0217	1.2001	0.98
19	0.089	1.094	0.99
28	0.276	0.903	0.99

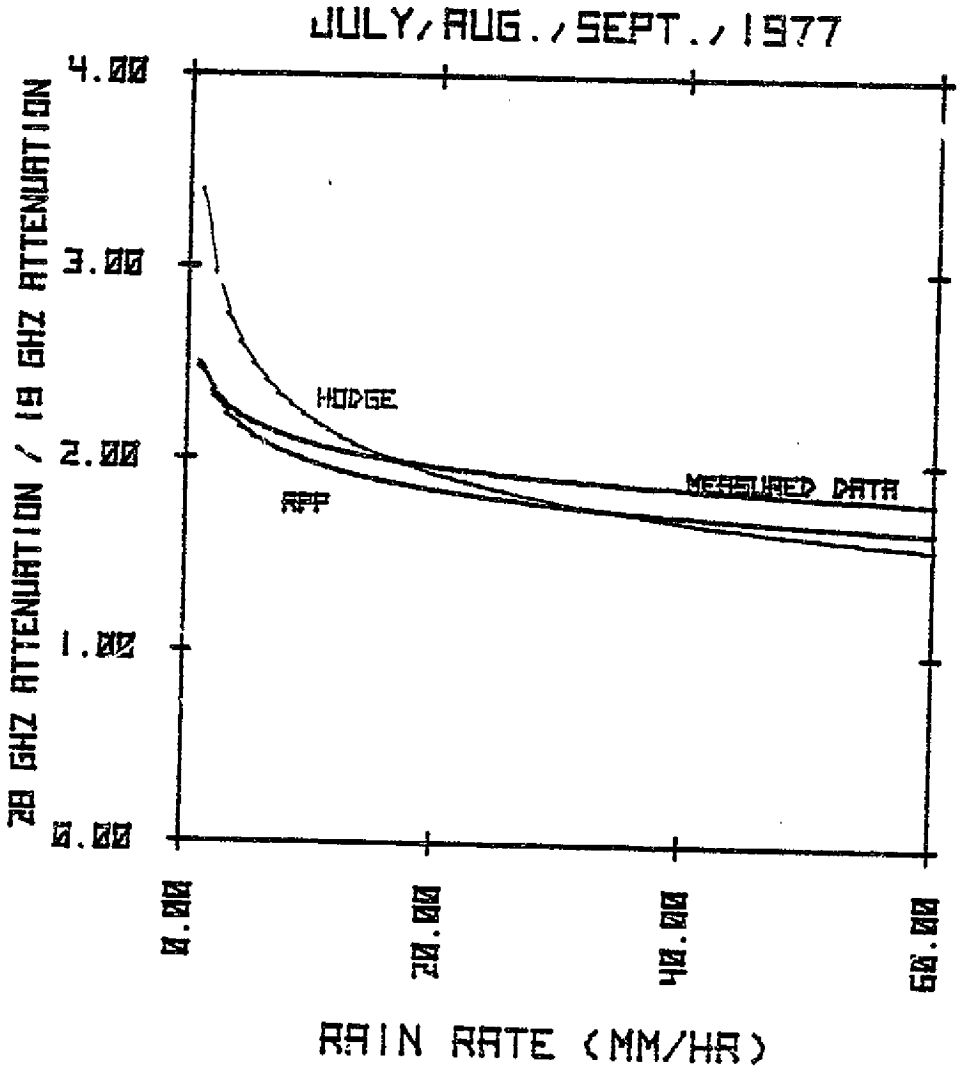

ORIGINAL PAGE IS
OF POOR QUALITY

Figure 4.4-5. Theoretical attenuation scaling, comparison of the Hodge and the scattering model formulations to measured data.

4.4.2 Isolation

Frequency scaling of isolation is more complicated than scaling attenuation. Isolation is very sensitive to changes in rain conditions and as a result significant scatter in isolation occurs. Isolation measurements are also very sensitive to antenna polarization parameters and tracking errors. As a consequence of the large variation in isolation for a single frequency, the scaling of isolation presents a difficult problem to communications engineers, researchers and experimenters.

For a particular set of system parameters, the scattering model can predict the frequency dependence of *mean* isolation. Figure 4.4-6 illustrates the frequency dependence of mean isolation for the system parameters of the VPI&SU earth station. The data presented in Fig. 4.4-6 can be represented with equations of the form

$$I_{m_2} = t\, I_{m_1}^{\,w} \quad \text{dB} \tag{4.4-4}$$

where I_{m_i} is the mean isolation in dB for the i^{th} frequency. The symbols t and w are constants containing the effects of the particular system parameters (canting angle, elevation angle, rain extent, etc.) on mean isolation. These values are tabulated in Table 4.4-3 for the VPI&SU experimental system. Although the data in Fig. 4.4-6 are presented without experimental verification, an insight into isolation scaling has been obtained.

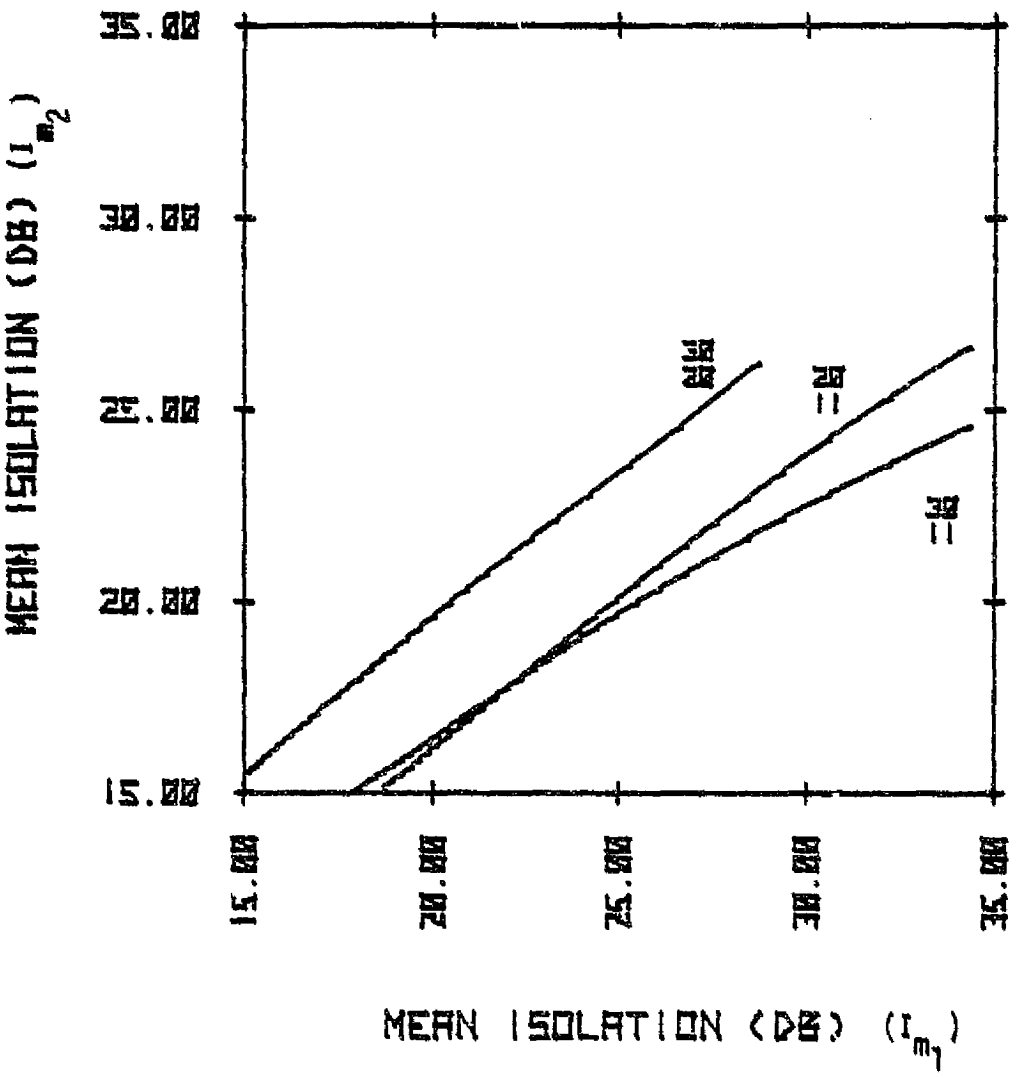

ORIGINAL PAGE IS
OF POOR QUALITY

Figure 4.4-6. Theoretical mean isolation versus mean isolation for 11, 20, and 30 GHz.

Table 4.4-3. Power curve fits to isolation versus isolation data presented in Fig. 4.4-6 ($15 \leq I_{m_i} \leq 40$)

Frequency Ratio	t	w	r^2
30/20	1.7238	0.8107	1.00
30/11	1.6371	0.7707	1.00
20/11	0.9642	0.9416	1.00

CHAPTER V

SUMMARY AND CONCLUSIONS

The effects of rain on millimeter wave propagation will influence the future design of satellite communications systems. Therefore, it is necessary to predict the impact of precipitation on satellite communications system performance prior to the specification of system parameters. To this end a theoretical model has been developed to predict the degradation in system performance due to precipitation. A new deterministic model has been presented that models an inhomogeneous rain by discretizing the rain into several piecewise homogeneous rain cells. The scattering properties of each homogeneous rain cell are described by effective scattering coefficients. These coefficients describe the changes in polarization, attenuation and phase shift that an incident field experiences as it propagates through an ensemble of particles with a distribution of particle type (rain or ice), particle shape, particle size, particle density, and particle orientation. A frequency independent synthetic storm algorithm also was developed to model the effects of nonuniform rain rates present on satellite communications links. As a result, the *scattering model* can predict accurately the effects of rain on a millimeter wave communications link for a variety of frequencies, elevation angles and locations.

After a detailed derivation of the scattering model, the predictions of the associated *Rain Propagation Prediction program* were compared to available measured data. The comparison of theory to experimental data covered a wide range of system parameters and

various site locations. Excellent agreement was obtained.

Although the scattering model has predicted accurately the observed rain effects on satellite link performance at various ground terminals, more experimental data are needed to further refine the synthetic storm algorithm. Data describing the distribution of canting angles and particle shape along the entire rain extent also would lead to further refinements of the physical modeling of the rain conditions present on a satellite link. After these refinements and further verification of the model with a more extensive experimental data base, the scattering model will provide the system design engineer with a low cost, reliable model to predict the effects of weather on arbitrary satellite communications systems.

CHAPTER VI

APPENDIX

6.1 Derivations

6.1.1 Derivation of the Generalized Single Particle Scattering Coefficients

In the development of the scattering model, a generalized single particle scattering coefficient was used to allow particles within a thin rain slab to have any arbitrary orientation. Thus, a canting angle distribution within the rain slab is possible. The derivation of the generalized single particle scattering coefficients is straight-forward and based on simple geometric principles [11].

Consider Fig. 6.1-1. An incident field $\dot{E}_x^i$ aligned with the arbitrary x-axis is incident on an arbitrary oblate particle canted at an angle θ with respect to the x-axis. $\dot{E}_x^i$ is decomposed into components $\dot{E}_v^i$ and $\dot{E}_h^i$ along the principal axes (v, h) of the oblate particle; respectively,

$$\begin{aligned} \dot{E}_v^i &= \dot{E}_x^i \sin\theta \\ \dot{E}_h^i &= \dot{E}_x^i \cos\theta \quad . \end{aligned} \tag{6.1-1}$$

$\dot{E}_v^i$ and $\dot{E}_h^i$ are scattered by the oblate particle producing $\dot{E}_v^s$ and $\dot{E}_h^s$,

$$\begin{aligned} \dot{E}_v^s &= f_v \dot{E}_v^i = f_v \dot{E}_x^i \sin\theta \\ \dot{E}_h^s &= f_h \dot{E}_h^i = f_h \dot{E}_x^i \cos\theta \end{aligned} \tag{6.1-2}$$

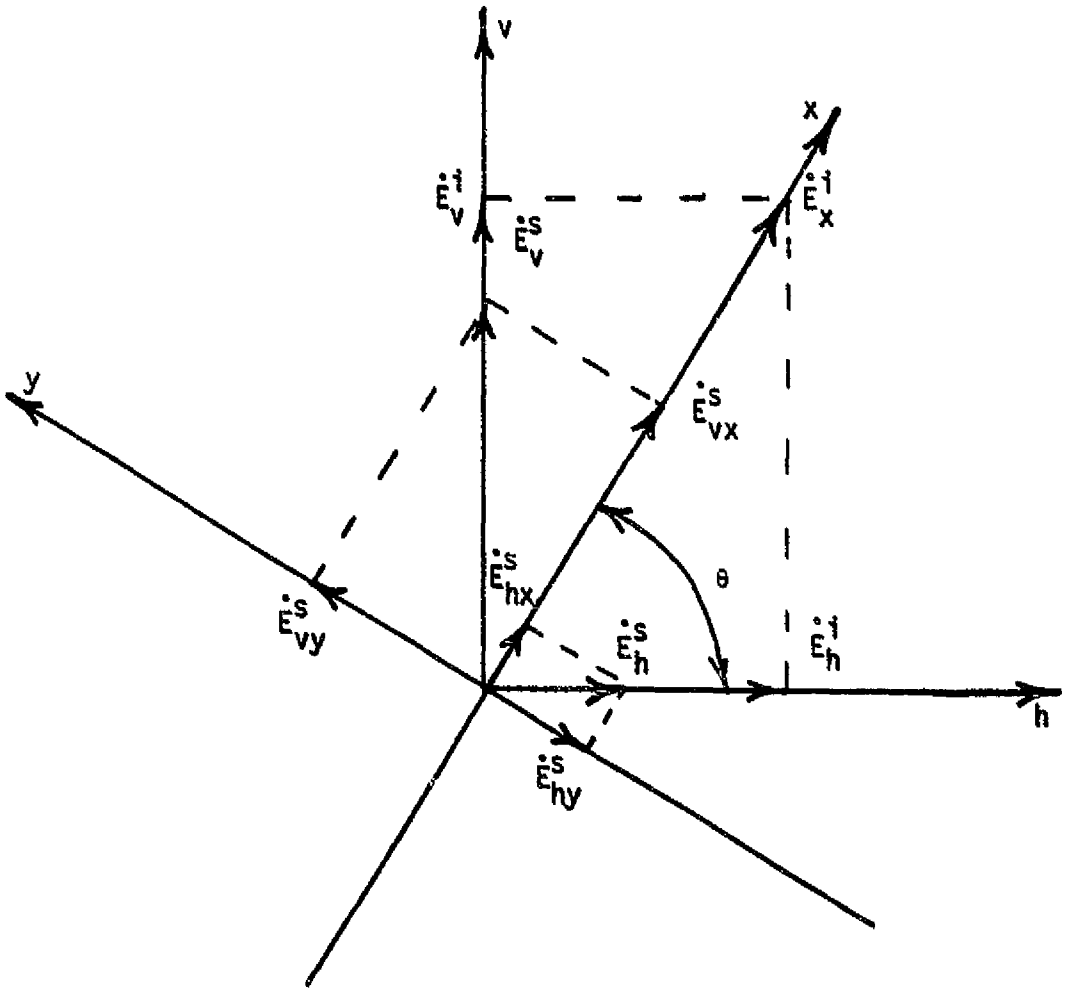

Figure 6.1-1. Geometry used in the derivation of the generalized single particle scattering coefficients.

where f_v and f_h are the complex scattering coefficients of the particle minor and major axis, respectively (f_v and f_h are defined in Sec. 3.1). $\dot{E}^s_v$ and $\dot{E}^s_h$ have components $\dot{E}^s_{vx}$ and $\dot{E}^s_{hx}$ along the x-axis and components $\dot{E}^s_{vy}$ and $\dot{E}^s_{hy}$ along the y-axis as a result of the rotation of the incident field by the oblate particle and are given by

$$\begin{aligned}
\dot{E}^s_{vx} &= \dot{E}^s_v \sin\theta = f_v \dot{E}^i_x \sin^2\theta \\
\dot{E}^s_{hx} &= \dot{E}^s_h \cos\theta = f_h \dot{E}^i_x \cos^2\theta \\
\dot{E}^s_{vy} &= \dot{E}^s_v \cos\theta = f_v \dot{E}^i_x \sin\theta\cos\theta \\
\dot{E}^s_{hy} &= \dot{E}^s_h \sin\theta = f_h \dot{E}^i_x \sin\theta\cos\theta \quad .
\end{aligned} \tag{6.1-3}$$

The total scattered field component along the x-axis is

$$\begin{aligned}
\dot{E}^s_x &= \dot{E}^s_{vx} + \dot{E}^s_{hx} \\
&= \dot{E}^i_x \{f_v \sin^2\theta + f_h \cos^2\theta\} \quad .
\end{aligned} \tag{6.1-4}$$

The total scattered field component along the y-axis is

$$\begin{aligned}
\dot{E}^s_y &= \dot{E}^s_{vy} - \dot{E}^s_{hy} \\
&= \dot{E}^i_x (f_v - f_h) \sin\theta\cos\theta \quad .
\end{aligned} \tag{6.1-5}$$

The scattering coefficient f_{xx} is defined as the ratio of $\dot{E}^s_x$ to $\dot{E}^i_x$,

$$f_{xx} = \frac{\dot{E}^s_x}{\dot{E}^i_x} = f_v \sin^2\theta + f_h \cos^2\theta \quad .$$

The scattering coefficient f_{xy} is defined as the ratio of $\dot{E}^s_y$ to $\dot{E}^i_x$,

$$f_{xy} = \frac{\dot{E}^s_y}{\dot{E}^i_x} = (f_v - f_h) \sin\theta \cos\theta \quad . \tag{6.1-6}$$

The coefficients f_{yx} and f_{yy} are obtained by replacing θ in Eqs. (6.1-5) and (6.1-6) with θ_c where

$$\theta_c = \theta - 90°$$

and then

$$f_{yx} = f_{xy} = (f_v - f_h) \sin\theta \cos\theta \tag{6.1-7}$$

and

$$f_{yy} = f_v \cos^2\theta + f_h \sin^2\theta \quad . \tag{6.1-8}$$

Equations (6.1-5), (6.1-6), (6.1-7) and (6.1-8) define the generalized single particle scattering coefficients as given in Eq. (3.1-1).

6.1.2 Evaluation of $\Sigma^{N_{i,k}} g_m$

Before the effective scattering coefficients of Eq. (3.2-13) can be determined, the evaluation of the summation $\Sigma^{N_{i,k}} g_m$ is necessary. The summation extends over all the particles within the finite rain slab of Fig. 3.2-1 in the i^{th} size interval and the k^{th} orientation interval. If the particles in the i^{th} and k^{th} intervals are numerous, the summation can be expressed as an integral,

$$\Sigma^{N_{i,k}} g_m = n_{i,k} \int_{Vol} g_m \, d_V = n_{i,k} \int_0^{\Delta\ell} \int_0^{2\pi} \int_0^{\infty} g_m \, \rho d\rho d\rho dz \tag{6.1-9}$$

where $n_{i,k}$ is the number of particles per unit volume in the i^{th} size

interval and the k^{th} orientation interval. Performing the integral yields

$$\sum_{g_m}^{N_{i,k}} = \eta_{i,k} \int_0^{\Delta\ell} \int_0^{2\pi} \int_0^{\infty} \frac{1}{z} e^{-j\, k_o\, \rho^2/2z}\, \rho d\rho d\phi dz$$

$$= 2\pi\, n_{i,k} \int_0^{\Delta\ell} \int_0^{\infty} \frac{1}{z} \{\rho\, e^{-j\, k_o\, \rho^2/2z}\}\, d\rho dz$$

$$= 2\pi\, n_{i,k} \int_0^{\Delta\ell} \frac{1}{z} \{-j\, z/k_o\}\, dz$$

$$= -j\, \frac{2\pi\, \Delta\ell}{k_o}\, n_{i,k}$$

$$= -j\, \lambda \Delta\ell\, n_{i,k} \qquad (6.1\text{-}10)$$

where the following indefinite integral [45] was used:

$$\int_0^{\infty} x\, e^{-r^2 x^2}\, dz = \frac{1}{2r^2} \quad .$$

Equation (6.1-10) is the result given in Eq. (3.2-7).

6.1.3 Derivation of N_V

N_V is the total number of raindrops per unit volume within a thin rain slab and is a function of rain rate and the distribution of drop size. Since drops of different size fall with different terminal velocities, they will contribute differently to the total measured ground rain rate. To account for this difference consider a time interval Δt over which all drops striking the ground will be summed to obtain the total rain accumulation. The drops in the drop size inter-

val $\bar{a}$ to $\bar{a} + d\bar{a}$ have a terminal velocity of $v_T(\bar{a})$ given below:

$$v_T(\bar{a}) = 4.6 \quad 2\bar{a} \qquad \text{m/sec} \tag{6.1-11}$$

where $\bar{a}$ is in mm [46]. The height above the ground corresponding to the height of the last drops in the time interval Δt to strike the ground is

$$h(\bar{a}) = v_T(\bar{a})\Delta t \quad \text{m}$$

$$= 6.5054\sqrt{\bar{a}}\ \Delta t \quad \text{m} \tag{6.1-12}$$

where $\bar{a}$ is in mm, v_T is in m/sec and h is in m. The volume of water accumulated on top of the ground per unit area of ground surface in the time interval Δt due to drops in the size interval $\bar{a}$ to $\bar{a} + d\bar{a}$ is then

$$\text{Vol}/_{m^2}(\bar{a}) = h(\bar{a})\ \frac{4\pi}{3}\ (\bar{a})^3\ n(\bar{a})d\bar{a} \tag{6.1-13}$$

where $n(\bar{a})$ is the number of drops per cubic meter of space in the size class $\bar{a}$ to $\bar{a} + d\bar{a}$. This volume of water equals the rain rate for the drops with drop size $\bar{a}$ to $\bar{a} + d\bar{a}$, $RR(\bar{a})d\bar{a}$, times the time interval. Using Eq. (6.1-12) in Eq. (6.1-13) and eliminating Δt yields

$$RR(\bar{a})d\bar{a} = v_T(\bar{a})\ \frac{4\pi}{3}\ (\bar{a})^3\ n(\bar{a})\ d\bar{a}\ . \tag{6.1-14}$$

The total rain rate is found by summing over all drop size contributions,

$$RR = \int RR(\bar{a})\ d\bar{a}$$

$$= \int_0^\infty v_T(\bar{a})\ \frac{4\pi}{3}\ (\bar{a})^3\ n(\bar{a},\ d\bar{a}\ . \tag{6.1-15}$$

Using the modified Laws and Parsons drop size distribution discussed in Sec. 3.6 gives

$$RR = \frac{4\pi}{3} (6.5054) N_V \int_0^\infty (\bar{a})^{7/2} s(\bar{a}) d\bar{a}$$

$$= \frac{4\pi}{3} (6.5054) N_V \{4(2^{9/2} - 1)(1/9 - 1/11) a_m^{7/2}\}$$

$$= 47.624 N_V a_m^{7/2} \text{ m/s} \qquad (6.1\text{-}16)$$

where a_m is the modal drop radius in mm. Rain rate should be in units of mm/hr, but the above expression arose from terminal velocity in m/s, drop volume in mm^3 and number density in per m^3 of space. Thus, to convert Eq. (6.1-16) into units of mm/hr,

$$RR = 47.624 N_V a_m^{7/2} \left\{\frac{10^3 \text{ mm}}{\text{m}}\right\} \left\{\frac{3600 \text{ s}}{\text{hr}}\right\} \left\{\frac{10^{-3} \text{ m}}{\text{mm}}\right\}^3$$

$$= 0.17144 N_V a_m^{7/2} \quad \text{mm/hr} \quad . \qquad (6.1\text{-}17)$$

To find the total number of raindrops per unit volume, the inverse of Eq. (3.6-17) yields

$$N_V = 5.8327 (a_m)^{-7/2} \qquad (6.1\text{-}18)$$

which is the result given in Eq. (3.6-4).

6.1.4 Derivation of Single Ice Particle Scattering Coefficients

In the derivation of the single ice particle scattering coefficients, the theory of Rayleigh scattering can be used for frequencies up to 30 GHz [30]. Assume that an incident electric field is propaga-

ting in the $\hat{z}$ direction and is incident on an ice particle in the hv plane as shown in Fig. 6.1-2. The ice particle can be spherical, oblate spheroidal, or prolate spheroidal in shape. A dipole moment is induced in each of the principal planes of the particle. The assumption is made that the size of the particle is sufficiently small to ignore higher multipole moments. Each of the components of the incident field along the principal planes (h, v) are considered to act separately in the excitation of the dipole moment in the respective component direction.

Battan [47] defines the dipole moments in terms of particle shape as follows:

$$m_h = 4\pi\, \varepsilon_o\{g,\, g'\}\dot{E}_h$$
$$m_v = 4\pi\, \varepsilon_o\{g,\, g'\}\dot{E}_v \qquad (6.1\text{-}19)$$

where g is a complex number describing the effects of particle geometry on the dipole moment associated with the particle's axis of revolution and g' is associated with the orthogonal axis. The definitions of g and g' are given below:

$$g = \frac{\varepsilon_{RO}^2\, V_p(\varepsilon_R^2 - 1)}{4\pi + (\varepsilon_R^2 - 1)P} \qquad (6.1\text{-}20)$$

$$g' = \frac{\varepsilon_{RO}^2\, V_p(\varepsilon_R^2 - 1)}{4\pi + (\varepsilon_R^2 - 1)(2\pi - P/2)} \qquad (6.1\text{-}21)$$

where for a prolate spheroid,

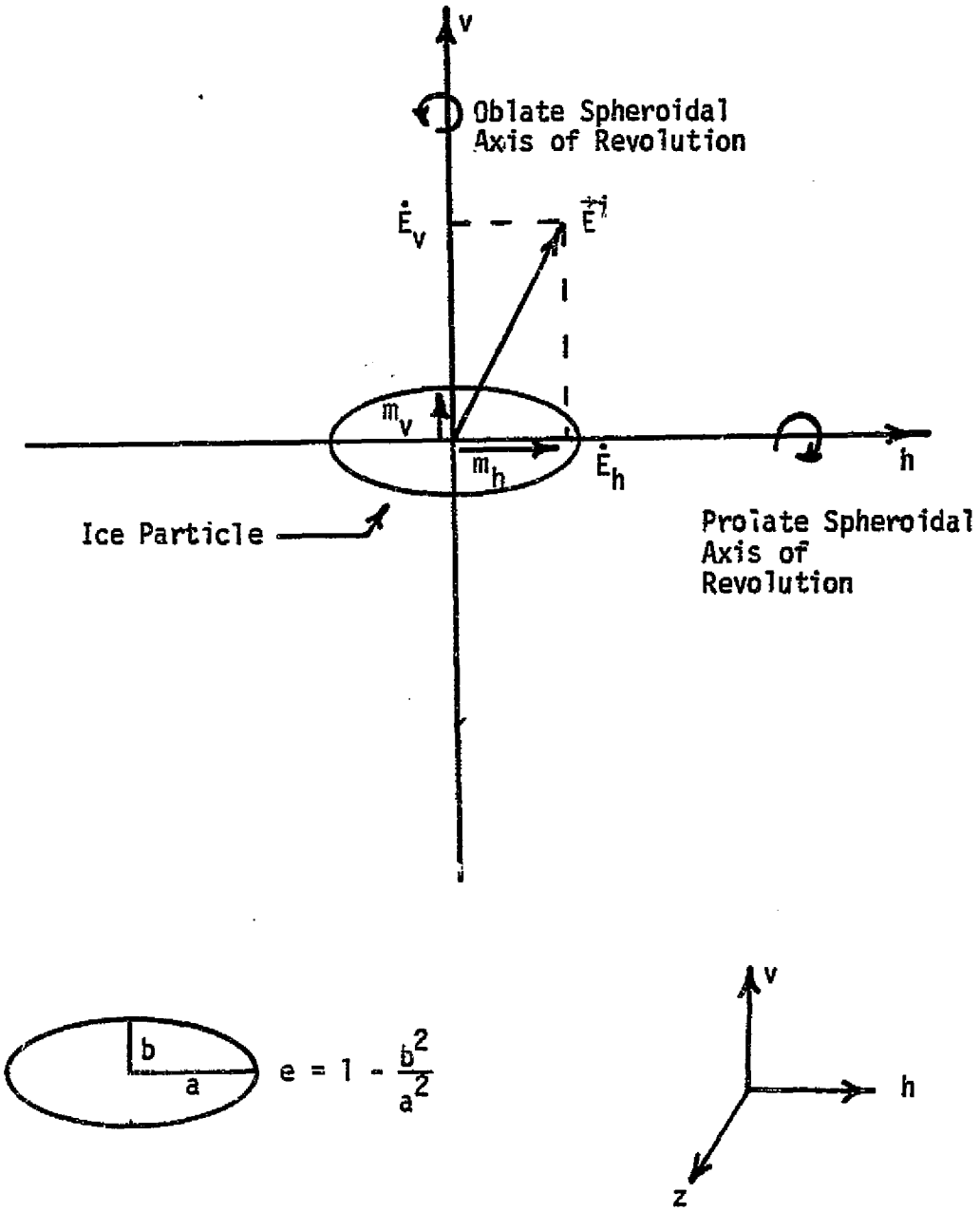

Figure 6.1-2. Geometry used in the derivation of the single ice particle scattering coefficients.

$$P_{PRO} = 4\pi \frac{(1 - e^2)}{e^2} \left(\frac{1}{2e} \ln\left(\frac{1 + e}{1 - e}\right) - 1\right) \qquad (6.1\text{-}22)$$

for an oblate spheroid,

$$P_{OBL} = \frac{4\pi}{e^2} \left(1 - \sqrt{\frac{1 - e^2}{e^2}} \sin^{-1} e\right) \qquad (6.1\text{-}23)$$

and for a spherical particle,

$$P = \frac{4\pi}{3} \quad . \qquad (6.1\text{-}24)$$

The various symbols appearing above are defined below:

ε_{RO}: complex refractive index of air $(\varepsilon_{RO} = 1)$

ε_R : complex refractive index of ice [47]
$(\varepsilon_R = 1.78 - j\ 0.0024$ @ 0° C)*

V_p : volume of the ice particle

e : eccentricity $(e = 1 - b^2/a^2)$.

If the eccentricity is close to one, i.e., a long narrow prolate spheroid or a flat platelike oblate spheroid Eq. (6.1-22) and Eq. (6.1-23) reduce to

$$P_{PRO} = 0$$
$$P_{OBL} = 4\pi \quad . \qquad (6.1\text{-}25)$$

Using Eq. (6.1-24) and Eq. (6.1-25) in Eq. (6.1-20) and Eq. (6.1-21)

---

* Haworth, McEwan, and Watson [30] evidently have a misprint in their publication.

and the results in Eq. (6.1-19) yield for the various particle shapes:

Prolate

$$m_h = \frac{1}{3}\bar{a}^3(\epsilon_R^2 - 1)\, 4\pi\, \epsilon_o\, \dot{E}^i_h$$
$$m_v = \frac{2}{3}\bar{a}^3 \frac{(\epsilon_R^2 - 1)}{(\epsilon_R^2 + 1)} 4\pi\, \epsilon_o\, \dot{E}^i_v \qquad (6.1\text{-}26)$$

Oblate

$$m_h = \frac{1}{3}\bar{a}^3(\epsilon_R^2 - 1)\, 4\pi\, \epsilon_o\, \dot{E}^i_h$$
$$m_v = \frac{1}{3}\bar{a}^3(1 - 1/\epsilon_R^2)\, 4\pi\, \epsilon_o\, \dot{E}^i_v \qquad (6.1\text{-}27)$$

Spherical

$$m_{h,v} = \bar{a}^3 \frac{(\epsilon_R^2 - 1)}{(\epsilon_R^2 + 2)}\, 4\pi\, \epsilon_o\, \dot{E}^i_{h,v} \qquad (6.1\text{-}28)$$

where

$\bar{a}$ is the equivolumetric particle radius in meters.

Now consider the radiation properties of an electric dipole. From Stratton [48] the radiated electric field is

$$\vec{E}^{RAD}(z) = \frac{k_o^2}{4\pi\, \epsilon_o} [\hat{z} \times (\vec{m} \times \hat{z})] \frac{e^{-jk_o z}}{z} \qquad (6.1\text{-}29)$$

cr,

$$E_h^{RAD} = \frac{k_o^2}{4\pi\,\varepsilon_o} m_h \frac{e^{-jk_o z}}{z}$$

$$E_v^{RAD} = \frac{k_o^2}{4\pi\,\varepsilon_o} m_v \frac{e^{-jk_o z}}{z} \quad . \tag{6.1-30}$$

Comparing Eq. (6.1-30) to the definition of the scattered field as defined by the scattering model, the single particle scattering coefficients can be determined as seen below:

$$\dot{E}^s_{h,v}(z) = \dot{E}^i_{h,v} f_{h,v} \frac{e^{-jk_o z}}{z} = \dot{E}^{RAD}_{h,v}(z)$$

$$= \frac{k_o^2}{4\pi\,\varepsilon_o} m_{h,v} \frac{e^{-jk_o z}}{z} \quad .$$

So,

$$f_{h,v} = \frac{k_o^2}{4\pi\,\varepsilon_o} m_{h,v}\, 1/\dot{E}^i_{h,v} \quad . \tag{6.1-31}$$

Using Eqs. (6.1-26), (6.1-27), and (6.1-28) in (6.1-31) yield the single particle scattering coefficients for each particle shape and are given below:

Prolate

$$f_h^{PRO} = \frac{\{4\pi\,\bar{a}^3\}}{3\lambda^2}\{6.812211 - j\,0.026842\}$$

$$f_v^{PRO} = \frac{\{4\pi\,\bar{a}^3\}}{3\lambda^2}\{3.268519 - j\,0.006179\} \tag{6.1-32}$$

Oblate

$$f_h^{OBL} = \frac{\{4\pi\,\bar{a}^3\}}{3\lambda^2}\{6.812211 - j\,0.026842\}$$

$$f_v^{OBL} = \frac{\{4\pi\ \bar{a}^3\}}{3\lambda^2}\ \{2.150047 - j\ 0.002674\} \qquad (6.1\text{-}33)$$

Spherical

$$f^{SPH} = \{\frac{4\pi\ \bar{a}^3\}}{3\lambda^2}\ \{3.95417 - j\ 0.009044\}\ . \qquad (6.1\text{-}34)$$

Equations (6.1-32), (6.1-33), and (6.1-34) define the *single* ice particle scattering coefficients. By summing over all the particle radii within an ice particle concentration, a general scattering coefficient can be obtained. Define

$$F_{h,v} = \sum_{\bar{a} = \bar{a}_1}^{\bar{a}_N} n(\bar{a})\ f_{h,v}(\bar{a}) \qquad (6.1\text{-}35)$$

where $n(\bar{a})$ is the number of particles with radius $\bar{a}$. Since $f_{h,v}$ is directly proportional to the volume of the particular particle size class and inversely proportional to λ^2,

$$F_{h,v} = \frac{V}{\lambda^2} A_{h,v} \qquad (6.1\text{-}36)$$

where V is the *total* volume of ice in a cubic meter of air and $A_{h,v}$ is a complex constant independent of frequency given in Table 3.6-1. This result along with the general scattering coefficient formulation, Eq. (3.1-1), and the elevation angle formulation presented in 3.6 yield Eq. (3.6-12).

6.2 The Rain Propagation Prediction Program (RPP)

6.2.1 General Description

The *Rain Propagation Prediction program* uses the scattering model and the synthetic storm algorithm to predict attenuation, isolation, and phase as a function of rain rate for a given set of system and rain parameters. A block diagram of the RPP program is found in Fig. 6.2-1. The single input format of Fig. 6.2-2 facilitates changing the system and rain parameters. Although the lack of data has caused certain restrictions to have been placed on the particle distributions along the rain extent, the scattering model and thus the RPP program can model an arbitrary inhomogeneous rain given the appropriate input parameters. The input parameters will be discussed in more detail in Sec. 6.2-2.

After reading the input parameters and calculating the clear weather isolation and phase, the RPP program prints an information header at the beginning of the output section as seen in Fig. 6.2-3. The rain conditions for each cell are then computed and the scattering matricies as defined by Eq. (3.3-1) are determined. After computing the wave exiting the rain medium and the wave-antenna interaction, the RPP program outputs rain rate, attenuation, isolation and phase data as seen in Fig. 6.2-4. Since curve fits to theoretical data are often useful, the RPP program outputs curve fit data for various combinations of rain rate, attenuation, and isolation data as seen in Fig. 6.2-5.

ORIGINAL PAGE IS
OF POOR QUALITY

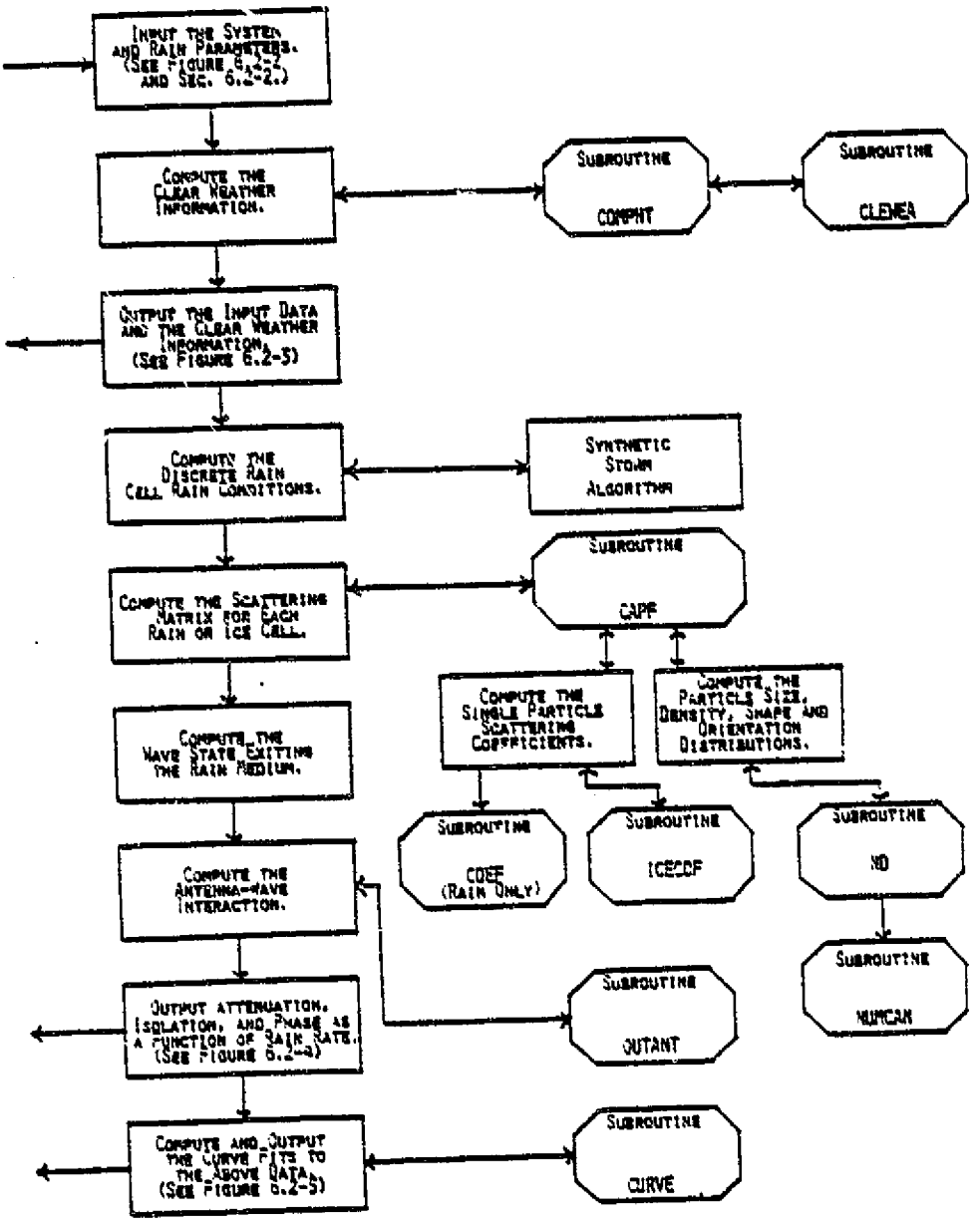

ORIGINAL PAGE IS
OF POOR QUALITY

Figure 6.2-1. Block diagram of the rain propagation prediction program (RPP).

```
11.0
33.0
1000010000 1000
   10   10   10
    3   60    3
 -43.35   0.00
 -44.01   0.00  44.11  90.00
 0.0 0.0-.66-.66-.66-.66-.66-.66-.66-.66
 1.0 1.0 1.0 1.0 1.0 1.0 1.0 1.0 1.0 1.0
 0.6 0.6 0.6 0.6 0.6 0.6 0.6 0.6 0.6 0.6
12.012.012.0[illegible].012.012.012.012.012.012.0
  0  0  0  0  0  0  0  0  0  0
    0
```

ORIGINAL PAGE IS
OF POOR QUALITY

Figure 6.2-2. Sample input data to the rain propagation prediction program (RPP).

```
***** RAIN PROPAGATION PREDICTION PROGRAM (RPP) *******

**********************************************************

THE DOWNLINK PROPAGATION FREQUENCY IS  11.0  GHZ
THE LOOK ANGLE, BETA, IS  33.0  DEGREES

**********************************************************

***** PROGRAM PARAMETERS *****

DO LOOP PARAMETERS
   TYPE          START     STOP      INCREMENT
1) RAIN EXTNT   10000      10000      1000
2) CANT ANGLE      10         10        10
3) RAIN RATE        3         60         3

BINNED COEFFICIENTS

             1     2     3     4     5     6     7     8     9     10
RAIN RATE   0.0   0.0  -0.7  -0.7  -0.7  -0.7  -0.7  -0.7  -0.7  -0.7
CANT ANGL   1.0   1.0   1.0   1.0   1.0   1.0   1.0   1.0   1.0   1.0
FRAC OBLT   0.6   0.6   0.6   0.6   0.6   0.6   0.6   0.6   0.6   0.6
SIGMA      12.0  12.0  12.0  12.0  12.0  12.0  12.0  12.0  12.0  12.0
ICE           0     0     0     0     0     0     0     0     0     0

***** CLEAR WEATHER INFORMATION *****

THE POLARIZATION PARAMETER EPSILON FOR THE INCIDENT WAVE IS                  -43.35  DEGREES
THE POLARIZATION PARAMETER TAU FOR THE INCIDENT WAVE  IS                      0.0   DEGREES
THE POLARIZATION PARAMETER EPSILON FOR THE CO ANTENNA POLARIZATION STATE IS   -44.01  DEGREES
THE POLARIZATION PARAMETER TAU FOR THE CO ANTENNA POLARAZATION STATE IS        0.0   DEGREES
THE POLARIZATION PARAMETER EPSILON FOR THE CROSS ANTENNA POLARIZATION STATE IS  44.11  DEGREES
THE POLARIZATION PARAMETER TAU FOR THE CROSS ANTENNA  STATE IS                90.00  DEGREES
THE CLEAR WEATHER ISOLATION REFERENCED TO THE ANTENNA PORTS IS                 37.55  DB
THE CLEAR WEATHER PHASE DIFFERENCE                                           -0.01  DEGREES
```

ORIGINAL PAGE IS
OF POOR QUALITY

Figure 6.2-3. Information header section for the output of the rain propagation prediction program corresponding to the input data of Fig. 6.2-2.

THE RAIN EXTENT IS 10000 METERS

THE MEAN ANGLE BETWEEN THE Y-AXIS AND THE DROP MINOR AXIS (THETA) IS 10 DEGREES

********** SCATTERING MODEL **********

RAIN RATE (MM/HR)	ATTEN (DB)	ISOL (DB)	PHASE (DEG)
3.00	1.95	31.83	299.96
6.00	2.90	29.51	290.61
9.00	3.73	27.80	285.81
12.00	4.39	26.63	283.15
15.00	5.03	25.61	281.28
18.00	5.66	24.68	279.79
21.00	6.21	23.94	278.72
24.00	6.76	23.24	277.74
27.00	7.25	22.66	276.98
30.00	7.73	22.12	276.30
33.00	8.20	21.60	275.65
36.00	8.67	21.11	275.09
39.00	9.13	20.66	274.59
42.00	9.61	20.20	274.07
45.00	10.07	19.76	273.60
48.00	10.51	19.37	273.19
51.00	10.94	19.01	272.82
54.00	11.34	18.68	272.50
57.00	11.77	18.32	272.12
60.00	12.20	17.98	271.76

ORIGINAL PAGE IS
OF POOR QUALITY

Figure 6.2-4. Rain propagation prediction program output, attenuation, isolation and phase as a function of rain rate corresponding to the input data of Fig. 6.2-2.

ORIGINAL PAGE IS
OF POOR QUALITY

CURVE FITS TO ABOVE DATA

	CURVE TYPE	ASSOCIATED EQUATION	A	B	R**2
ATTEN VS RR	POWER	ATTEN = A*RR**B	0.9525	0.6197	0.9994
ISOL VS RR	LOG	ISOL = A+B*LN(RR)	38.4404	-4.9078	0.9888
ISOL VS ATTEN	LOG	ISOL = A+B*LN(ATTEN)	38.0867	-7.9350	0.9933

Figure 6.2-5. Rain propagation prediction program output, curve fits to the data in Fig. 6.2-4.

6.2.2 RPP Users Guide

The RPP program was designed to provide an efficient tool to predict the effects of precipitation on satellite communications system performance. The RPP program is written in the FORTRAN programming language, and the program listing is found in Sec. 6.2.3. This section explains the steps in the operational procedure of the RPP program. Each step corresponds to a line of input data in Fig. 6.2-2.

Step 1

Input the operating frequency in GHz in an F5.1 format.*

Step 2

Input the system elevation angle in degrees in an F5.1 format.

Step 3

Input the effective physical rain extent (L) *do loop* parameters in meters, *LSTRT*, *LSTOP*, and *LINC*. The input format is I5. The *do loop* parameters allow finer control over the rain extent parameter. To implement the synthetic storm algorithm consult Fig. 3.6-5.

---

* The scattering coefficients f_v and f_h are limited to 11.0, 14.0, 20.0, and 30.0 GHz. To increase the frequency selection, curve regressions for published f_v and f_h coefficients at other frequencies are easily obtained and the RPP program is easily modified.

Step 4

Input the mean canting angle ($\bar{\theta}_\mu$) *do loop* parameters *ANSTRT*, *ANSTOP*, and *ANINC* in degrees {$|\bar{\theta}_\mu| < 45°$}. The format is I5.

Step 5

Input the rain rate do loop parameters *RRSTRT*, *RRSTOP*, and *RRINC* in mm/hr {RR < 250 mm/hr}. The format is I5.

Step 6

Input the clear weather wave polarization state parameters ε_w and τ_w in degrees. The format is F7.2.

Step 7

Input the co and cross antenna polarization state parameters ε_{co}, τ_{co}, ε_{cross} and τ_{cross} in degrees. The format is F7.2.

Step 8

Input the x_i coefficients of the synthetic storm algorithm for each rain cell. To model a uniform rain path $x_{1\to10} = 0$. *Note that cell one is closest to the receive antenna.* The format is F4.1.

Step 9

If a distribution of mean canting angles is desired along

the propagation path, input the multiplicative factors for each *rain* cell $(\overline{\theta}_{\mu_i} = B_i \overline{\theta}_{\mu_1})$. If a uniform distribution along the rain path is desired $B_{1\rightarrow 10} = 1.0$. The format is F4.1.

Step 10

Input the *fraction* of oblate raindrops C_i in each *rain* cell. The format is F4.1.

Step 11

Input the standard deviation of the canting angle distribution of σ_i of each *rain* cell in degrees. The format is F4.1.

Step 12

Input a "0" to indicate a rain cell or input a "1" to indicate an ice cell for each cell along the propagation path. For an ice cell, steps 9, 10 and 11 are overridden and the assumptions of Sec. 3.6.5 apply. The format is I3.

Step 13

Input a "0" for a downlink. Input a "1" for an uplink, The format is I5.

By controlling steps 1 through 13, a wide range of system and rain parameters can be modeled and their effects on the performance

of an arbitrary satellite communications link can be determined.

```
C                                                                       RPP00010
C                          6.2.3  RPP Program Listing                   RPP00020
C                                                                       RPP00030
C***********************************************************          RPP00040
C*                                                                      RPP00050
C*    RAIN PROPAGATION PREDICTION PROGRAM (RPP)                         RPP00060
C*                                                                      RPP00070
C*    THIS PROGRAM OUTPUTS THEORETICAL RAIN PROPAGATION                 RPP00080
C*    DATA (ATTENUATION, ISOLATION, AND PHASE) FOR A                    RPP00090
C*    VARIETY OF FREQUENCIES, ELEVATION ANGLES AND LOCATIONS            RPP00100
C*    AS A FUNCTION OF GROUND RAIN RATE.                                RPP00110
C*    THE INPUT FORMAT ALLOWS THE RAIN PATH TO BE SUBDIVIDED            RPP00120
C*    INTO TEN SEGMENTS WHICH PROVIDE ARBITRARY VARIATION               RPP00130
C*    OF THE PROPAGATION MEDIUM PARAMETERS.                             RPP00140
C*                                                                      RPP00150
C*    PROPAGATION MODEL:    SCATTERING MODEL                            RPP00160
C*                                                                      RPP00170
C*    PROGRAMMER:           RUSSELL R. PERSINGER                        RPP00180
C*                                                                      RPP00190
C*    CONSULTING ADVISORS: DR. WARREN L. STUTZMAN                       RPP00200
C*                         AND ROBERT E. CASTLE                         RPP00210
C*                                                                      RPP00220
C*    THIS PROGRAM WAS DEVELOPED IN PARTIAL                             RPP00230
C*    FULFILLMENT OF THE REQUIREMENTS FOR THE DEGREE                    RPP00240
C*    OF MASTER OF SCIENCE IN ELECTRICAL ENGINEERING;                   RPP00250
C*    HOWEVER, ITS DEVELOPMENT WAS SUPPORTED BY NASA                    RPP00260
C*    WITH IMPORTANT ADDITIVE SUPPORT FROM THE DEFENSE                  RPP00270
C*    COMMUNICATIONS AGENCY AND THE US ARMY RESEARCH OFFICE.            RPP00280
C*                                                                      RPP00290
C***********************************************************          RPP00300
C                                                                       RPP00310
C                                                                       RPP00320
```

```
      DIMENSION ICE(10),SIGMA(10)                                       RPP00330
      DIMENSION BIN(10)                                                 RPP00340
      DIMENSION A(10),B(10),C(10)                                       RPP00350
      DIMENSION THETA(15),RRATE(15),RRATEL(300),PE(15)                  RPP00360
      DIMENSION PHASEL(300),ISOL1(300),ATTENL(300)                      RPP00370
      DIMENSION PXX(15),PXY(15),PYX(15),PYY(15)                         RPP00380
      INTEGER LSTRT,LSTOP,LINC                                          RPP00390
      INTEGER ANSTRT,ANSTOP,ANINC                                       RPP00400
      INTEGER RRSTRT,RRSTOP,RRINC                                       RPP00410
      INTEGER BIN,DIREC                                                 RPP00420
      REAL ISOL                                                         RPP00430
      REAL ISOLI,LOKANG                                                 RPP00440
      COMPLEX MINUSJ                                                    RPP00450
      COMPLEX*16 CONSNT                                                 RPP00460
      COMPLEX*16 EXO,EYO,EXC,EYC,EXX,EYX                                RPP00470
      COMPLEX*16 FV,FH,FSPH,DIFF                                        RPP00480
      COMPLEX*16 P1,P2,P3,P4                                            RPP00490
      COMPLEX*16 EXN,EYN                                                RPP00500
      COMPLEX*16 PXX,PXY,PYX,PYY                                        RPP00510
      COMPLEX*16 FXX,FXY,FYY                                            RPP00520
      COMPLEX*16 SXX,SXY,SYX,SYY                                        RPP00530
      COMPLEX*16 LAMDA1,LAMDA2,ALPHA0,ALPHA1                            RPP00540
C                                                                       RPP00550
      COMMON/BLOC1/MINUSJ,CONV                                          RPP00560
C                                                                       RPP00570
C                                                                       RPP00580
C*************************************************************************RPP00590
C*                                                                      RPP00600
C*    FIRST THE PROGRAM READS ALL NECESSARY VARIABLE VALUES INTO        RPP00610
C*    MEMORY AND WRITES THIS INFORMATION OUT AS A HEADER AT THE         RPP00620
C*    BEGINNING OF THE OUTPUT SECTION.                                  RPP00630
C*    ALSO INCLUDED IN THIS SECTION ARE THE CLEAR WEATHER CONDITIONS    RPP00640
```

ORIGINAL PAGE IS
OF POOR QUALITY

```
C*    AND AS A RESULT, UNIT VECTORS DESCRIBING THE SYSTEM POLARIZATIONS RPP00650
C*    ARE COMPUTED.                                                    RPP00660
C*                                                                     RPP00670
C*    FREQ IS FREQUENCY IN GHZ ( 11.0, 14.0, 20.0, 30.0 ONLY )         RPP00680
C*    LOKANG IS ELEVATION ANGLE IN DEGREES (0...90)                    RPP00690
C*    LSTRT,LSTOP, AND LINC ARE THE RAIN EXTENT PARAMETERS             RPP00700
C*    IN METERS                                                        RPP00710
C*    ANSTRT, ANSTOP, AND ANINC ARE CANTING ANGLE PARAMETERS           RPP00720
C*    IN DEGREES                                                       RPP00730
C*    RRSTRT, RRSTOP, AND RRINC ARE RAIN RATE PARAMETERS IN MM/HR      RPP00740
C*    ALL EPS'S AND TAU'S ARE IN DEGREES                               RPP00750
C*    BIN ONE IS LOCATED AT THE GROUND ANTENNA                         RPP00760
C*    A(1,...10), B(1,...10), AND C(1,...10) ARE MULTIPLICATIVE FACTORS RPP00770
C*    ASSOCIATED WITH THE RAIN EXTENT BINS                             RPP00780
C*     A(I) CONTROLS THE ITH BIN RAIN RATE                             RPP00790
C*     THE VALUES OF A(I) ARE SET IN ACCORDANCE WITH THE STORM ALGORITHMRPP00800
C*     B(I) CONTROLS THE ITH BIN CANTING ANGLE                         RPP00810
C*     C(I) CONTROLS THE ITH BIN PERCENT OBLATENESS                    RPP00820
C*     THE ABSOLUTE VALUE OF THETA(I) IS ALWAYS LESS THAN 45 DEGREES   RPP00830
C*     RRATE(I) IS ALWAYS LESS THAN 250 MM/HR                          RPP00840
C*    SIGMA(I) IS THE STANDARD DEVIATION OF THE CANTING ANGLE          RPP00850
C*    DISTRIBUTION FOR THE ITH BIN. (EQUAL TO ZERO OR 10<SIGMA<50)     RPP00860
C*    IF ICE(I) IS EQUAL TO 1, THE ITH BIN IS FILLED WITH ICE PARTICLES RPP00870
C*    IF ICE(I) IS EQUAL TO 0, THE ITH BIN IS FILLED WITH RAIN         RPP00880
C*    DIREC EQUALS ONE FOR UPLINK                                      RPP00890
C*    DIREC EQUALS ZERO FOR DOWNLINK                                   RPP00900
C*                                                                     RPP00910
C*********************************************************************RPP00920
C                                                                      RPP00930
      READ(5,100) FREQ                                                 RPP00940
      READ(5,100) LOKANG                                               RPP00950
      READ(5,101) LSTRT,LSTOP,LINC                                     RPP00960
```

```
      READ(5,101) ANSTRT,ANSTOP,ANINC                                   RPP00970
      READ(5,101) RRSTRT,RRSTOP,RRINC                                   RPP00980
      READ(5,102) EPSW,TAUW                                             RPP00990
      READ(5,103) EPSC,TAUC,EPSX,TAUX                                   RPP01000
      READ(5,104) (A(I),I=1,10)                                         RPP01010
      READ(5,104) (B(I),I=1,10)                                         RPP01020
      READ(5,104) (C(I),I=1,10)                                         RPP01030
      READ(5,104) (SIGMA(I),I=1,10)                                     RPP01040
      READ(5,105) (ICE(I),I=1,10)                                       RPP01050
      READ(5,101) DIREC                                                 RPP01060
C                                                                       RPP01070
  100 FORMAT(F4.1)                                                      RPP01080
  101 FORMAT(I5,I5,I5)                                                  RPP01090
  102 FORMAT(F7.2,F7.2)                                                 RPP01100
  103 FORMAT(4(F7.2))                                                   RPP01110
  104 FORMAT(10(F4.1))                                                  RPP01120
  105 FORMAT(10I3)                                                      RPP01130
C                                                                       RPP01140
      WRITE(6,200)                                                      RPP01150
      WRITE(6,221)                                                      RPP01160
      IF(DIREC.EQ.1) WRITE(6,2031) FREQ                                 RPP01170
      IF(DIREC.EQ.0) WRITE(6,2030) FREQ                                 RPP01180
      WRITE(6,201) LOKANG                                               RPP01190
      WRITE(6,221)                                                      RPP01200
      WRITE(6,202)                                                      RPP01210
      WRITE(6,204)                                                      RPP01220
      WRITE(6,205)                                                      RPP01230
      WRITE(6,206) LSTRT,LSTOP,LINC                                     RPP01240
      WRITE(6,207) ANSTRT,ANSTOP,ANINC                                  RPP01250
      WRITE(6,208) RRSTRT,RRSTOP,RRINC                                  RPP01260
      WRITE(6,209)                                                      RPP01270
      WRITE(6,210)                                                      RPP01280
```

ORIGINAL PAGE IS
OF POOR QUALITY

```
      WRITE(6,211) (A(I),I=1,10)                                        RPP01290
      WRITE(6,212) (B(I),I=1,10)                                        RPP01300
      WRITE(6,213) (C(I),I=1,10)                                        RPP01310
      WRITE(6,2131) (SIGMA(I),I=1,10)                                   RPP01320
      WRITE(6,2132) (ICE(I),I=1,10)                                     RPP01330
      WRITE(6,214)                                                      RPP01340
      WRITE(6,215) EPSW                                                 RPP01350
      WRITE(6,216) TAUW                                                 RPP01360
      WRITE(6,217) EPSC                                                 RPP01370
      WRITE(6,218) TAUC                                                 RPP01380
      WRITE(6,219) EPSX                                                 RPP01390
      WRITE(6,220) TAUX                                                 RPP01400
C                                                                       RPP01410
  200 FORMAT(1H1,3X,'***** RAIN PROPAGATION PREDICTION PROGRAM (RPP) ***RPP01420
     1****')                                                            RPP01430
  201 FORMAT(/,3X,'THE ELEVATION ANGLE, BETA, IS  ',F4.1,2X,'DEGREES')  RPP01440
  202 FORMAT(//,3X,'***** PROGRAM PARAMETERS *****')                    RPP01450
 2031 FORMAT(//,3X,'THE UPLINK PROPAGATION FREQUENCY IS',2X,F4.1,2X,'GHZRPP01460
     1')                                                                RPP01470
 2030 FORMAT(//,3X,'THE DOWNLINK PROPAGATION FREQUENCY IS',2X,F4.1,2X,  RPP01480
     1'GHZ')                                                            RPP01490
  204 FORMAT(//,3X,'DO LOOP PARAMETERS')                                RPP01500
  205 FORMAT(/,3X,'   TYPE          START     STOP     INCREMENT')      RPP01510
  206 FORMAT(/,3X,'1) RAIN EXTNT ',I6,5X,I6,4X,I6)                      RPP01520
  207 FORMAT(/,3X,'2) CANT ANGLE ',I6,5X,I6,4X,I6)                      RPP01530
  208 FORMAT(/,3X,'3) RAIN RATE  ',I6,5X,I6,4X,I6)                      RPP01540
  209 FORMAT(//,3X,'BINNED COEFFICIENTS')                               RPP01550
  210 FORMAT(//,15X,'1',5X,'2',5X,'3',5X,'4',5X,'5',5X,'6',5X,'7',5X,'8'RPP01560
     1,5X,'9',5X,'10')                                                  RPP01570
  211 FORMAT(/,3X,'RAIN RATE',2X,10(F4.1,2X))                           RPP01580
  212 FORMAT(/,3X,'CANT ANGL',2X,10(F4.1,2X))                           RPP01590
  213 FORMAT(/,3X,'FRAC OBLT',2X,10(F4.1,2X))                           RPP01600
```

```
2131 FORMAT(/,3X,'SIGMA     ',2X,10(F4.1,2X))                                    RPP01610
2132 FORMAT(/,3X,'ICE       ',2X,10(I4,2X))                                      RPP01620
 214 FORMAT(//,3X,'***** CLEAR WEATHER INFORMATION *****')                       RPP01630
 215 FORMAT(//,3X,'THE POLARIZATION PARAMETER EPSILON FOR THE INCIDENT RPP01640
    1WAVE IS',21X,F7.2,2X,'DEGREES')                                           RPP01650
 216 FORMAT(/,3X,'THE POLARIZATION PARAMETER TAU FOR THE INCIDENT WAVE RPP01660
    1 IS',24X,F7.2,2X,'DEGREES')                                               RPP01670
 217 FORMAT(/,3X,'THE POLARIZATION PARAMETER EPSILON FOR THE CO ANTENNARPP01680
    1 POLARIZATION STATE IS',5X,F7.2,2X,'DEGREES')                             RPP01690
 218 FORMAT(/,3X,'THE POLARIZATION PARAMETER TAU FOR THE CO ANTENNA POLRPP01700
    1ARAZATION STATE IS',9X,F7.2,2X,'DEGREES')                                 RPP01710
 219 FORMAT(/,3X,'THE POLARIZATION PARAMETER EPSILON FOR THE CROSS ANTERPP01720
    1NNA POLARIZATION STATE IS',2X,F7.2,2X,'DEGREES')                          RPP01730
 220 FORMAT(/,3X,'THE POLARIZATION PARAMETER TAU FOR THE CROSS ANTENNA RPP01740
    1 STATE IS',18X,F7.2,2X,'DEGREES')                                         RPP01750
 221 FORMAT(//,3X,'**************************************************RPP01760
    1****')                                                                    RPP01770
 222 FORMAT(1H1,2X,'THE RAIN EXTENT IS  ',I5,'  METERS')                       RPP01780
 223 FORMAT(//,3X,'THE MEAN ANGLE BETWEEN THE Y-AXIS AND THE DROP MINORRPP01790
    1 AXIS (THETA) IS  ',I5,'  DEGRESS')                                       RPP01800
 224 FORMAT(////,25X,'************ SCATTERING MODEL **************', RPP01810
    1/)                                                                        RPP01820
 225 FORMAT(//,3X,'RAIN RATE (MM/HR)',5X,'ATTEN (DB)',9X,'ISOL (DB)',8XRPP01830
    1,'PHASE (DEG)',//)                                                        RPP01840
 226 FORMAT(/,10X,F6.2,11X,F6.2,12X,F6.2,11X,F7.2)                             RPP01850
 227 FORMAT(//////'   CURVE FITS TO ABOVE DATA')                               RPP01860
 228 FORMAT(///,21X,'CURVE TYPE',6X,'ASSOCIATED EQUATION',7X,'A',11X,'BRPP01870
    1',9X,'R**2')                                                              RPP01880
 229 FORMAT(//,'   ATTEN VS RR',8X,'POWER',12X,'ATTEN = A*RR**B',4X,3(FRPP01890
    18.4,4X))                                                                  RPP01900
 230 FORMAT(//,'   ISOL VS RR',10X,'LOG',12X,'ISOL = A+B*LN(RR)',3X,3(FRPP01910
    18.4,4X))                                                                  RPP01920
```

ORIGINAL PAGE IS OF POOR QUALITY

```
  231 FORMAT(//,'    ISOL VS ATTEN',7X,'LOG',10X,'ISOL = A+B*LN(ATTEN)',2RPP01930
     1X,3(F8.4,4X))                                                     RPP01940
C                                                                       RPP01950
C                                                                       RPP01960
      PI=3.14159265                                                     RPP01970
      CONV=PI/180.                                                      RPP01980
      LOKANG=LOKANG*CONV                                                RPP01990
      MINUSJ=(0.,-1.)                                                   RPP02000
C                                                                       RPP02010
      CALL COMPNT(EPSW,TAUW,EXO,EYO)                                    RPP02020
      CALL COMPNT(EPSC,TAUC,EXC,EYC)                                    RPP02030
      CALL COMPNT(EPSX,TAUX,EXX,EYX)                                    RPP02040
C                                                                       RPP02050
      EYC=DCONJG(EYC)                                                   RPP02060
      EYX=DCONJG(EYX)                                                   RPP02070
C                                                                       RPP02080
      CALL CLEWEA(EXO,EYO,EXC,EYC,EXX,EYX)                              RPP02090
C                                                                       RPP02100
C*************************************************************************RPP02110
C*                                                                      RPP02120
C*     THE REST OF THE PROGRAM USES THE  SCATTERING MODEL               RPP02130
C*     TO COMPUTE ATTENUATION, ISOLATION, AND PHASE AS A FUNCTION       RPP02140
C*     OF RAIN RATE AND OUTPUTS THEM IN AN ORGANIZED FORM.              RPP02150
C*                                                                      RPP02160
C*************************************************************************RPP02170
C                                                                       RPP02180
      IF(ANSTRT.LT.0) FLAG=1.0                                          RPP02190
      IF(ANSTRT.LT.0) ANSTOP=ANSTOP+360                                 RPP02200
      IF(ANSTRT.LT.0) ANSTRT=ANSTRT+360                                 RPP02210
C                                                                       RPP02220
      ANSTRT=ANSTRT + ANINC                                             RPP02230
      ANSTOP=ANSTOP + ANINC                                             RPP02240
```

ORIGINAL PAGE IS OF POOR QUALITY

```
C                                                                       RPP02250
      DO 1 II=LSTRT,LSTOP,LINC                                          RPP02260
      DO 1 JJ=ANSTRT,ANSTOP,ANINC                                       RPP02270
C                                                                       RPP02280
      RAINL=II                                                          RPP02290
      JJJ=JJ-ANINC                                                      RPP02300
      JJJJ=JJJ                                                          RPP02310
      IF(FLAG.EQ.1.0) JJJJ=JJJ-360                                      RPP02320
C                                                                       RPP02330
      WRITE(6,222) II                                                   RPP02340
      WRITE(6,223) JJJJ                                                 RPP02350
      WRITE(6,224)                                                      RPP02360
      WRITE(6,225)                                                      RPP02370
C                                                                       RPP02380
      III=0                                                             RPP02390
      THETA(1)=JJJ*CONV                                                 RPP02400
      IF(THETA(1).GT.PI) THETA(1)=THETA(1)-2.*PI                        RPP02410
C                                                                       RPP02420
      DO 2 KK=RRSTRT,RRSTOP,RRINC                                       RPP02430
C                                                                       RPP02440
C     SET UP THE BINNED PARAMETERS                                      RPP02450
C                                                                       RPP02460
      RRATE(1)=KK                                                       RPP02470
C                                                                       RPP02480
C     III IS THE NUMBER OF RAIN RATE ENTRIES... LESS THAN 300           RPP02490
C                                                                       RPP02500
      III=III + 1                                                       RPP02510
      RRATE1(III)=KK                                                    RPP02520
C                                                                       RPP02530
      DO 3 I=1,10                                                       RPP02540
C                                                                       RPP02550
      K=I+1                                                             RPP02560
```

```
      IF(K.EQ.11) GO TO 9                                                RPP02570
      RRATE(K)=(RRATE(1)/10.0)**A(K)*RRATE(1)                            RPP02580
      THETA(K)=B(K)*THETA(1)                                             RPP02590
    9 PE(I)=C(I)                                                         RPP02600
C                                                                        RPP02610
      IF(RRATE(K).LT.1.00) RRATE(K)=1.0                                  RPP02620
      IF(RRATE(K).GT.250.0) RRATE(K)=250.0                               RPP02630
      IF(THETA(K).GT.0.7854) THETA(K)=0.7854                             RPP02640
      IF(THETA(K).LT.-0.7854) THETA(K)=-0.7854                           RPP02650
    3 CONTINUE                                                           RPP02660
C                                                                        RPP02670
C     SCATTERING MODEL                                                   RPP02680
C                                                                        RPP02690
      DELTAL=1.0                                                         RPP02700
      CONSNT=MINUSJ*DELTAL*0.3/FREQ                                      RPP02710
      NN=RAINL/(DELTAL*10.0)                                             RPP02720
C                                                                        RPP02730
C     COMPUTE THE SYSTEM MATRICES FOR EACH DISCRETE BIN                  RPP02740
C     USING THE CAYLEY-HAMILTON THEOREM.                                 RPP02750
C                                                                        RPP02760
      I1=0                                                               RPP02770
      BIN(1)=1                                                           RPP02780
C                                                                        RPP02790
      DO 4 I=1,10                                                        RPP02800
C                                                                        RPP02810
C     CHECK FOR UNIQUE BINS, IF PREVIOUSLY COMPUTED DO NOT RECOMPUTE     RPP02820
C                                                                        RPP02830
      IF(I.EQ.1) GO TO 13                                                RPP02840
C                                                                        RPP02850
      DO 8 K1=1,I1                                                       RPP02860
C                                                                        RPP02870
      K2=BIN(K1)                                                         RPP02880
```

```
C                                                                       RPP02890
      IF((THETA(I).EQ.THETA(K2)).AND.(PE(I).EQ.PE(K2)).AND.(RRATE(I)    RPP02900
     1.EQ.RRATE(K2)).AND.(ICE(I).EQ.ICE(K2)).AND.(SIGMA(I).EQ.SIGMA(K2))RPP02910
     1) GO TO 7                                                         RPP02920
C                                                                       RPP02930
    8 CONTINUE                                                          RPP02940
   13 CONTINUE                                                          RPP02950
C                                                                       RPP02960
      AMODE=0.5 +0.45*ALOG10(RRATE(I))                                  RPP02970
C                                                                       RPP02980
      IF(ICE(I).NE.1) GO TO 14                                          RPP02990
      CALL ICECOF(FREQ,AMODE,FXX,FYY,FXY,LOKANG,RRATE,I,THETA)          RPP03000
      GO TO 15                                                          RPP03010
C                                                                       RPP03020
   14 CALL CAPF(PE,AMODE,FXX,FYY,FXY,FREQ,LOKANG,RRATE,I,THETA,SIGMA)   RPP03030
   15 CONTINUE                                                          RPP03040
C                                                                       RPP03050
      SXX=1.+CONSNT*FXX                                                 RPP03060
      SYY=1.+CONSNT*FYY                                                 RPP03070
      SXY=CONSNT*FXY                                                    RPP03080
      SYX=SXY                                                           RPP03090
C                                                                       RPP03100
      LAMDA1=(SXX+SYY)/2.+CDSQRT(((SXX+SYY)**2)/4.+SXY**2-SXX*SYY)      RPP03110
      LAMDA2=(SXX+SYY)/2.-CDSQRT(((SXX+SYY)**2)/4.+SXY**2-SXX*SYY)      RPP03120
C                                                                       RPP03130
      ALPHA0=(LAMDA2*(LAMDA1**NN)-LAMDA1*(LAMDA2**NN))/(LAMDA2-LAMDA1)  RPP03140
      ALPHA1=(LAMDA2**NN - LAMDA1**NN)/(LAMDA2-LAMDA1)                  RPP03150
C                                                                       RPP03160
      PXX(I)=ALPHA0+ALPHA1*SXX                                          RPP03170
      PXY(I)=ALPHA1*SXY                                                 RPP03180
      PYX(I)=PXY(I)                                                     RPP03190
      PYY(I)=ALPHA0+ALPHA1*SYY                                          RPP03200
```

ORIGINAL PAGE IS
OF POOR QUALITY

```
C                                                                       RPP03210
      I1=I1+1                                                           RPP03220
      BIN(I1)=I                                                         RPP03230
      GO TO 4                                                           RPP03240
    7 CONTINUE                                                          RPP03250
C                                                                       RPP03260
      PXX(I)=PXX(K2)                                                    RPP03270
      PXY(I)=PXY(K2)                                                    RPP03280
      PYX(I)=PYX(K2)                                                    RPP03290
      PYY(I)=PYY(K2)                                                    RPP03300
C                                                                       RPP03310
    4 CONTINUE                                                          RPP03320
C                                                                       RPP03330
      DO 5 I=1,9                                                        RPP03340
C                                                                       RPP03350
      IF(DIREC.EQ.1) GO TO 11                                           RPP03360
C                                                                       RPP03370
      J=11-I                                                            RPP03380
      K=J-1                                                             RPP03390
      GO TO 12                                                          RPP03400
   11 CONTINUE                                                          RPP03410
      K=I+1                                                             RPP03420
      J=I                                                               RPP03430
   12 CONTINUE                                                          RPP03440
C                                                                       RPP03450
      P1=PXX(K)*PXX(J) + PYX(K)*PXY(J)                                  RPP03460
      P2=PXX(K)*PYX(J) + PYX(K)*PYY(J)                                  RPP03470
      P3=PXY(K)*PXX(J) + PYY(K)*PYX(J)                                  RPP03480
      P4=PXY(K)*PYX(J) + PYY(K)*PYY(J)                                  RPP03490
C                                                                       RPP03500
      PXX(K)=P1                                                         RPP03510
      PYX(K)=P2                                                         RPP03520
```

ORIGINAL PAGE IS
OF POOR QUALITY

```
      PXY(K)=P3                                                          RPP03530
      PYY(K)=P4                                                          RPP03540
C                                                                        RPP03550
    5 CONTINUE                                                           RPP03560
C                                                                        RPP03570
C     COMPUTE THE RESULTING X AND Y COMPONENTS EXITING THE RAIN MEDIUM   RPP03580
C                                                                        RPP03590
      EXN=P1*EXO + P2*EYO                                                RPP03600
      EYN=P3*EXO + P4*EYO                                                RPP03610
C                                                                        RPP03620
C     COMPUTE THE ANTENNA OUTPUTS DUE TO RAIN AND POLARIZATION MISMATCH  RPP03630
C                                                                        RPP03640
      CALL OUTANT(EXN,EYN,EXC,EYC,EXX,EYX,III,ISOL1,ATTEN1,PHASE1)       RPP03650
C                                                                        RPP03660
    2 CONTINUE                                                           RPP03670
C                                                                        RPP03680
C     NOW OUTPUT THE DATA IN AN ORGANIZED FORM                           RPP03690
C                                                                        RPP03700
      DO 6 I=1,III                                                       RPP03710
      WRITE(6,226) RRATE1(I),ATTEN1(I),ISOL1(I),PHASE1(I)                RPP03720
    6 CONTINUE                                                           RPP03730
C                                                                        RPP03740
C     PERFORM LINEAR REGRESSIONS ON OUTPUT DATA                          RPP03750
C                                                                        RPP03760
      WRITE(6,227)                                                       RPP03770
      WRITE(6,228)                                                       RPP03780
      CALL CURVE(RRATE1,ATTEN1,III,AA,BB,R,2)                            RPP03790
      WRITE(6,229) AA,BB,R                                               RPP03800
      CALL CURVE(RRATE1,ISOL1,III,AA,BB,R,3)                             RPP03810
      WRITE(6,230) AA,BB,R                                               RPP03820
      CALL CURVE(ATTEN1,ISOL1,III,AA,BB,R,3)                             RPP03830
      WRITE(6,231) AA,BB,R                                               RPP03840
```

```
C                                                                       RPP03850
    1 CONTINUE                                                          RPP03860
C                                                                       RPP03870
      WRITE(6,1000)                                                     RPP03880
 1000 FORMAT(1H1)                                                       RPP03890
      STOP                                                              RPP03900
      END                                                               RPP03910
      SUBROUTINE COMPNT(EPS,TAU,EX,EY)                                  RPP03920
C                                                                       RPP03930
C     THIS SUBROUTINE RETURNS THE X AND Y COMPONENTS GIVEN AN EPSILON   RPP03940
C     AND TAU (IN DEGREES) DESCRIBING AN ARBITRARY POLARIZATION STATE   RPP03950
C                                                                       RPP03960
      COMPLEX*16 EX,EY                                                  RPP03970
      COMPLEX MINUSJ                                                    RPP03980
      COMMON/BLOC1/MINUSJ,CONV                                          RPP03990
C                                                                       RPP04000
      EPSR=EPS*CONV                                                     RPP04010
      TAUR=TAU*CONV                                                     RPP04020
C                                                                       RPP04030
      IF(ABS(EPSR).EQ.(45.*CONV)) GO TO 1                               RPP04040
      IF(EPSR.EQ.0.) GO TO 2                                            RPP04050
      IF(TAUR.EQ.0.) GO TO 3                                            RPP04060
      IF(TAUR.EQ.(90.*CONV)) GO TO 4                                    RPP04070
C                                                                       RPP04080
      T1=TAN(2.*EPSR)                                                   RPP04090
      T2=SIN(2.*TAUR)                                                   RPP04100
      DELTR=ATAN2(T1,T2)                                                RPP04110
      GAMR=0.5*ARCOS(COS(2*EPSR)*COS(2*TAUR))                           RPP04120
      GO TO 100                                                         RPP04130
    1 DELTR=2.*EPSR                                                     RPP04140
      GAMR=45.*CONV                                                     RPP04150
      GO TO 100                                                         RPP04160
```

```
    2 DELTR=0.                                                          RPP04170
      GAMR=TAUR                                                         RPP04180
      GO TO 100                                                         RPP04190
    3 DELTR=SIGN(1.,EPSR)*90.*CONV                                      RPP04200
      GAMR=ABS(EPSR)                                                    RPP04210
      GO TO 100                                                         RPP04220
    4 DELTR=SIGN(1.,EPSR)*90.*CONV                                      RPP04230
      GAMR=90.*CONV-ABS(EPSR)                                           RPP04240
  100 CONTINUE                                                          RPP04250
C                                                                       RPP04260
      EX=COS(GAMR)                                                      RPP04270
      EY=SIN(GAMR)*CEXP(-MINUSJ*DELTR)                                  RPP04280
C                                                                       RPP04290
      RETURN                                                            RPP04300
      END                                                               RPP04310
      SUBROUTINE CLEWEA(EXO,EYO,EXC,EYC,EXX,EYX)                        RPP04320
C                                                                       RPP04330
C     THIS SUBROUTINE OUTPUTS THE CLEAR WEATHER ISOLATION AND PHASE     RPP04340
C                                                                       RPP04350
      REAL ISOCL                                                        RPP04360
      COMPLEX MINUSJ                                                    RPP04370
      COMPLEX*16 EXO,EYO,EXC,EYC,EXX,EYX                                RPP04380
      COMPLEX*16 VWAC,VWAX                                              RPP04390
      REAL*8 VWACM,VWAXM                                                RPP04400
      REAL*8 REAL,AIMAG                                                 RPP04410
C                                                                       RPP04420
      COMMON/BLOC1/MINUSJ,CONV                                          RPP04430
      COMMON/BLOC2/VWACM                                                RPP04440
C                                                                       RPP04450
      VWAC=EXO*EXC + EYO*EYC                                            RPP04460
      VWAX=EXO*EXX + EYO*EYX                                            RPP04470
      VWACR=REAL(VWAC)                                                  RPP04480
```

ORIGINAL PAGE IS
OF POOR QUALITY

```
      VWACI=AIMAG(VWAC)                                                 RPP04490
      VWACM=CDABS(VWAC)                                                 RPP04500
      IF((VWACI.EQ.0.).AND.(VWACR.EQ.0.)) GO TO 1                       RPP04510
      VWACPR=ATAN2(VWACI,VWACR)                                         RPP04520
      VWACPH=VWACPR/CONV                                                RPP04530
      GO TO 2                                                           RPP04540
    1 VWACPH=0.                                                         RPP04550
    2 CONTINUE                                                          RPP04560
      VWAXR=REAL(VWAX)                                                  RPP04570
      VWAXI=AIMAG(VWAX)                                                 RPP04580
      VWAXM=CDABS(VWAX)                                                 RPP04590
      IF(VWAXI.EQ.0. .AND. VWAXR.EQ.0.) GO TO 3                         RPP04600
      VWAXPR=ATAN2(VWAXI,VWAXR)                                         RPP04610
      VWAXPH=VWAXPR/CONV                                                RPP04620
      GO TO 4                                                           RPP04630
    3 VWAXPH=0.                                                         RPP04640
    4 CONTINUE                                                          RPP04650
C                                                                       RPP04660
      PHASCW=VWAXPH-VWACPH                                              RPP04670
C                                                                       RPP04680
      IF(VWAXM.EQ.0.) GO TO 5                                           RPP04690
C                                                                       RPP04700
      ISOCL=20.*DLOG10(VWACM/VWAXM)                                     RPP04710
      WRITE(6,8) ISOCL                                                  RPP04720
    8 FORMAT(/,3X,'THE CLEAR WEATHER ISOLATION REFERENCED TO THE ANTENNARPP04730
     1 PORTS IS',19X,F6.2,2X,'DB')                                      RPP04740
C                                                                       RPP04750
      GO TO 7                                                           RPP04760
    5 WRITE(6,6)                                                        RPP04770
    6 FORMAT(/,3X,'THE CLEAR WEATHER ISOLATION IS INFINITY')            RPP04780
    7 CONTINUE                                                          RPP04790
      WRITE(6,9) PHASCW                                                 RPP04800
```

ORIGINAL PAGE IS
OF POOR QUALITY

```
    9 FORMAT(/,3X,'THE CLEAR WEATHER PHASE DIFFERENCE',46X,F7.2,          RPP04810
     12X,'DEGREES')                                                      RPP04820
C                                                                        RPP04830
      RETURN                                                             RPP04840
      END                                                                RPP04850
      SUBROUTINE ICECOF(FREQ,AMODE,FXX,FYY,FXY,LOKANG,RRATE,I,THETA)     RPP04860
C                                                                        RPP04870
C     THIS SUBROUTINE RETURNS TO THE CALLING PROGRAM THE EFFECTIVE       RPP04880
C     SCATTERING COEFFICIENTS FOR A SLAB OF ICE PARTICLES.  THE SLAB     RPP04890
C     HAS 50% PROLATE PARTICLES AND 50% OBLATE PARTICLES.  THE           RPP04900
C     SCATTERING COEFFICIENTS ARE A FUNCTION OF PARTICLE SIZE AND        RPP04910
C     ORIENTATION.  THE PARTICLES ALL HAVE THE SAME CANTING ANGLE        RPP04920
C     THETA.  THE COEFFICENTS ARE DERIVED FROM RAYLEIGH SCATTERING       RPP04930
C     TECHNIQUES.                                                        RPP04940
C     THE PARTICLE ECCENTRICITY IS VERY CLOSE TO ONE.                    RPP04950
C                                                                        RPP04960
      DIMENSION ICE(10),RRATE(15),THETA(15)                              RPP04970
      REAL LOKANG                                                        RPP04980
      COMPLEX*16 FXX,FXY,FYY,APROX,APROY,AOBLX,AOBLY,ASPH                RPP04990
C                                                                        RPP05000
C                                                                        RPP05010
C     ICE CONCENTRATION INCREASES WITH RAIN RATE.                        RPP05020
C     IF ONLY CONSIDERING ICE IN THE PATH, RAIN RATE IS MEANINGLESS,     RPP05030
C     BUT IT CONTROLS PARTICLE CONCENTRATION.                            RPP05040
C     RR=1,VOLICE=E-8...RR=50,VOLICE=E-6                                 RPP05050
C                                                                        RPP05060
      VOLICE=RRATE(I)*(24.434608*1E-9)/SQRT(AMODE)                       RPP05070
C                                                                        RPP05080
      CON=VOLICE*(FREQ**2)/0.18                                          RPP05090
      CSTH=COS(THETA(I))**2                                              RPP05100
      SNTH=SIN(THETA(I))**2                                              RPP05110
      CSLA=COS(LOKANG)**2                                                RPP05120
```

```
      SNLA=SIN(LOKANG)**2                                                RPP05130
C                                                                        RPP05140
      APROX=(6.812211,-0.026842)                                         RPP05150
      APROY=(3.268519,-0.006179)                                         RPP05160
      AOBLX=(6.812211,-0.026842)                                         RPP05170
      AOBLY=(2.150047,-0.002674)                                         RPP05180
      ASPH=(3.95417,-0.009044)                                           RPP05190
C                                                                        RPP05200
      AOBLX=ASPH*CSLA + AOBLX*SNLA                                       RPP05210
      AOBLY=ASPH*CSLA + AOBLY*SNLA                                       RPP05220
C                                                                        RPP05230
      FXX=CON*(SNTH*(APROY+AOBLY) + CSTH*(APROX+AOBLX))                  RPP05240
      FYY=CON*(CSTH*(APROY+AOBLY) + SNTH*(APROX+AOBLX))                  RPP05250
      FXY=CON*(APROY+AOBLY-APROX-AOBLX)*SIN(THETA(I))*COS(THETA(I))      RPP05260
C                                                                        RPP05270
      RETURN                                                             RPP05280
      END                                                                RPP05290
      SUBROUTINE CAPF(PE,AMODE,FXX,FYY,FXY,FREQ,LOKANG,RRATE,II,THETA,SIRPP05300
     1GMA)                                                               RPP05310
C                                                                        RPP05320
C     THIS SUBROUTINE RETURNS TO THE CALLING PROGRAM THE COMPLEX         RPP05330
C     SCATTERING COEFFICIENTS FXX,FXY,FYX,FYY.  THESE COEFFICIENTS       RPP05340
C     INCLUDE THE EFFECTS OF A DROP SIZE DISTRIBUTION AND A              RPP05350
C     CANTING ANGLE DISTRIBUTION. (THE ABSOLUTE VALUE OF THE CANTING     RPP05360
C     ANGLE RANGE IS LESS THAN 100 DEGREES)                              RPP05370
C                                                                        RPP05380
      DIMENSION RRATE(15),THETA(15),PE(15),N(20,28)                      RPP05390
      DIMENSION SIGMA(10)                                                RPP05400
      INTEGER P,Q                                                        RPP05410
      REAL LOKANG,N                                                      RPP05420
      COMPLEX*16 FXX,FXY,FYY                                             RPP05430
      COMPLEX*16 FV,FH,FSPH,DIFF                                         RPP05440
```

ORIGINAL PAGE IS
OF POOR QUALITY

```
C                                                                       RPP05450
      CALL ND(RRATE,II,N,AMODE,THETA,SIGMA)                             RPP05460
C                                                                       RPP05470
      FXX=(0.0,0.0)                                                     RPP05480
      FYY=(0.0,0.0)                                                     RPP05490
      FXY=(0.0,0.0)                                                     RPP05500
C                                                                       RPP05510
      DO 1 P=2,28                                                       RPP05520
C                                                                       RPP05530
      RADIUS=0.125/2.0 + (P-1)*0.125                                    RPP05540
C                                                                       RPP05550
      CALL COEF(FREQ,RADIUS,FV,FH,FSPH,DIFF,LOKANG)                     RPP05560
C                                                                       RPP05570
      DO 1 Q=1,20                                                       RPP05580
C                                                                       RPP05590
      THETAS=-1.832596 + 0.174533*Q                                     RPP05600
C                                                                       RPP05610
      IF(SIGMA(II).EQ.0.0) THETAS=THETA(II)                             RPP05620
C                                                                       RPP05630
      SNTH=SIN(THETAS)**2                                               RPP05640
      CSTH=COS(THETAS)**2                                               RPP05650
C                                                                       RPP05660
      FXX=FXX + N(Q,P)*((1.-PE(II))*FSPH+PE(II)*(FV*SNTH+FH*CSTH))      RPP05670
      FYY=FYY + N(Q,P)*((1-PE(II))*FSPH+PE(II)*(FV*CSTH+FH*SNTH))       RPP05680
      FXY=FXY + N(Q,P)*PE(II)*DIFF*SIN(THETAS)*COS(THETAS)              RPP05690
C                                                                       RPP05700
    1 CONTINUE                                                          RPP05710
      RETURN                                                            RPP05720
      END                                                               RPP05730
      SUBROUTINE ND(RRATE,II,N,AMODE,THETA,SIGMA)                       RPP05740
C                                                                       RPP05750
C     THIS SUBROUTINE RETURNS TO THE CALLING PROGRAM                    RPP05760
```

```
C      THE NUMBER OF DROPS IN THE QTH CANTING ANGLE CLASS AND                RPP05770
C      THE PTH DROP SIZE CLASS.                                              RPP05780
C                                                                            RPP05790
       DIMENSION CANNUM(20),AREA(20),SIGMA(20)                               RPP05800
       DIMENSION RRATE(15),THETA(15),N(20,28)                                RPP05810
       INTEGER P,Q                                                           RPP05820
       REAL N,NUMTOT                                                         RPP05830
C                                                                            RPP05840
       NUMTOT=RRATE(II)*5.83333/(AMODE**3.5)                                 RPP05850
C                                                                            RPP05860
       IF(SIGMA(II).EQ.0.0) GO TO 2                                          RPP05870
C                                                                            RPP05880
       CALL NUMCAN(NUMTOT,THETA,CANNUM,II,SIGMA)                             RPP05890
C                                                                            RPP05900
       GO TO 4                                                               RPP05910
     2 CONTINUE                                                              RPP05920
       DO 3 J=1,20                                                           RPP05930
       CANNUM(J)=NUMTOT/20.0                                                 RPP05940
     3 CONTINUE                                                              RPP05950
     4 CONTINUE                                                              RPP05960
       DELTAA=0.125                                                          RPP05970
C                                                                            RPP05980
       DO 1 Q=1,20                                                           RPP05990
       DO 1 P=2,28                                                           RPP06000
C                                                                            RPP06010
       RADIUS=0.125/2.0 + (P-1)*0.125                                        RPP06020
C                                                                            RPP06030
       IF(RADIUS.LE.AMODE) N(Q,P)=CANNUM(Q)*DELTAA*RADIUS/AMODE**2           RPP06040
       IF(RADIUS.GT.AMODE)N(Q,P)=CANNUM(Q)*2.*DELTAA*(1.-.5*RADIUS/AMODE)    RPP06050
      1/AMODE                                                                RPP06060
       IF(RADIUS.GT.(2.*AMODE)) N(Q,P)=0.0                                   RPP06070
C                                                                            RPP06080
```

ORIGINAL PAGE IS
OF POOR QUALITY

```
    1 CONTINUE                                                          RPP06090
      RETURN                                                            RPP06100
      END                                                               RPP06110
      SUBROUTINE NUMCAN(NUMTOT,THETA,CANNUM,II,SIGMA)                   RPP06120
C                                                                       RPP06130
C     THIS SUBROUTINE RETURNS TO THE CALLING PROGRAM THE                RPP06140
C     NUMBER OF DROPS IN ALL THE DISCRETE INTERVALS.                    RPP06150
C     THE DISTRIBUTION IS THE NORMAL DISTRIBUTION.                      RPP06160
C     SIGMA CAN EQUAL ZERO OR GREATER THAN 10 DEGREES                   RPP06170
C                                                                       RPP06180
      DIMENSION AREA(20),CANNUM(20)                                     RPP06190
      DIMENSION SIGMA(10)                                               RPP06200
      DIMENSION THETA(15)                                               RPP06210
      REAL NUMTOT                                                       RPP06220
C                                                                       RPP06230
      SIGMAP=SIGMA(II)*0.017453                                         RPP06240
C                                                                       RPP06250
      IF(SIGMAP.LT.0.17453) SIGMAP=.17453                               RPP06260
C                                                                       RPP06270
C                                                                       RPP06280
      DO 1 I=1,19                                                       RPP06290
C                                                                       RPP06300
      K=I-1                                                             RPP06310
      THETAP=-1.57079 + K*0.174533                                      RPP06320
      U=(THETAP-THETA(II))/1.4142136/SIGMAP                             RPP06330
C                                                                       RPP06340
      IF(U.LT.0.0) AREA(I)=0.5*ERFC(ABS(U))                             RPP06350
      IF(U.EQ.0.0) AREA(I)=0.5                                          RPP06360
      IF(U.GT.0.0) AREA(I)=0.5*ERF(U) + 0.5                             RPP06370
C                                                                       RPP06380
    1 CONTINUE                                                          RPP06390
      CANNUM(1)=NUMTOT*AREA(1)                                          RPP06400
```

ORIGINAL PAGE IS
OF POOR QUALITY

```
      CANNUM(20)=NUMTOT*(1.0-AREA(19))                                  RPP06410
C                                                                       RPP06420
      IF(CANNUM(20).LT.1.E-10) CANNUM(20)=0.0                           RPP06430
C                                                                       RPP06440
      DO 2 I=1,18                                                       RPP06450
C                                                                       RPP06460
      K=I+1                                                             RPP06470
C                                                                       RPP06480
      CANNUM(K)=NUMTOT*(AREA(K)-AREA(I))                                RPP06490
C                                                                       RPP06500
      IF(CANNUM(K).LT.1.E-10) CANNUM(K)=0.0                             RPP06510
C                                                                       RPP06520
    2 CONTINUE                                                          RPP06530
C                                                                       RPP06540
      RETURN                                                            RPP06550
      END                                                               RPP06560
      SUBROUTINE COEF(FREQ,AMODE,FV,FH,FSPH,DIFF,LOKANG)                RPP06570
C                                                                       RPP06580
C     THIS SUBROUTINE RETURNS TO THE CALLING PROGRAM THE SCATTERING     RPP06590
C     COEFFICIENTS FOR SPHERICAL AND OBLATE RAIN DROPS.                 RPP06600
C     THE COEFFICIENTS ARE A FUNCTION OF FREQUENCY AND DROP SIZE        RPP06610
C     AND ELEVATION ANGLE.  THE COEFFICIENTS USED ARE THOSE OF UZUNOGLU,RPP06620
C     EVANS AND HOLT.                                                   RPP06630
C                                                                       RPP06640
      COMPLEX CMPLX                                                     RPP06650
      DOUBLE PRECISION U1,U2,U3,U4,U5                                   RPP06660
      REAL LOKANG                                                       RPP06670
C                                                                       RPP06680
      COMPLEX*16 FV,FH,FSPH,DIFF     .                                  RPP06690
C                                                                       RPP06700
      IF(AMODE.LT.0.25) AMODE=0.25                                      RPP06710
      IF((INT(FREQ).EQ.11).AND.(AMODE.GT.3.5)) AMODE=3.5                RPP06720
```

```
      IF((INT(FREQ).EQ.14).AND.(AMODE.GT.3.5)) AMODE=3.5                RPP06730
      IF((INT(FREQ).EQ.20).AND.(AMODE.GT.3.0)) AMODE=3.0                RPP06740
      IF((INT(FREQ).EQ.30).AND.(AMODE.GT.3.0)) AMODE=3.0                RPP06750
C                                                                       RPP06760
      U1=AMODE                                                          RPP06770
      U2=AMODE**2                                                       RPP06780
      U3=AMODE**3                                                       RPP06790
      U4=AMODE**4                                                       RPP06800
      U5=AMODE**5                                                       RPP06810
C                                                                       RPP06820
C                                                                       RPP06830
C                                                                       RPP06840
C     11.0 GHZ COEFFICIENTS                                             RPP06850
C                                                                       RPP06860
      IF(INT(FREQ).NE.11) GO TO 1                                       RPP06870
C                                                                       RPP06880
C     SPHERICAL DROP COEFFICIENTS                                       RPP06890
C                                                                       RPP06900
      IF(AMODE.GT.1.00) GO TO 10                                        RPP06910
C                                                                       RPP06920
      EOR=-0.0020548+0.01638947*U1-0.0417568*U2+0.08832213*U3           RPP06930
      EOI=-0.0025154+0.0192855 3*U1-0.04568!6*U2+0.0365147*U3           RPP06940
      GO TO 11                                                          RPP06950
   10 CONTINUE                                                          RPP06960
C                                                                       RPP06970
      EOR=-1.28155706+2.83287718*U1-2.07399678*U2+0.60190887*U3         RPP06980
     1-0.00984194*U4-0.01096165*U5                                      RPP06990
      EOI=2.60278025-7.52434662*U1+8.14691632*U2-4.12133971*U3          RPP07000
     1+0.99089467*U4-0.08731788*U5                                      RPP07010
C                                                                       RPP07020
      GO TO 12                                                          RPP07030
   11 CONTINUE                                                          RPP07040
```

ORIGINAL PAGE IS
OF POOR QUALITY

```
C                                                                       RPP07050
C     OBLATE DROP COEFFICIENTS                                          RPP07060
C                                                                       RPP07070
      EV90R=-0.001322+0.01036867*U1-0.025372*U2+0.07072533*U3           RPP07080
      EV90I=-0.0024306+0.01861967*U1-0.0440732*U2+0.03507413*U3         RPP07090
      EH90R=-0.0023684+0.01878307*U1-0.0473704*U2+0.09255573*U3         RPP07100
      EH90I=-0.0030366+0.02320527*U1-0.0546296*U2+0.04299093*U3         RPP07110
      DIFFR=-0.0010464+0.0084144*U1-0.0219984*U2+0.0218304*U3           RPP07120
      DIFFI=-0.000606+0.0045856*U1-0.0106064*U2+0.0079168*U3            RPP07130
C                                                                       RPP07140
      GO TO 1000                                                        RPP07150
   12 CONTINUE                                                          RPP07160
C                                                                       RPP07170
      EV90R=-0.3653892+0.32540943*U1+0.45280976*U2-0.53907398*U3        RPP07180
     1+0.20309215*U4-0.02432204*U5                                      RPP07190
      EV90I=2.20618555-6.19251766*U1+6.43873903*U2-3.090414*U3          RPP07200
     1+0.70600211*U4-0.0607173*U5                                       RPP07210
      EH90R=2.09022706-7.07345119*U1+9.03639726*U2-5.33156215*U3        RPP07220
     1+1.49716423*U4-0.15747063*U5                                      RPP07230
      EH90I=3.28654422-9.68217951*U1+10.71102231*U2-5.5491184*U3        RPP07240
     1+1.36694565*U4-0.12512466*U5                                      RPP07250
      DIFFI=1.08034369-3.48962081*U1+4.2722407*U2-2.45868344*U3         RPP07260
     1+0.66093861*U4-0.06440692*U5                                      RPP07270
C                                                                       RPP07280
      IF(AMODE.GT.2.0) GO TO 120                                        RPP07290
C                                                                       RPP07300
      DIFFR=-0.32599997+0.7531995*U1-0.57039996*U2+0.15039999*U3        RPP07310
      GO TO 1000                                                        RPP07320
C                                                                       RPP07330
  120 CONTINUE                                                          RPP07340
C                                                                       RPP07350
      DIFFR=11.94200847-14.59334299*U1+5.80600359*U2-0.7346671*U3       RPP07360
```

ORIGINAL PAGE IS
OF POOR QUALITY

```
C                                                                       RPP07370
      GO TO 1000                                                        RPP07380
C                                                                       RPP07390
    1 CONTINUE                                                          RPP07400
C                                                                       RPP07410
C     14 GHZ COEFFICIENTS                                               RPP07420
C                                                                       RPP07430
      IF(INT(FREQ).NE.14) GO TO 2                                       RPP07440
C                                                                       RPP07450
C     SPHERICAL DROP COEFFECIENTS                                       RPP07460
C                                                                       RPP07470
      IF(AMODE.GT.1.00) GO TO 20                                        RPP07480
C                                                                       RPP07490
      EOR=-0.001376+0.012776*U1-0.040134*U2+0.128736*U3                 RPP07500
      EOI=-0.008796+0.06731467*U1-0.1588*U2+0.12418133*U3               RPP07510
C                                                                       RPP07520
      GO TO 21                                                          RPP07530
   20 CONTINUE                                                          RPP07540
C                                                                       RPP07550
      EOR=-12.1370793+34.85683676*U1-37.84887378*U2+19.48995359*U3      RPP07560
     1-4.69149894*U4+0.42548477*U5                                      RPP07570
      EOI=-8.4550178+22.97909617*U1-23.38444001*U2+11.09553161*U3       RPP07580
     1-2.41694538*U4+0.19907664*U5                                      RPP07590
C                                                                       RPP07600
      GO TO 22                                                          RPP07610
   21 CONTINUE                                                          RPP07620
C                                                                       RPP07630
C     OBLATE DROP COEFFICIENTS                                          RPP07640
C                                                                       RPP07650
      EV90R=-0.000248+0.00335467*U1-0.013928*U2+0.10002133*U3           RPP07660
      EV90I=-0.008436+0.06455867*U1-0.152256*U2+0.11893333*U3           RPP07670
      EH90R=-0.000656+0.007656*U1-0.029656*U2+0.122656*U3               RPP07680
```

```
      EH90I=-0.010366+0.079154*U1-0.18596*U2+0.143872*U3                RPP07690
      DIFFR=-0.000408+0.00430133*U1-0.015728*U2+0.0226346?*U3           RPP07700
      DIFFI=-0.00193+0.01459533*U1-0.033704*U2+0.024938?7*U3            RPP07710
C                                                                       RPP07720
      GO TO 1000                                                        RPP07730
   22 CONTINUE                                                          RPP07740
C                                                                       RPP07750
      EV90R=-4.48493663+12.45481829*U1-12.90182271*U2+6.32901913*U3     RPP07760
     1-1.42805671*U4+0.11875301*U5                                      RPP07770
      EV90I=-0.1923376+0.3425132*U1-0.196242*U2+0.07468968*U3           RPP07780
C                                                                       RPP07790
      IF(AMODE.GT.2.5) GO TO 24                                         RPP07800
C                                                                       RPP07810
      EH90I=1.10278458-3.74696237*U1+4.48042001*U2-2.22964317*U3        RPP07820
     1+0.42010037*U4                                                    RPP07830
      DIFFR=-0.15268404+0.39830845*U1-0.3527577*U2+0.1176?014*U3        RPP07840
      DIFFI=-1.29960041+2.93303524*U1-2.15255009*U2+0.5206384*U3        RPP07850
C                                                                       RPP07860
      IF(AMODE.GT.2.00) GO TO 25                                        RPP07870
C                                                                       RPP07880
      EH90R=-1.02599992+2.30733317*U1-1.60799988*U2+0.4266664*U3        RPP07890
C                                                                       RPP07900
      GO TO 1000                                                        RPP07910
   24 CONTINUE                                                          RPP07920
C                                                                       RPP07930
      EH90I=2.51000033-2.03000022*U1+0.62000004*U2                      RPP07940
      DIFFR=-15.85152202+18.27189723*U1-6.68140666*U2+0.79411153*U3     RPP07950
      DIFFI=22.32321586-44.48681458*U1+30.17926125*U2-8.46925555*U3     RPP07960
     1+0.85300427*U4                                                    RPP07970
C                                                                       RPP07980
      GO TO 1000                                                        RPP07990
   25 CONTINUE                                                          RPP08000
```

```
C                                                                       RPP08010
      EH90R=-19.65+20.6567*U1-6.66*U2+0.6933*U3                         RPP08020
C                                                                       RPP08030
      GO TO 1000                                                        RPP08040
    2 CONTINUE                                                          RPP08050
C                                                                       RPP08060
C     20 GHZ COEFFICIENTS                                               RPP08070
C                                                                       RPP08080
      IF(INT(FREQ).NE.20) GO TO 3                                       RPP08090
C                                                                       RPP08100
C     SPHERICAL DROP COEFFICIENTS                                       RPP08110
C                                                                       RPP08120
      IF(AMODE.GT.1.0) GO TO 30                                         RPP08130
C                                                                       RPP08140
      EOR=0.020296-0.145276*U1+0.297656*U2+0.008224*U3                  RPP08150
C                                                                       RPP08160
      EOI=-0.015488+0.12709133*U1-0.334568*U2+0.30583467*U3             RPP08170
C                                                                       RPP08180
      GO TO 31                                                          RPP08190
   30 CONTINUE                                                          RPP08200
C                                                                       RPP08210
      EOR=3.35567152-8.61818659*U1+7.8157989*U2-2.68217917*U3           RPP08220
     1+0.3108073*U4                                                     RPP08230
      EOI=1.85636463-3.70750898*U1+2.19599302*U2-0.25148145*U3          RPP08240
C                                                                       RPP08250
      GO TO 32                                                          RPP08260
   31 CONTINUE                                                          RPP08270
C                                                                       RPP08280
C     OBLATE COEFFICIENTS                                               RPP08290
C                                                                       RPP08300
      EV90R=0.02454800-0.17912133*U1+0.384448*U2-0.07447467*U3          RPP08310
      EV90I=-0.013492+0.11190533*U1-0.299032*U2+0.27853867*U3           RPP08320
```

ORIGINAL PAGE IS
OF POOR QUALITY

```
      EH90R=0.02282-0.16596667*U1+0.34976*U2-0.03061333*U3                RPP08330
      EH90I=-0.015178+0.12623933*U1-0.33848*U2+0.31533867*U3              RPP08340
      DIFFR=0.000072+0.00175467*U1-0.015488*U2+0.03426133*U3              RPP08350
      DIFFI=-0.001686+0.014334*U1-0.039448*U2+0.0368*U3                   RPP08360
C                                                                         RPP08370
      GO TO 1000                                                          RPP08380
   32 CONTINUE                                                            RPP08390
C                                                                         RPP08400
      EV90R=1.56037246-3.97019757*U1+3.66524972*U2-1.24458239*U3          RPP08410
     1+0.14526662*U4                                                      RPP08420
      EV90I=4.77376463-13.63610787*U1+14.83397997*U2                      RPP08430
     1-7.66136891*U3+1.96881573*U4-0.19749381*U5                          RPP08440
      EH90R=4.63026679-11.97374109*U1+11.0254653*U2                       RPP08450
     1-4.0050613*U3+0.50244373*U4                                         RPP08460
      EH90I=-1.5390057+6.3417866*U1-9.35328879*U2+6.20987895*U3           RPP08470
     1-1.74544867*U4+0.17820925*U5                                        RPP08480
      DIFFR=3.06989428-8.00354339*U1+7.36021547*U2                        RPP08490
     1-2.76047886*U3+0.3571771*U4                                         RPP08500
      DIFFI=-6.31274803+19.97783334*U1-24.1872053*U2+13.8712166*U3        RPP08510
     1-3.71425705*U4+0.3757024*U5                                         RPP08520
C                                                                         RPP08530
      GO TO 1000                                                          RPP08540
    3 CONTINUE                                                            RPP08550
C                                                                         RPP08560
      IF(INT(FREQ).NE.30) GO TO 2000                                      RPP08570
C                                                                         RPP08580
C     30 GHZ COEFFICIENTS                                                 RPP08590
C                                                                         RPP08600
C     SPHERICAL DROP COEFFICIENTS                                         RPP08610
C                                                                         RPP08620
      IF(AMODE.GT.1.0) GO TO 40                                           RPP08630
C                                                                         RPP08640
```

ORIGINAL PAGE IS
OF POOR QUALITY

```
      EOR=0.028004-0.221564*U1+0.530744*U2+0.022816*U3                  RPP08650
      EOI=-0.007072+0.09329866*U1-0.390112*U2+0.55688533*U3             RPP08660
C                                                                       RPP08670
      GO TO 41                                                          RPP08680
   40 CONTINUE                                                          RPP08690
C                                                                       RPP08700
      EOR=-1.95096901+3.4107597*U1-0.82790307*U2-0.39982485*U3          RPP08710
     1+0.1291964*U4                                                     RPP08720
      EOI=5.77798866-16.3876166*U1+16.10102407*U2-6.06482662*U3         RPP08730
     1+0.82747918*U4                                                    RPP08740
C                                                                       RPP08750
      GO TO 42                                                          RPP08760
   41 CONTINUE                                                          RPP08770
C                                                                       RPP08780
C     OBLATE DROP COEFFICIENTS                                          RPP08790
C                                                                       RPP08800
      EV90R=0.03542-0.2838733*U1+0.7038*U2-0.15834666*U3                RPP08810
      EV90I=0.013876-0.064756*U1-0.026904*U2+0.290784*U3                RPP08820
      EH90R=0.031652-0.252652*U1+0.614952*U2-0.049952*U3                RPP08830
      EH90I=-0.000532+0.04746533*U1-0.299512*U2+0.50957867*U3           RPP08840
      DIFFR=-0.003768+0.03122133*U1-0.088848*U2+0.10839467*U3           RPP08850
      DIFFI=-0.014408+0.11222133*U1-0.272608*U2+0.21879467*U3           RPP08860
C                                                                       RPP08870
      GO TO 1000                                                        RPP08880
   42 CONTINUE                                                          RPP08890
C                                                                       RPP08900
      EV90R=3.93161268-10.97208846*U1+11.43870068*U2                    RPP08910
     1-4.78953064*U3+0.69447892*U4                                      RPP08920
      EV90I=3.12729055-9.08249632*U1+9.16246329*U2                      RPP08930
     1-3.47227982*U3+0.47789632*U4                                      RPP08940
      EH90R=-6.97583584+16.79179963*U1-13.53607686*U2                   RPP08950
     1+4.63811854*U3-0.57535653*U4                                      RPP08960
```

C-3

```
      EH90I=-1.39373246+1.72736066*U1-0.14076091*U2+0.05474057*U3        RPP08970
      DIFFR=-10.90744851+27.76388807*U1-24.97477753*U2                   RPP08980
     1+9.42764918*U3-1.26983545*U4                                       RPP08990
      DIFFI=5.33984552-17.20920477*U1+20.7812541*U2                      RPP09000
     1-11.64360435*U3+3.07942984*U4-0.30370378*U5                        RPP09010
C                                                                        RPP09020
 1000 CONTINUE                                                           RPP09030
C                                                                        RPP09040
      ALPH=1.576796-LOKANG                                               RPP09050
      CSLA=0.001*COS(ALPH)**2                                            RPP09060
      SNLA=0.001*SIN(ALPH)**2                                            RPP09070
      FVR=CSLA*EOR+SNLA*EV90R                                            RPP09080
      FVI=-CSLA*EOI-SNLA*EV90I                                           RPP09090
      FHR=CSLA*EOR+SNLA*EH90R                                            RPP09100
      FHI=-CSLA*EOI-SNLA*EH90I                                           RPP09110
      DIFFR=-SNLA*DIFFR                                                  RPP09120
      DIFFI=SNLA*DIFFI                                                   RPP09130
      EOR=0.001*EOR                                                      RPP09140
      EOI=-0.001*EOI                                                     RPP09150
C                                                                        RPP09160
      FV=CMPLX(FVR,FVI)                                                  RPP09170
      FH=CMPLX(FHR,FHI)                                                  RPP09180
      FSPH=CMPLX(EOR,EOI)                                                RPP09190
      DIFF=CMPLX(DIFFR,DIFFI)                                            RPP09200
C                                                                        RPP09210
      GO TO 3000                                                         RPP09220
C                                                                        RPP09230
 2000 WRITE(6,2001)                                                      RPP09240
 2001 FORMAT(//,3X,'FREQUENCY NOT ALLOWED, ONLY 11,14,20,30 GHZ ALLOWED'RPP09250
     1)                                                                  RPP09260
C                                                                        RPP09270
      STOP                                                               RPP09280
```

ORIGINAL PAGE IS
OF POOR QUALITY

```
 3000 CONTINUE                                                          RPP09290
C                                                                       RPP09300
      RETURN                                                            RPP09310
      END                                                               RPP09320
      SUBROUTINE OUTANT(EXN,EYN,EXC,EYC,EXX,EYX,I,ISOL1,ATTEN1,PHASE1)  RPP09330
C                                                                       RPP09340
C     THIS SUBROUTINE TAKES THE X AND Y COMPONENTS OF THE WAVE EXITING  RPP09350
C     THE RAIN CELL (EXN,EYN) AND USES THE COMPLEX VECTOR METHOD        RPP09360
C     TO COMPUTE VALUES FOR ATTENUATION, ISOLATION, AND PHASE AS A      RPP09370
C     RESULT OF THE RAIN MEDIUM AND POLARIZATION MISMATCH EFFECTS OF THERPP09380
C     RECEIVE ANTENNA                                                   RPP09390
C     THIS DATA IS STORED IN PROGRAM MEMORY FOR LATER OUTPUT            RPP09400
C                                                                       RPP09410
      REAL ISOL1                                                        RPP09420
      COMMON/BLOC1/MINUSJ,CONV                                          RPP09430
      COMMON/BLOC2/VHACM                                                RPP09440
C                                                                       RPP09450
      DIMENSION PHASE1(100),ATTEN1(100),ISOL1(100)                      RPP09460
C                                                                       RPP09470
      COMPLEX MINUSJ                                                    RPP09480
      COMPLEX*16 EXC,EYC,EXX,EYX                                        RPP09490
      COMPLEX*16 VWPAC,VWPAX                                            RPP09500
      COMPLEX*16 EXN,EYN                                                RPP09510
      REAL*8 VWPACM,VWPAXM                                              RPP09520
      REAL*8 REAL,AIMAG                                                 RPP09530
C                                                                       RPP09540
      VWPAC=EXN*EXC + EYN*EYC                                           RPP09550
      VWPAX=EXN*EXX + EYN*EYX                                           RPP09560
C                                                                       RPP09570
C                                                                       RPP09580
      VWPACR=REAL(VWPAC)                                                RPP09590
      VWPACI=AIMAG(VWPAC)                                               RPP09600
```

```
      VWPACM=CDABS(VWPAC)                                                RPP09610
      VWPACR=ATAN2(VWPACI,VWPACR)                                        RPP09620
      VWPACP=VWPACR/CONV                                                 RPP09630
C                                                                        RPP09640
      VWPAXR=REAL(VWPAX)                                                 RPP09650
      VWPAXI=AIMAG(VWPAX)                                                RPP09660
      VWPAXM=CDABS(VWPAX)                                                RPP09670
      VWPAXR=ATAN2(VWPAXI,VWPAXR)                                        RPP09680
      VWPAXP=VWPAXR/CONV                                                 RPP09690
      IF(VWPAXM.LE.0.000001) VWPAXP=0.0                                  RPP09700
C                                                                        RPP09710
      PHASE1(I)=VWPAXP-VWPACP                                            RPP09720
C                                                                        RPP09730
      IF(PHASE1(I).LT.0.0) PHASE1(I)=PHASE1(I)+360.0                     RPP09740
C                                                                        RPP09750
      ISOL1(I)=20.*DLOG10(VWPACM/VWPAXM)                                 RPP09760
      ATTEN1(I)=20.*DLOG10(VWACM/VWPACM)                                 RPP09770
C                                                                        RPP09780
      RETURN                                                             RPP09790
      END                                                                RPP09800
      SUBROUTINE CURVE(X,Y,III,A,B,R,K)                                  RPP09810
C*********************************************************************** RPP09820
C*                                                                       RPP09830
C*   THIS SUBROUTINE PERFORMS A LINEAR REGRESSION ON ARRAYS X,Y          RPP09840
C*                                                                       RPP09850
C*   POWER FITS,LOG FITS, AND EXPONENTIAL FITS ARE DONE BY               RPP09860
C*   TAKING THE LOG OF THE INPUT DATA WHERE APPROPRIATE                  RPP09870
C*                                                                       RPP09880
C*   THE CALL STATEMENT FOR THIS SUBROUTINE IS                           RPP09890
C*                                                                       RPP09900
C*     CALL CURVE(X,Y,III,A,B,R,K)                                       RPP09910
C*                                                                       RPP09920
```

```
C*        WHERE                                                          RPP09930
C*          X IS A SINGLE DIMENSIONED ARRAY WITH III ENTRIES             RPP09940
C*          Y IS A SINGLE DIMENSIONED ARRAY WITH III ENTRIES             RPP09950
C*          A AND B ARE THE RETURNED COEFFICENTS                         RPP09960
C*          R IS THE RETURNED CORRELATION COEFFICENT R**2                RPP09970
C*          K IS THE FLAG FOR THE TYPE OF CURVE FIT                      RPP09980
C*             K=1   LINEAR FIT   Y=A+B*X                                RPP09990
C*             K=2   POWER FIT  Y=A*X**B                                 RPP10000
C*             K=3   LOG FIT  Y=A+B*LN(X)                                RPP10010
C*             K=4   EXP FIT  Y=A*EXP(B*X)                               RPP10020
C*                                                                       RPP10030
C*************************************************************************RPP10040
C                                                                        RPP10050
      DIMENSION X(300),Y(300)                                            RPP10060
C                                                                        RPP10070
      IF (III.LE.1) GOTO 50                                              RPP10080
C                                                                        RPP10090
      X1=0                                                               RPP10100
      X2=0                                                               RPP10110
      Y1=0                                                               RPP10120
      Y2=0                                                               RPP10130
      XY=0                                                               RPP10140
      DO 10 I=1,III                                                      RPP10150
      XX=X(I)                                                            RPP10160
      YY=Y(I)                                                            RPP10170
      IF(K.EQ.1) GO TO 20                                                RPP10180
      IF(K.EQ.4) GO TO 30                                                RPP10190
      XX=ALOG(XX)                                                        RPP10200
      IF(K.EQ.3) GO TO 20                                                RPP10210
30    YY=ALOG(YY)                                                        RPP10220
20    X1=X1+XX                                                           RPP10230
      X2=X2+XX*XX                                                        RPP10240
```

ORIGINAL PAGE IS
OF POOR QUALITY

```
      Y1=Y1+YY                                                          RPP10250
      Y2=Y2+YY*YY                                                       RPP10260
      XY=XY+XX*YY                                                       RPP10270
10    CONTINUE                                                          RPP10280
      XN=FLOAT(III)                                                     RPP10290
      B=(XN*XY-X1*Y1)/(XN*X2-X1*X1)                                     RPP10300
      A=Y1/XN-B*X1/XN                                                   RPP10310
      R=(XN*XY-X1*Y1)**2/((XN*X2-X1*X1)*(XN*Y2-Y1*Y1))                  RPP10320
      IF(K.EQ.1.OR.K.EQ.3) RETURN                                       RPP10330
      A=EXP(A)                                                          RPP10340
      RETURN                                                            RPP10350
50    A=1.0                                                             RPP10360
      B=1.0                                                             RPP10370
      R=0.0                                                             RPP10380
      RETURN                                                            RPP10390
      END                                                               RPP10400
```

ORIGINAL PAGE IS
OF POOR QUALITY